UNIVERSITY OF BIRMINGHAM

EXPERIMENTAL AND SIMULATION INVESTIGATION OF THE GASOLINE ENGINE AFTERTREATMENT SYSTEM

by

YUANZHUO MEI

A thesis submitted to the University of Birmingham for the degree of

DOCTOR OF PHILOSOPHY

Department of Mechanical Engineering

School of Engineering

College of Engineering and Physical Science

The University of Birmingham

June 2021

ABSTRACT

Nowadays, lean burn strategy for gasoline direct injection (GDI) engine is gaining increasing popularity due to its superior fuel economy and lower greenhouse gas emissions. However, it is technically challenging to meet the stringent emissions regulations on NO_x with a conventional three-way catalyst (TWC). Moreover, low-temperature emissions control, especially during engine cold start, has been another focal point to researchers. To this end, it is urgently demanding to introduce strategies for improving the low-temperature and lean-NO_x removal performance of gasoline engine aftertreatment catalysts. Applying chemical promotors (i.e., hydrogen) was shown to be beneficial for enhancing catalysts activity but has been barely studied for lean burn GDI engine exhaust.

The work presented in this thesis investigates the potential of adding hydrogen to improve the gasoline engine aftertreatment performance in reducing vehicle emissions. Corresponding experimental works were performed using a gasoline research engine testing bench with modified aftertreatment system consisting of catalysts, heating devices and hydrogen introduction system. Precious hydrogen injection set-up was designed and built to allow both continuous and periodical hydrogen injection strategy. Simulation studies were carried out using a one-dimensional model developed via AVL Boost to model the catalyst light-off performance, providing auxiliary information to reveal the

underlying causes of hydrogen effect.

The hydrogen effect was studied using a TWC and a lean NO_x trap (LNT) catalyst. Firstly, the impact of adding small amount of hydrogen upstream TWC was examined. It was found that hydrogen addition (0.5%) upstream of the TWC greatly reduced its light-off temperatures. The poor lean NO_x removal efficiency over TWC was also enhanced, but the overall efficiency was still not very satisfactory. Therefore, the implementation of a LNT downstream the TWC was studied. The TWC-LNT system performance under various conditions was examined to help understanding the real exhaust chemistry over the catalysts. Periodical engine rich operation is required for the LNT regeneration, thereby causing associated fuel penalty (3.51%) compared to constant lean operation. Therefore, the concept of periodically injecting hydrogen to regenerate LNT instead of the cyclic engine rich operation was assessed. When engine was operating under lean/stoichiometric cycling operation, it was observed that injecting hydrogen during the stoichiometric phase has potential to improve the LNT NO_x removal performance and the engine fuel economy simultaneously. Subsequently, the effect of hydrogen addition on LNT performance at various temperatures (especially low temperature) was investigated. The influence of hydrogen injection amount and injection strategy was also assessed. Overall, the experimental results indicate that hydrogen addition upstream can improve the low temperature performance of lean gasoline engine aftertreatment catalysts.

ACKNOWLEDGEMENTS

Firstly, I would like to thank my supervisors Professor Athanasios (Thanos) Tsolakis and Dr Jose Martin Herreros sincerely for their support, guidance, and expertise throughout my PhD research project. Their dedicated supervision is incredibly useful. Also, I would like to thank Dr Soheil Zeraati Rezaei and Dr Omid Doustdar for giving me useful comments on my research topic and helping me with my experimental works. I gratefully appreciate the EPS college of University of Birmingham for providing me a scholarship which supported my PhD project.

ESPRC is acknowledged for supporting this work with the project FACE (ESPRC: ref. EP/P03117X/1). I also want to thank Johnson Matthey Plc. for providing the testing catalyst and Shell for providing the testing gasoline fuel. Thanks to AVL for providing access to its Advanced Simulation Technologies and software technical support within the frame of the University Partnership Program. This thesis was partly proofread for conventions of language, grammar and spelling by Janet's Proofreading Service.

I would like to thank my family and friends for their support and care during the whole PhD study. Also, I would like to thank my fiancé Mr. Tianchu Jiang for his encouragement and support. Lastly, I would like to thank myself for persevering and not giving up.

TABLE OF CONTENT

LIST OF TABLES

LIST OF FIGURES

LIST OF ABBREVIATIONS

AC	Alternating current
AFR	Air-fuel ratio
BDC	Bottom dead centre
BMEP	Brake mean effective power
BSFC	Brake specific fuel consumption
CAD	Crank angle degree
CC	Close-coupled
CFD	Computational fluid dynamics
cGPF	Catalysed GPF
CI	Compression ignition
COV	Coefficient of variation
CPSI	Cells per square inch
DI	Direct injection
DISI	Direct injection spark ignition
DOC	Diesel oxidation catalysts
DOHC	Dual overhead camshaft
DPF	Diesel particulate filter
ECU	Electronic computer unit

EIMS	Electron Impact Ionization Mass Spectrometer
EGR	Exhaust gas recirculation
ER	Eley-Rideal
EVC	Exhaust valve close
FTIR	Fourier transform infra-red
FTP-75	Federal Test Procedure 75
GA	Genetic algorithm
GDI	Gasoline direct injection
GHSV	Gas hourly space velocity
GHG	Greenhouse gas
GPF	Gasoline particulate filter
GSA	Geometric surface area
HC	Hydrocarbon
ICE	Internal combustion engine
IMEP	Indicated mean effective pressure
IVO	Intake valve open
LDV	Light duty vehicle
LH	Langmuir-Hinshelwood
LNT	Lean-NO_x trap
MFB	Mass fraction burned
NEDC	New European drive cycle

NRTC	Nonroad transient cycle
NSR	NO_x storage reduction
PFI	Port fuel injection
PM	Particulate matter
ppm	part per million (concentration)
REGR	Reformed exhaust gas recirculation
rpm	Revolutions per minute
SCR	Selective catalytic reduction
SD	Standard deviation
SI	Spark ignition
SR	Steam reforming
TWC	Three-way catalyst
VVT	Variable valve timing
WGS	Water-gas shift
WHR	Waste heat recovery

LIST OF SYMBOLS

A_{geo} the geometrical surface of the catalyst and is defined as $A_{geo} = \frac{4*d_H}{(d_H+d_W)^2}$

c_p the specific heat capacity, $\mathrm{J}/(kg * K)$

d_H hydraulic channel diameter, m

d_w monolith wall thickness, m

$D_{eff,j}$ diffusion coefficient of species j in the gas mixture, m^2/s

Gz Graetz number

h_j the total enthalpy of species j, kJ/mol

Δh_i the heat enthalpy of catalytic surface reaction i, kJ/mol

K_D friction coefficient

k_h heat transfer coefficient

k_m mass transfer coefficient

$M_{j,g}$ the molar mass of species j

n Engine speed, rpm

Nu Nusselt number

p pressure, Pa

P Engine brake power, W

Pr Prandtl number

R redox ratio of the exhaust gas composition

Re Reynolds number, and can be obtained by $Re = d_H * v * \rho * \mu^{-1}$

Sc Schmidt number

Sh Sherwood number

t time, s

T Engine brake torque, Nm

T_g gas temperature, K

T_s solid temperature, K

v_g gas velocity, m/s

$v_{i,j}$ the stoichiometric coefficient of reactant j in the catalytic surface reaction i

$y_{j,g}$ the molar concentration of species j in the bulk gas

y_j^L the surface molar concentraiton of species j

z axial coordinate

Greek symbols

α heat transfer coefficient between the gas phase and the solid walls

ε_g open frontal area, and can be derived from $\varepsilon_g = \frac{{d_H}^2}{(d_H + d_w)^2}$, m^2

λ_g thermal conductivity of the gas mixture, $W/(m^2K)$

λ engine operation lambda

μ fluid dynamic viscosity, $\mathrm{kg/m} \cdot s$

ρ_g molar density of the gas, $\mathrm{mol/m}^3$

φ pipe channel shape factor

ς generic friction coefficient

$\omega_{j,g}$ the mass fraction of species j in the bulk gas

Subscripts

i catalytic surface reaction

j gas species

s solid, surface

CHAPTER 1 INTRODUCTION

1.1 Overview

Nowadays, saving energy and reducing environmental pollutants are gaining global attention due to the increasing concern about the adverse effect of pollutants on both human health and environment and the continuously growing demand for energy. The overall trend of the automotive industry is shifting from traditional internal combustion engines (ICEs) towards more environmental-friendly power technologies like fuel cells, hybridisation, and electrification to approach the goal of carbon neutral in the forthcoming future. However, light-duty vehicles (LDVs) powered by ICEs are still dominated the automobile market and the total number is estimated to double the 2015's level and approach approximate 2 billion worldwide by 2040 according to the estimation by Smith et al. [1]. The rapidly growing number of LDVs results in increasing demand for the fossil fuels, and the associated pollutants emissions are also a heavy burden to the environment. Thus, it is of great necessity to innovate cleaner and more fuel economy engine and aftertreatment technologies. Governments from worldwide have developed relevant regulations which stimulate the automotive industry to attain great advance in improving vehicle fuel economy and reducing the regulated vehicular emissions. In the European Union, standards and legal controls on on-road vehicle tailpipe emissions have been

implemented since 1992 and have become increasingly stringent in recent years. As for the latest EURO 6 legislation for light-duty petrol vehicles, a limit on both particle mass concentration (0.0045 g/km) and particle number concentration (6 x 10^{11} #/km) from SI engines was stipulated with the limit on CO, HC, and NO_x emissions of 1.0, 0.10, and 0.060 g/km [2].

Gasoline engine with lean operation is gaining widely attention from researchers and the automotive industry due to its pronounced advantage in improving fuel economy and reducing greenhouse gas emissions (CO_2) compared to the stoichiometric-burn engines. However, NO_x emissions control for lean-burn gasoline engines to meet the rigorous legislation remains a major challenge since the traditional TWCs exhibit poor activity in lean NO_x reduction. This has impeded the commercialisation of the lean-burn fuel efficient gasoline engines in the European Union. The low-temperature emissions control (e.g., during engine cold start) is another challenge. It has been reported that over 90% cumulative tailpipe HC emissions were released from a 3.5 L turbocharged GDI engine over the Federal Test Procedure 75 (FTP-75) cycle in the first 250 seconds when the TWC is at low temperatures [3]. Therefore, the research and development of modern and advanced aftertreatment technology is of great significance.

In the past decades, relevant studies have been carried out to develop techniques to address those two issues, including the utilization of novel catalyst support materials to improve the low temperature performance, the utilization of a close-coupled catalyst configuration to achieve rapid warm-up, and the implementation of additional NO_x

reduction devices. Apart from those technologies, it is also reported that the presence of hydrogen is beneficial for improving the catalyst low-temperature performance, including promoting the catalytic oxidation of CO and HC [4-7] as well as the catalytic reduction of NO_x [8, 9]. Katare et al. reported that the diesel oxidation catalyst (DOC) activity was greatly promoted with the CO and HC light-off being advanced by around 20 ^oC with the presence of hydrogen in the feed exhaust gas (see Figure 1-1) [6]. In a more recent publication of Herreros et. al. (2014), the influence of upstream hydrogen injection on DOCs were assessed [10]. However, there is a lack of investigation on catalysts employed on gasoline engine under lean-burn conditions. For this reason, the hydrogen impact on gasoline engine aftertreatment system needs to be examined.

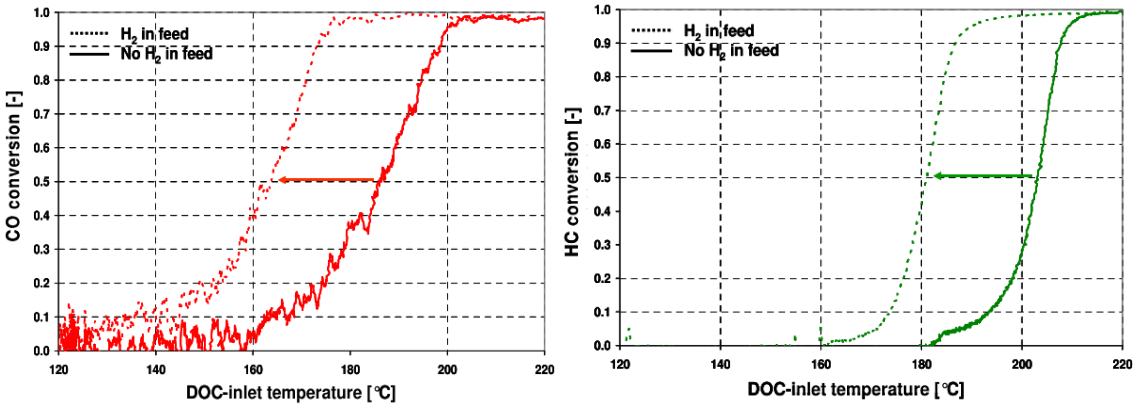

Figure 1-1. Enhancement on CO and HC light-off over a DOC by the presence of hydrogen (adapted from Katare, 2009) [6]

1.2 Thesis aims and objectives

The aim of this work is to study the role of hydrogen in improving the performance of a lean-burn GDI engine aftertreatment system, including a TWC, and a LNT catalyst. To

achieve the aim, specific objectives are listed as below:

1. To determine the impact of hydrogen addition on the light-off activity of a TWC under engine stoichiometric and lean operations
2. To understand the underlying causes of the hydrogen promotional effect on TWC's oxidation and reduction activity
3. To study the performance of the TWC-LNT catalysts for a lean-burn gasoline engine under various engine operating conditions (cold start and standard engine lean/rich cycling operations)
4. To understand the NO_x storage, regeneration, and reduction process over the LNT catalyst under a real gasoline engine exhaust environment
5. To understand the effect of upstream TWC and operating temperature on LNT performance
6. To determine the effect of hydrogen addition to the exhaust feed to LNT on the LNT performance
7. To determine the temperature dependence of the hydrogen addition effect on LNT performance
8. To identify the feasibility of using hydrogen addition to regenerate the LNT catalyst instead of running engine at periodical rich

1.3 Research outline

In present thesis, the major focus is on the investigation of hydrogen effect on the catalyst performance of a lean-burn gasoline engine. The investigation involves experimental and modelling study on a TWC and a LNT catalyst. Regarding the hydrogen effect on TWC, different amounts of hydrogen addition to the exhaust feed to TWC inlet were studied and the hydrogen effect on TWC performance was analysed in terms of the light-off temperatures of regulated emissions (CO, THC, NO_x). Regarding the study LNT catalyst, different amounts of hydrogen were added into the exhaust feed to LNT inlet under various engine operating conditions to explore the potential beneficial effect of hydrogen addition, including promoting the LNT activity (CO, THC, NO_x conversion and N_2O selectivity) and improving the engine fuel economy. Beside those, an AVL-Boost model is used to simulate the TWC light-off and provide insights into the underlying cause of the hydrogen effect.

1.4 Thesis outline

This thesis consists of seven chapters, including introduction, literature review, research methodology and three chapters of major outcomes, conclusions and further work suggestion.

In Chapter 1, the aim, and objectives as well as the outline and novelty of my research will be introduced. The challenge that is going to be addressed is also included.

Chapter 2: Literature Review

This chapter presents relevant background on GDI engine combustion and emissions as well as the implementation and development of aftertreatment technology, particularly the three-way catalyst and lean NO_x trap catalyst. Introduction of related emission regulations (from Euro 1 to Euro 6), the novel fuel technology and the ICE engine revolution are also included. Additionally, relevant literatures regarding experimental and simulation studies on the impact of hydrogen on catalyst activity will be reviewed and briefly introduced. In addition, the science of engineering gap which will be filled in the present work will be covered as well.

Chapter 3: Methodology

This chapter is about the research methods utilized in present work in terms of experimental and simulation approaches. The experimental section explains the experimental set-up, engine instrumentation, emissions measurement instruments, data acquisition and record system, and general experimental procedures. In the simulation section, details regarding the computational fluid dynamics (CFD) and thermodynamics model, relative chemical kinetic mechanisms, and the parameters optimization process will be provided.

Chapter 4: Effect of hydrogen addition on the light-off performance of a TWC

In Chapter 4, the investigation on hydrogen effect on a commercial TWC's light-off performance is presented. With different amount of hydrogen addition upstream, the TWC's light-off activity was experimentally investigated. Engine was running at speed

of 2100 rpm, brake mean effective power (BMEP) of 2.2 bar, and lean air-fuel ratio at λ = 1 and 1.08. The light-off temperatures and overall conversion of CO, THC, and NO_x have been compared to the baseline condition without hydrogen addition to identify the hydrogen effect. An AVL Boost model was built to simulate the TWC light-off performance and good agreement was achieved between model prediction and experiment. The estimated chemical reaction parameters revealed the underlying cause of hydrogen effect. This chapter highlights the potential of adding small amount of hydrogen to enhance the TWC's low temperature activity and its lean NO_x conversion.

Chapter 5: Study of a TWC-LNT system performance on a gasoline engine

This chapter examines TWC-LNT catalysts system performance under different conditions on a gasoline engine, including cold-start, and transient lean/rich cycle. The concentration profiles of key exhaust species were collected at various locations along the exhaust pipeline to analyse the catalysts performance and the gasoline-based exhaust chemistry during the alternation of engine lean and rich operation. In addition, the temperature and the upstream TWC effect on LNT activity was examined. The importance of this chapter is that it provides detailed investigation of how the TWC-LNT catalysts system functions under different conditions for a gasoline research engine. Moreover, the study on LNT's cold start performance and NO_x storage memory phenomenon provides insights for optimizing the emissions control system of hybrid electric vehicles, which typically experience frequent engine starts and stops in urban driving.

Chapter 6: Effect of hydrogen addition on the performance of a LNT catalyst

Chapter 6 is mainly focused on the exploration of the influence of hydrogen addition on LNT performance through experimental approach. Both constant and periodical hydrogen addition strategies were studied. Engine was operating at 2100 rpm of speed, BEMP load of 1.68 bar, and different air-fuel-ratio operations. For the investigation on constant hydrogen addition, engine was running at standard LNT operating condition – transient lean/rich cycle, and various amount of hydrogen was added to the exhaust feed to LNT inlet to investigate the hydrogen effect on LNT performance, especially at low temperature. For the periodical hydrogen addition study, using hydrogen as reductant instead of gasoline fuel (rich operation) to purge the LNT catalyst was examined under engine lean operations. The importance of this chapter is that it provides key information on how different amount of hydrogen addition affects LNT catalyst under different circumstances, including enhancing THC and NO_x conversion, moderating N_2O formation, and improving the fuel economy.

Chapter 7: Conclusions and Future Work

This chapter is the last chapter of this thesis, summarising the major findings obtained from present research work. Additionally, the suggestion of any potential further works on this research topic will be included.

1.5 Contribution to knowledge

The novelty of present research is outlined as below:

- This thesis demonstrates the hydrogen promotional effect on catalysts performance for a lean-burn gasoline direct engine, including both TWC and LNT catalyst.
- This thesis provides detailed simulation analysis of how hydrogen is able to improve the TWC light-off.
- This thesis investigates the temperature effect on a LNT catalyst under real gasoline engine lean exhaust.
- This thesis studies the low temperature performance TWC-LNT catalysts during engine start-up.
- This thesis examines the feasibility of injecting hydrogen to regenerate the LNT under gasoline direct injection engine lean operation.
- Unlike most of other studies, the experimental studies in present thesis were conducted using engine testing bench incorporated with catalysts rather than using synthetic exhaust gas mixtures.

CHAPTER 2 LITERATURE REVIEW

2.1 Introduction

In this chapter, an introduction to background knowledge and a literature review regarding relevant research works is presented. The experimental works in this thesis were carried out using a GDI engine test bench, thereby a brief introduction to the GDI engine's development history, combustion and regulated emissions formation is firstly presented. Afterwards, the aftertreatment devices implemented for modern gasoline engines are introduced, including TWC and the lean-NO_x abatement systems, especially the LNT catalyst. In addition, the influence of hydrogen addition on different catalytic converters will be described. Subsequently, traditional hydrogen storage and on-board hydrogen production technology will be briefly introduced. Through this PhD research, the catalytic converter modelling provided supplementary information to the laboratory testing. Thus, the models developed and utilized by other researchers to simulate the fluid dynamics, thermodynamics and chemical reactions over the monolithic catalyst converter were reviewed in detail. In addition, the scientific of gap which will be filled in the present work will be covered as well.

2.2 The GDI engine combustion

The increased pressure to reduce the carbon dioxide (CO_2) emissions and improve engine fuel economy has emphasised the necessity for innovating cleaner and more advanced engine technologies, which has led to the evolution of the GDI engines. The idea of developing a direct injection system for gasoline engines was first proposed by Rolls-Royce Crecy for military use during the 1930s. Since then extensive studies have been carried out by many automotive manufacturers to apply direct injection strategies to automotive applications [11]. In the 1990's, GDI engines were substantially introduced into the Japanese and European market and then gradually they took place of their counterpart –traditional port fuel injection (PFI) technology, because of their superior performance in engine efficiency and fuel economy [12]. It was reported that the GDI engines' market share rapidly rose from virtually 0% to over 30% in the EU during the past decades [13].

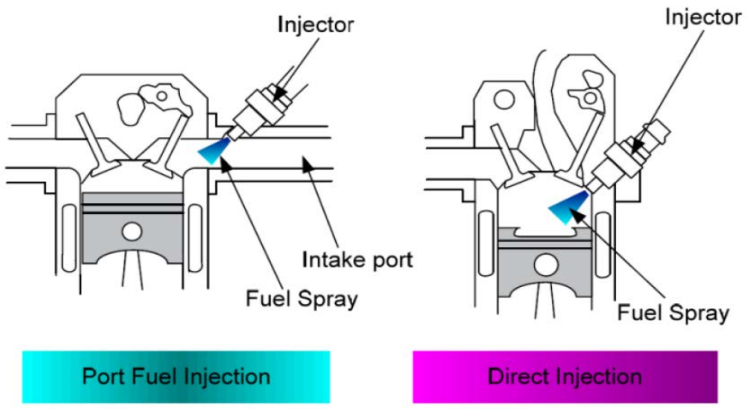

Figure 2-1. Typical air/fuel mixture preparation systems for gasoline engine (adapted from Zhao, 2010) [14]

As indicated by the name, the major difference between the GDI engine and the PFI engine is the approach of fuel injection. For the PFI engine, fuel is injected into the intake port first via injectors mounted in the intake manifold; while in the GDI engine, the high-pressure liquid fuel (50-150 bar) is directly injected into the combustion chamber through injectors mounted close to the cylinder head with precise control of the fuel injection amount and timing, thereby providing more accurate fuel metering than the PFI approach. Different strategies for air/fuel mixture preparation in gasoline engines are illustrated by Figure 2-1. There are several inherent benefits of applying the direct injection strategy. For example, high injection pressure is associated with better fuel spray atomisation, thereby resulting in more stable combustion and reduced HC emissions. It was suggested by Takagi that a 30 % reduction in HC emissions during cold start was achieved by a Nissan prototype GDI engine compared to that for a comparable PFI engine [15]. Also, an engine with the DI strategy was reported to have enhanced transient response and less variation from cylinder to cylinder [16]. Furthermore, the superior charge cooling effect provided by direct injection is another advantage. The cylinder charge temperature can be significantly reduced through heat extraction from the surrounding air via fuel evaporation, which enables the GDI engines to run under full-load condition with higher compression ratio and without the risk of causing knocking combustion. Thereby, higher engine efficiency and lower fuel consumption can be achieved simultaneously. Moreover, the charge cooling effect can

be beneficial for engine downsizing. Namely, a large displacement naturally aspirated engine can be replaced with a smaller but highly boosted engine without being limited by the tendency of knocking combustion, thereby allowing the operation at higher load and wide-open throttle conditions. Apart from these advantages, there are still several drawbacks of the GDI engine. One of the major disadvantages is that GDI engines with stratified charge combustion have higher particulate matter (PM) emissions, and relatively higher unburned HC and NO_x emissions at high load than PFI engines [16-18]. Also, there are issues regarding the accumulation of deposits at the injection nozzle and potential negative impact on engine combustion and vehicle emissions [16, 19, 20].

Additionally, GDI engines can provide more flexible options of combustion mode compared to PFI engines which usually operate with homogenous charge. The GDI engine can operate under both homogenous and stratified conditions depending on the fuel injection timing as indicated in Figure 2.2. For highly efficient full-load operation, the GDI engine runs under stochiometric condition with early injection (during induction) to obtain a homogenous mixture; while for the part-load operation, lean-burn combustion strategy is adopted to improve engine efficiency by reducing the pumping loss. Lean-burn combustion can be achieved through direct injection, because the in-cylinder air/fuel ratio (AFR) range can be extended from the original 20:1, which is limited by gasoline propagating flame front to 100:1 via stratified charge combustion [11]. To achieve the stratified mixture, the fuel injection commences during the compression stroke which results in higher efficiency under part-load operation. In

addition, fast and efficient engine stop and start operation can be realized by using direct injection, which is also shown to be advantageous to improve the three-way catalyst light-off performance at cold start and decrease the overall CO_2 emissions simultaneously [11, 16].

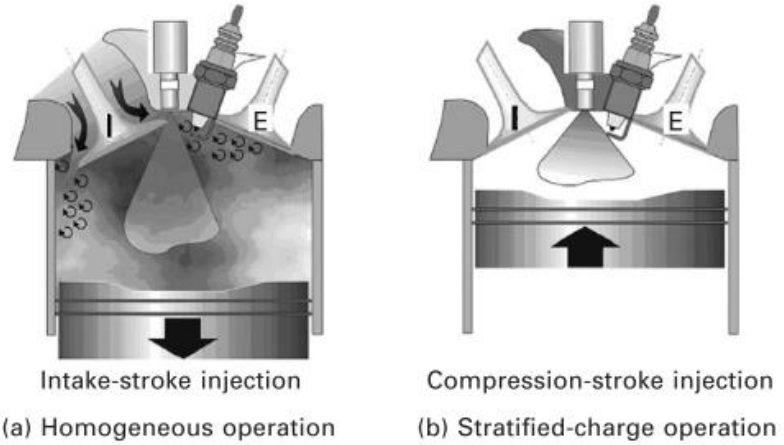

Figure 2.2. Schematic illustration of (a) homogeneous and (b) stratified-charge operation (Adapted from Spicher and Heidenreich, 2010) [21]

2.3 Engine exhaust emissions

In recent years, increasing worldwide attention has been given to air pollutants, which have been reported to have a seriously detrimental impact on public health, atmospheric visibility, and climate [22-24]. Automobile exhaust emissions are reported to be one of these main contributors of the air pollutants. Gasoline engine exhaust emissions are primarily comprised of gaseous emissions, including unburnt hydrocarbons (HCs), carbon monoxide (CO) and nitrogen oxides (NO_x), and particulate matter (PM) to a small extent. To reduce emissions from on-road vehicles, the 'Clean Air Act' was firstly

proposed and implemented in California decades ago [25]. As for the legal controls in the European Union, the revolution of the EURO emission regulations for light duty commercial petrol vehicles are summarised in

Table 2-1. Besides these, regulations on green-house gas (GHG) emissions have also been proposed in several regions, including the US, India, China, and the EU. The European Green Deal was proposed with an ambitious target of a 90% reduction in the GHG emissions from transport compared to the 1990 levels, and the achievement of being climate-neutral by 2050. The latest legislation introduced in 2019 targets a reduction in the fleet-average CO_2 emissions from new light-duty vehicles by 15% in 2025 and by 37.5% in 2030, compared to the 2020's emission levels of 95g CO_2/km [26]. Additionally, it is expected that the next stage of emission standards - Euro 7 regulation will be introduced soon to further reduce the tailpipe CO_2 emission levels [27].

Table 2-1- Evolution of EURO emission legislation for light-duty petrol vehicles [2]

Year/Stage	CO	HC	NMHC	NO_x	PM	PN
Unit			(g/km)			(#/km)
1992 (Euro 1)	2.72	-	-	-	-	-
1996 (Euro 2)	2.2	-	-	-	-	-
2000 (Euro 3)	2.3	0.20	-	0.15	-	-
2005 (Euro 4)	1.0	0.10	-	0.08	-	-
2009 (Euro 5a)	1.0	0.10	0.068	0.060	0.005*	-

2011 (Euro 5b)	1.0	0.10	0.068	0.060	0.0045*	-
2014 (Euro 6)	1.0	0.10	0.068	0.060	0.0045*	6×10^{11}
2020 (Euro 6d)	1.0	0.10	0.068	0.060	0.0045*	6×10^{11}

NMHC: Non-methane hydrocarbons; *only applicable to vehicles powered by DI engines.

2.3.1 CO, HC and PM emissions

Carbon monoxide is a colourless, odourless, poisonous, and flammable chemical substance which has lower density than air. Although it is generally non-toxic, it could be physically dangerous or even fatal if a person is exposed to a high concentration of CO over a certain period. This toxic effect on human health has been demonstrated that CO reduces the capability of haemoglobin for oxygen storage and transportation to all other parts of the body (especially the brain), which can possibly result in headache, dizziness, tissue damage or even death [28]. Carbon monoxide is formed during combustion and is primarily concentrated in fuel-rich regions, where the oxygen level is insufficient for complete fuel combustion; while as for fuel-lean mixture, a significant level of CO is also present due to dissociation, and the concentration strongly relies on the temperature. As the combustion temperature decreases, the CO concentration decreases [29]. In the expansion stroke, the CO formation process is still taking place, but the formation rate significantly drops as the burnt gas temperature reduces [30]. The CO emission from gasoline engine could be affected by several factors, including the ignition timing, spark timing, load, and the fuel/air equivalence ratio. Among all those factors, the fuel/air

equivalence ratio is the dominant factor to the formation of CO. As illustrated in Figure 2-3, for fuel-rich mixtures, the CO emissions concentrations rise greatly with the increasing ratio, and the CO concentrations vary slightly as the equivalence ratio changes for the fuel-lean mixtures.

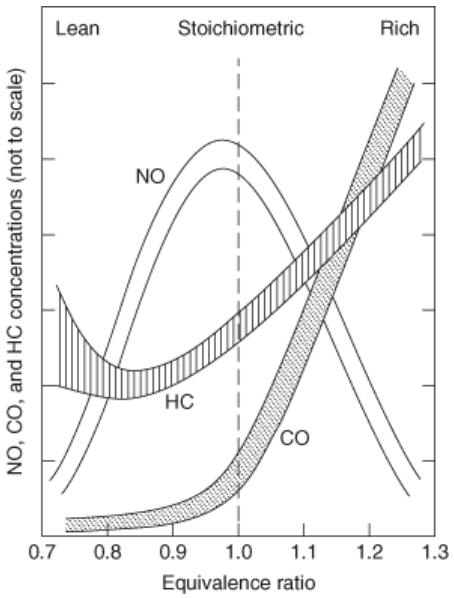

Figure 2-3. HC, CO and NO_x emissions from a conventional SI engine as a function of the fuel/air equivalence ratio (Adapted from Heywood, 1988) [30]

Unburnt hydrocarbons (HC) are also a result of incomplete combustion. The relation between HC emissions and the equivalence ratio is demonstrated in Figure 2-3. It can be seen that HC emissions are generally lower for leaner mixture apart from the ultra-lean region where the engine operation is erratic, and the combustion quality is poor. There are several sources which contribute to HC emissions. Unburned air-fuel mixtures, which are trapped in the crevices (regions such as piston ring grooves or valve seats) by the elevated in-cylinder pressure, are considered to be one of major sources. The entrances of theses crevices are too narrow for the flame to enter, so these unburned

air-fuel mixtures escape from combustion; and thereby form unburned HCs. The oil/fuel films formed on the cylinder wall, piston and cylinder head are reported to be another contributor of HC emissions, as they absorb the hydrocarbons contained in the fuel prior to combustion. Unburned HC emissions can be formed on the combustion chamber wall as well. When the flame approaches the combustion chamber wall, an ultra-thin quench layer comprising unburned and partially burned air-fuel mixtures is left after the flame is extinguished by the cold wall [30]. Sometimes when combustion is too slow or starts too late, misfire or partial burn occurs, thereby resulting in massive amount of unburnt HC fuel. Furthermore, short-circuiting makes unburnt mixture flow into the exhaust during the valve overlap period, which is another source for HC formation. It should be mentioned that HC emissions can be greatly reduced during cold start by utilising the direct injection approach. This benefit of the DI strategy has been experimentally verified by some researchers [15, 31, 32]. For example, Shimotani et al. [31] reported that only the first few cycles are required for GDI engines to reach stable operation during cold start, and the PFI engines normally need more than 10 cycles to reach stable operation. Accordingly, the formation and growth of fuel film, misfire and partial burn are alleviated in GDI engines which contributes to the decrease of HC emissions. For DISI engines with stratified charge, the HC emission level and PM emission level are generally several times higher than those emitted from engines with homogenous operation.

Generally, gasoline exhaust PM consists of ultrafine particles and nanoparticles that

contain volatile organic compounds, while the soot fraction is smaller compared to those from diesel particles [33]. The majority of PM is initially originated in fuel-rich regions in the engine cylinder. After leaving the cylinder, it undergoes complex physical and chemical processes in the exhaust system and atmosphere, including nucleation, coagulation, surface growth, oxidation [34]. Generally, engine exhaust particle size distribution can be classified into three modes based on the average diameter of particles: nuclei mode (also called nucleation mode), accumulation mode, and coarse mode [33]. In the past, diesel engine PM emissions have been a focal point for engine manufacturers and researchers, with particle emissions from SI engines being neglected. However, increasingly concerns have been raised about PM emissions from SI engines due to the considerable PM emissions from GDI engines. Related studies report that PM emissions from a GDI engine are higher than those from an equivalent PFI engine, [18] and in some cases, they are even close in number to those from diesel engines [17]. In addition, SI engine emissions are regarded as a major source of the ultrafine and nanometre range particles, which are reported to have adverse effects on human health, the environment, and public infrastructure [35-37]. Therefore, the issue of GDI engine PM emissions needs to be addressed to satisfy the increasingly stringent PM regulations. Similar to the diesel particulate filter (DPF) employed for CI engines, the utilisation of a gasoline particulate filter (GPF) has been reported to be effective in reducing the gasoline PM emissions [38-40]. Additionally, the implementation of reformed exhaust gas recirculation (REGR) was proved to be beneficial in lowering GDI engine PM generation [41, 42].

2.3.2 NO_x emissions

The mixture of nitric oxide (NO) and nitrogen dioxide (NO_2) is referred to NO_x, and typically NO accounts for over 90%. The majority of NO is formed during combustion, and it will be subsequently oxidised to NO_2 in the environment. However, it is the small fraction – NO_2, which was found to have an adverse effect on both the environment (acid deposition, eutrophication) and human health (causes inflammation of the respiratory system) [29]. In addition, NO_2 can react with non-methane hydrocarbons in the presence of ultra-violet light to form a photochemical smog, which is considered as one of the major sources of ground level ozone production. The fundamentals of NO_x formation in engine exhausts have been comprehensively described in multiple publications [29, 30, 43]. The general process will be briefly introduced here: NO mainly originates from the oxidation of atmospheric nitrogen in a gasoline engine, since there is a negligible amount of nitrogen contained in gasoline fuels. It is reported that NO formation generally takes place in both the flame front and the post-flame gas, where the temperature and pressure is high enough [30]. Generally, the formed NO will be rapidly converted to NO_2. However, in SI engine exhaust, the NO_2/NO ratio is extremely low, which is believed to result from the fact that the NO_2 decomposition rate is considerably higher than its formation rate. Relevant studies imply that NO formation is highly dependent on the flame speed, temperature, pressure, and fuel/air equivalence ratio [29]. The increment in NO_x emissions is related to lower flame speed, which provides a longer time for NO_x formation [29]. As can be seen from Figure 2-3 that the NO_x emissions level can be

described as a bell curve with the highest value being observed with the equivalence ratio between 0.95 to 1.0 where the fuel/air mixture is slightly lean. The explanation given by Heywood suggested that lower NO_x emissions can be attributed to the reduced burned gas temperatures in the richer region and the increased oxygen concentration in the leaner region [30].

There are several commonly used approaches to control NO_x emissions; including retardation of the ignition, implementation of exhaust gas recirculation (EGR), and aftertreatment catalysts, such as the NO_x trap catalyst, $DeNO_x$ catalyst and selective catalytic reduction (SCR) catalyst, which will be discussed in section 2.4. Retarding ignition (spark timing) is associated with later combustion, which is shown to be effective in reducing the in-cylinder peak pressure and temperature, thereby reducing the NO_x emissions. However, it is unfavourable for the engine power output and fuel economy. As for the application of EGR, increasing the concentration of residual gas in the cylinder can lower both the flame temperature and speed, which is proved to be beneficial for the control of NO_x emissions; but applying EGR is potentially disadvantageous for engine efficiency. Also, it is pointed out that the utilisation of EGR can result in a higher HC emissions level [44].

2.4 Aftertreatment devices for modern gasoline vehicles

To suppress the adverse environmental effect of engine emissions and meet the

increasingly stringent European exhaust emissions' regulations, more and more advanced technologies have been proposed and implemented in the automotive industry, including aftertreatment components – the TWC converter, lean-NO_x control devices and particle filters. Generally, TWC is capable of effectively converting the CO and HC emissions, and lean- NO_x control devices are gaining more attention with the increasing popularity of lean-burn strategy. Gasoline particle filters (GPF) are introduced into the gasoline engine aftertreatment system since the legal requirements on gasoline particle emissions were tightened.

2.4.1 Three-way catalytic (TWC) converter

Oxidation catalysts were first employed by automotive manufacturers for commercial purposes in the U.S. and Japan in 1974 [45]. Afterwards, they were introduced into the EU and the implementation of catalytic converters became mandatory for petrol vehicles from 1993 [46].

Since then, they have been rapidly developed and have become the most widely applied aftertreatment control technology for the abatement of harmful engine emissions from gasoline-powered vehicles including unburned hydrocarbons (HCs), CO, and NO_x. The major function of the catalysts is to rapidly convert these three pollutants to their corresponding harmless products CO_2, H_2O, and N_2. Accordingly, this kind of catalyst is named as a three-way catalyst. The reactions are largely speeded up over the catalyst surface compared to that for ordinary conditions. The basic principle for any catalytic

reaction is that the energy barrier is significantly lowered over the catalyst surface. The main catalytic reactions occurring over the TWC are given by Reaction 2-1 to Reaction 2-8, including the oxidation reactions, water gas shift (WGS) reaction, and hydrocarbon steam reforming (SR) reaction.

$$\mathrm{CO} + \frac{1}{2}O_2 \xrightarrow{\text{oxidation}} CO_2 \qquad \text{Reaction 2-1}$$

$$H_2 + \frac{1}{2}O_2 \xrightarrow{\text{oxidation}} H_2\mathrm{O} \qquad \text{Reaction 2-2}$$

$$C_\mathrm{x}H_\mathrm{y} + (\mathrm{x} + \frac{y}{4})O_2 \xrightarrow{\text{oxidation}} \mathrm{x}CO_2 + \frac{y}{2}H_2\mathrm{O} \qquad \text{Reaction 2-3}$$

$$2\mathrm{NO} + 2\mathrm{CO} \xrightarrow{\text{Reduction}} 2CO_2 + N_2 \qquad \text{Reaction 2-4}$$

$$2\mathrm{NO} + 2H_2 \xrightarrow{\text{Reduction}} 2H_2\mathrm{O} + N_2 \qquad \text{Reaction 2-5}$$

$$(2\mathrm{x} + \frac{y}{2})\mathrm{NO} + C_\mathrm{x}H_\mathrm{y} \xrightarrow{\text{Reduction}} \mathrm{x}CO_2 + \frac{y}{2}H_2\mathrm{O} + (\mathrm{x} + \frac{y}{4})N_2 \qquad \text{Reaction 2-6}$$

$$\mathrm{CO} + H_2O \xrightarrow{\text{WGS}} CO_2 + H_2 \qquad \text{Reaction 2-7}$$

$$C_\mathrm{x}H_\mathrm{y} + \mathrm{x}H_2\mathrm{O} \xrightarrow{\text{SR}} \mathrm{x}CO + (\mathrm{x} + \frac{\mathrm{y}}{2})H_2 \qquad \text{Reaction 2-8}$$

It is well known that the TWC works most efficiently and achieves a simultaneous conversion of CO, HCs, and NO_x with air/fuel stoichiometry. For fuel rich combustions ($\lambda<1$), the shortage of oxygen results in the incomplete combustion of the fuel, thereby producing more engine output unburned HCs and CO compared to the stoichiometric condition. The presence of excess HCs and CO in the exhaust makes it difficult for the TWC to fully convert those two species. As for the fuel lean conditions ($\lambda>1$), the TWC

performance exhibits totally different trend. The NO_x reduction is strongly affected by the excess of oxygen and the lack of CO in the exhaust. Figure 2-4. presents the TWC performance in CO, HC and NO conversion under varying air-fuel ratio.

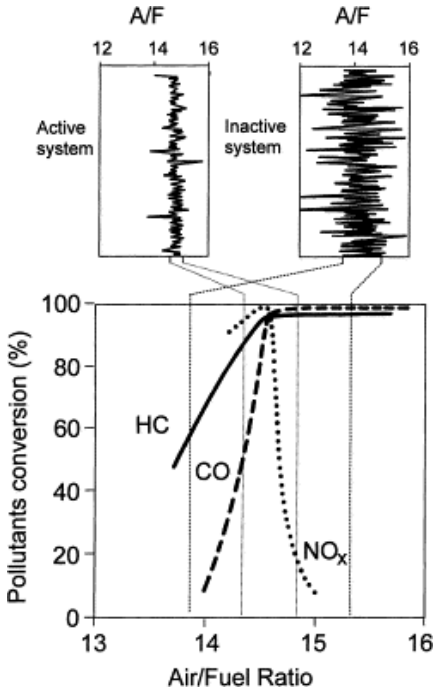

Figure 2-4. TWC response to air-fuel ratio (Adapted from Kašpar et al., 2003) [47]

As shown in Figure 2-5, a TWC generally consists of a honeycomb-structured monolith made of cordierite ($2MgO{\cdot}2Al_2O_3{\cdot}5SiO_2$) or stainless steel with a thin layer of porous materials deposited on its internal surface [48]. The axial direction of the honeycomb channels follows the same path as the exhaust gas flow passing through. The porous materials, also called washcoat, primarily contains γ-Al_2O_3 which provides high surface area support. Ceria (CeO_2) is added as an oxygen storage promoter. It was reported to be beneficial for CO, HCs, and NO_x conversion with the transient oscillating A/F ratios due to its rapid oxygen storage/release capacity. Generally, oxygen can be adsorbed and released by ceria as a function of the exhaust gas A/F ratio via the Ce^{4+}/Ce^{3+} redox

reactions.

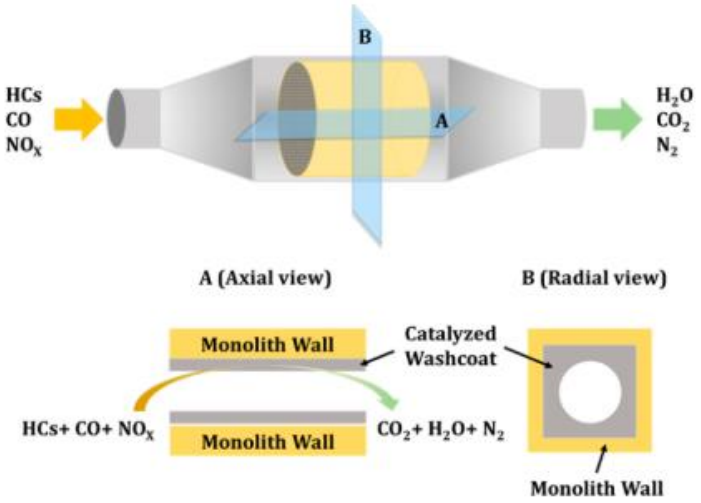

Figure 2-5. Schematic of a washcoated monolith TWC converter (Adapted from Zheng et al., 2015) [49]

There are other materials added to the washcoat as well for different purposes. For example, baria (BaO) is added as a stabiliser to maintain the surface area. Sometimes zirconia (ZrO_2) is incorporated into the ceria framework and it was reported that its introduction can effectively enhance the catalyst reduction behaviour compared to pure ceria [50]. The noble metals, which are the actual catalytical promoters, account for only 1% to 2% of the total washcoat weight. Nowadays, Pt, Pd, and Rh are usually used for the commercial TWCs. The stringent regulation on NO_x emissions has emphasised the necessity of Rh due to its superior performance in improving NO reduction behaviour. Additionally, it was found that the incorporation of Rh into Pt has a synergistic effect that helps to improve Pt and Rh activity simultaneously [51]. Therefore, prior to the introduction of Pd, Pt/Rh catalysts have dominated the automotive industry's catalyst market for many years. The addition of Pd to the conventional Pt/Rh catalyst is really a

breakthrough technology because of Pd's superior catalytical activity in facilitating HCs oxidation and better thermal stability.

The conversion efficiency of a conventional TWC can reach approximately 100% for the three aforementioned pollutants (CO, THC, and NO_x) when the operating temperature is sufficient, generally above 400 °C [3]. However, there are some challenges regarding the catalytic activity at low operating temperatures, especially during engine cold start. It was reported by Heck and Farrauto (2001) that it takes 60 to 120s for a conventional TWC to reach its light-off temperature and within this period approximately 70% of regulated pollutants are emitted [52]. A more recent study by Chen and Chang (2015) indicated that in the case of a 2010 vehicle powered by a 3.5 L turbocharged GDI engine, over 90% cumulative tailpipe HC emissions over the Federal Test Procedure 75 (FTP-75) cycle were released in the first 250 seconds when the TWC is at low temperatures [3]. Therefore, it is essential to develop advanced engine combustion strategies and aftertreatment techniques to reduce cold start emissions, and thereby reducing the associated environmental impact. Regarding the optimization in engine combustion, it was reported that a great reduction in regulated pollutant emissions is attained through optimising the fuel injection parameters, employing EGR, applying the REGR system, etc [53-55]. Apart from that, numerous studies were carried out to improve the low temperature performance of aftertreatment systems, including the utilisation of a close-coupled catalyst (CCC) configuration to achieve a rapid warm-up for TWC, implementation of HC traps to provide supplementary HC removal, utilisation of an electrically heated catalyst to reduce

the light-off time, and using novel support materials ($Al_2O_3/CeO_2/ZrO_2$ mixed oxide) for a TWC to reduce the light-off temperature [3, 56-58].

In addition to the inherent issues of low catalyst activity during engine cold start, the poor NO_x reduction performance of a TWC under lean conditions is another challenge. To meet the rigorous limitation on NO_x emission, advanced technologies have been researched and employed for gasoline engine lean NO_x abatement, such as implementing additional NO_x reduction devices, which will be discussed in the next section. Regarding the NO_x reduction over the TWC, apart from the harmless N_2, generally, NH_3 and N_2O are formed as undesirable by-products. Despite the disadvantages, NH_3 and N_2O can also bring some benefits. Recently, the concept of integrating an upstream TWC and a passive ammonia-SCR was proposed and studied [59, 60]. It is suggested that NH_3 produced over a TWC can be stored by the downstream ammonia-SCR, and subsequently, is released and functions as a NO_x reductant under a certain condition; which can not only solve the NH_3 slip issue of the TWC, but also reduce the expense of carrying an additional urea storage tank for the SCR. As for N_2O, it is found to be favourably formed at low temperatures over the catalyst, [61, 62] and was reported to be beneficial in soot removal. Davies and co-workers experimentally studied the catalysed chemistry of simultaneous soot oxidation and NO_x reduction over a silver-based catalyst, suggesting that the oxidation of trapped soot can be effectively initiated by N_2O which is formed via non-selective NO_x reduction by NH_3 at low exhaust gas temperature [63]. This finding pointed out the potential of utilising N_2O to trigger the low-temperature soot removal process; thus,

achieving the goal of removing the undesired N_2O and soot simultaneously.

2.4.2 Lean NO_x abatement for lean-burn gasoline engine

The lean-burn strategy is becoming more and more favourable for gasoline engines due to the improved fuel consumption performance and reduced greenhouse gas emissions. However, the lean combustion will strongly attenuate the TWC's performance in NO reduction, as indicated by Figure 2-4. Since the introduction of the Euro 5 legislation, the limitation on NO_x emissions has become more rigorous, which has emphasised the necessity of incorporating other NO_x reduction devices into the lean burn engine aftertreatment system. There are three generally employed ways for NO_x removal from lean-burn exhaust emissions: the direct decomposition of NO_x; the LNT catalyst; and the SCR catalyst (urea-SCR, HC-SCR, and H_2-SCR) [64]. Unlike the LNT and SCR, the first approach removes NO_x directly via $NO \rightarrow \frac{1}{2} N_2 + \frac{1}{2} O_2$ rather than the reduction reaction by other reductants, such as H_2, CO, HC, and NH_3. However, the activation energy of the decomposition process is very high. Although Cu-Zeolite is reported to be the best NO_x decomposition catalyst so far, it is found to have poor activity [65].

With the presence of surplus oxygen, NO_x removal over the SCR catalyst is achieved via selective reduction by reducing agents (such as H_2, HC, CO, and NH_3). The SCR catalyst can be operated under two different modes: (1) active control mode where the required reductants will be externally injected; and (2) passive control mode without any external addition. For example, for the active urea-SCR, NO_x removal is achieved by NH_3 via

external liquid urea injection through the following steps as illustrated in Figure 2-6. First, the injected aqueous urea is atomised into an upstream hydrolysis catalyst, thereby reacting with water to produce NH_3 and CO. Afterwards, the NO_x contained in the exhaust will be reduced by ammonia and converted into nitrogen over the SCR catalyst. However, there is one noticeable drawback of this type of catalyst, which is the requirement of an on-board urea tank with additional dosing system, leading to a cost penalty, the necessity for extra space, and thus, more complexity of the system's design.

Additionally, relevant problems such as NH_3-slip, ash odor, and catalyst deterioration cannot be ignored [66]. Regarding the passive-SCR system, it can be achieved via coupling a TWC upstream of the SCR catalyst to generate on-board the required amount of ammonia for NO_x reduction [59, 60, 67]. However, this requires complex control of the engine operation. Additionally, it is quite challenging to achieve the right balance between the quantity of NH_3 generated during the rich phase and the amount of NO_x to be reduced during the lean phase to ensure optimum NO_x removal efficiency with fewer ammonia slips and fuel penalty.

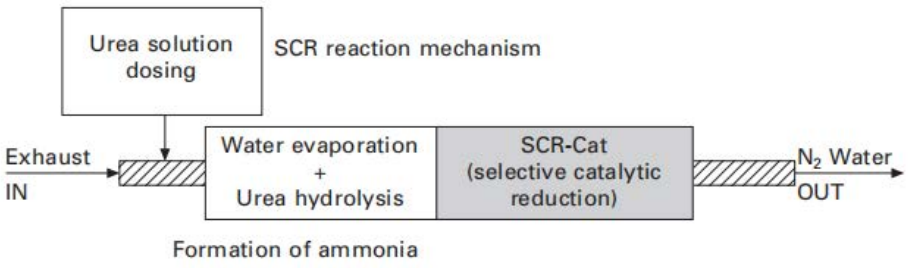

Figure 2-6. Graphical illustration of the urea-SCR (active control) reaction mechanism (Adapted from Zhao, 2010) [14]

As for the HC-SCR, the major issue is its low NO_x reduction efficiency at low temperatures [68, 69]. The H_2-SCR NO_x control technology has also been studied due to the superior NO_x reducing activity of hydrogen at low temperatures [70-72]. Also, it is more environmentally friendly to use the H_2-SCR technology as hydrogen is a non-carbon-containing reductant, thereby producing less CO_2 compared to the HC-SCR. The H_2-SCR NO_x removal activity varies over different noble metal-based catalysts [73]. It was reported that NO-H_2 reduction activity was found to be the highest over Pt-based catalysts at low temperature ($T < 200$ ºC) [74, 75], and relatively higher N_2 selectivity can be generally achieved over the Pd-based catalysts [71, 76].

The LNT (also called NO_x storage reduction catalyst, NSR) was originally implemented in a diesel engine's aftertreatment system and subsequently adopted for the lean-burn gasoline engine. The NO_x removal is achieved by the storage, regeneration, and reduction process in periodic lean/rich exhaust environment, as illustrated in Figure 2-7. Under lean condition with excess oxygen in the exhaust, NO_x is stored in the form of nitrites or nitrates on the storage component, such as $Ba(NO_3)_2$, $Ba(NO_2)_2$. Take the nitrite route as an example, the NO_x storage proceeds via Reaction 2-9 to Reaction 2-11. While switching to a fuel rich condition, the LNT will be regenerated via in-cylinder fuel injection or additional fuel injection to the exhaust stream. The stored NO_x is released (see Reaction 2-12 to Reaction 2-14), and then reduced to N_2 by reductants (see Reaction 2-15 to Reaction 2-17). Generally, C_3H_6 is selected as the representative HC in the catalytical reaction mechanism, thereby C_3H_6 is used for Reaction 2-14 and Reaction 2-17. Although

N_2 is the most desirable product during the NO_x reduction, NH_3 and N_2O can be also formed as by-products under certain conditions. The combination of a 60-120s storage phase and a 3-5s regeneration phase is typically employed in practice [64].

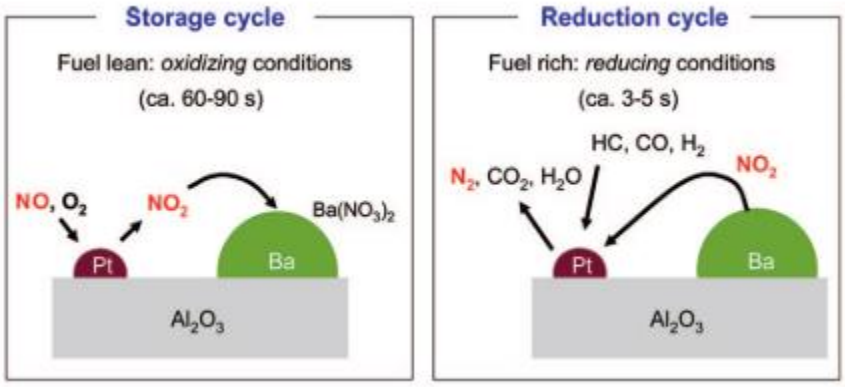

Figure 2-7. Graphical illustration of the LNT catalyst operating principle (Adapted from Roy and Baiker, 2009) [64]

$$\mathrm{NO} + \frac{1}{2}O_2 \overset{\text{oxidation}}{\Longleftrightarrow} NO_2 \qquad \text{Reaction 2-9}$$

$$\mathrm{Ba}CO_3 + 2\mathrm{N}O_2 + \frac{1}{2}O_2 \overset{\text{storage}}{\Longleftrightarrow} \mathrm{Ba}(NO_3)_2 + CO_2 \qquad \text{Reaction 2-10}$$

$$\mathrm{Ba}CO_3 + 2\mathrm{N}O + \frac{3}{2}O_2 \overset{\text{storage}}{\Longleftrightarrow} \mathrm{Ba}(NO_3)_2 + CO_2 \qquad \text{Reaction 2-11}$$

$$\mathrm{Ba}(NO_3)_2 + 3\mathrm{C}O \xrightarrow{\text{regeneration}} \mathrm{Ba}CO_3 + 2\mathrm{N}O + 2CO_2 \qquad \text{Reaction 2-12}$$

$$\mathrm{Ba}(NO_3)_2 + 3H_2 + CO_2 \xrightarrow{\text{regeneration}} \mathrm{Ba}CO_3 + 2\mathrm{N}O + 2H_2O \qquad \text{Reaction 2-13}$$

$$\mathrm{Ba}(NO_3)_2 + \frac{1}{3}C_3H_6 \xrightarrow{\text{regeneration}} \mathrm{Ba}CO_3 + 2\mathrm{N}O + H_2O \qquad \text{Reaction 2-14}$$

$$\mathrm{NO} + CO \xrightarrow{\text{reduction}} \frac{1}{2}N_2 + CO_2 \qquad \text{Reaction 2-15}$$

$$\mathrm{NO} + H_2 \xrightarrow{\text{reduction}} \frac{1}{2}N_2 + H_2O \qquad \text{Reaction 2-16}$$

$$\mathrm{NO} + \frac{1}{9}C_3H_6 \xrightarrow{\text{reduction}} \frac{1}{2}N_2 + \frac{1}{3}H_2O + \frac{1}{3}CO_2 \qquad \text{Reaction 2-17}$$

Generally, the LNT consists of a NO_x storage component (an alkaline or earth–alkaline metal, such as Ba, K, Na), precious metals (Pt, Pd, Rh) and supporting materials (Al_2O_3, CeO_2, TiO_2) [64]. One of the typical formulations of the LNT catalysts is Pt–Ba/Al_2O_3. Similar to the conventional TWC, precious metals play an important role in catalysing surface reactions, including catalysing NO, CO and HCs oxidation under lean conditions and NO_x reduction by reducing agents (such as CO, HC, and H_2) under rich condition. In modern aftertreatment system of a lean burn gasoline engine, the LNT is usually placed in the underfloor position and integrated with a close-coupled (cc) TWC to provide optimal performance in emissions control. Whereas NO_x storage and regeneration under

different lambda conditions is challenging since an advanced and complicated engine control system is required to ensure a fast lean-to-rich periodical switch without causing any torque oscillations. Additionally, it was reported that sulphur poisoning can adversely affect the LNT performance; thus it is necessary to use fuels and lubricants with low-sulphur content [77]. Moreover, additional reductants (i.e., fuel) are required for LNT purging which is associated with fuel penalty.

The LNT performance can be affected by several factors, including the operating temperature, the lean/rich phase duration, and the exhaust gas components (such as H_2, HC, CO and NH_3). Forzatti et al. [78] reported that the NO_x reduction by CO did not commence until 180 ^oC through performing a CO-temperature-programmed surface reaction (TPSR) study over a $Pt/Ba/Al_2O_3$ based LNT catalyst. Li et al. [79] examined the effect of LNT inlet temperature on NO_x adsorption over a $Pt/Ba/Al_2O_3$ based catalyst via an integrated study of engine bench tests and chemical kinetics simulation via CHEMKIN. The results indicated that the inlet temperature of 300 ^oC leads to the best NO_x adsorption performance compared to 200 and 400 ^oC. It is suggested that the adsorption reaction activity is inhibited at a lower temperature and the $Ba(NO_3)_2$ is not stable at a relatively high temperature. DiGiulio et al. [80] evaluated the performance of a commercial LNT ($Pt-Pd-Rh/Ba/CeO_2$) catalyst under different operating conditions via a laboratory bench flow reactor, using synthetic gas to simulate the engine exhaust under different lambda conditions. The results indicated that the optimum operating temperature for the LNT catalyst is 300-450 ^oC, where the measured NO_x conversion can approximately reach

100%. Similar to Abdulhamid's finding [81], DiGiulio et al. observed that CO and C_3H_6 show poor activity in reducing NO_x compared to H_2 at temperatures below 200 ^oC.

The lean/rich cycle timing plays an important role in controlling NO_x removal efficiency. DiGiulio et al. [80] tested the effect of the lean/rich period length on a commercial LNT NO_x removal performance through a different lean/rich cycle protocols study. As mentioned above, DiGiulio suggested that the 300-450 ^oC is the optimum operating temperature for the LNT catalyst when using the typical lean period duration of 60s. When extending the lean period length to 120 s or 180 s, the observed high NO_x conversion temperature window was narrowed to approximately 350-400 ^oC. As for the impact of the rich-phase duration, it was observed that the cycle averaged NO_x removal efficiency was increased from 59% to 87% through increasing the rich-phase duration from the previous 5s to 15s at 250 ^oC; while at 400 ^oC, the opposite effect can be found where the extra 10 s of the rich-phase duration leads to a drop of the NO_x conversion efficiency from 76% to 54%. Therefore, it was suggested that NO_x conversion efficiency can be increased either by extending the rich-cycle length at a lower temperature or reducing the rich-cycle duration at a higher temperature.

The TWC-LNT system has also been experimentally studied. James et al. examined the performance of a TWC-LNT coupled system via real engine bench testing [82]. The integrated system consisted of two c-c TWCs and an underfloor LNT. Although the LNT was implemented downstream of the TWC, there was still a large amount of NO_x exiting the LNT. The NO_x slip is believed to result from the high levels of NO_x emitted during

lean operation and the relatively lower storage capacity of the LNT.

2.4.3 Gasoline particulate filter (GPF)

As aforementioned, the major drawback of GDI engines is its relatively higher PM emissions than that from PFI engines. Due to the increasing popularity of GDI engines over the automobile market, it is necessary to develop advanced gasoline engine combustion and aftertreatment technology for PM control, thereby meeting the stringent PM regulations. Implementing GPF and cGPF (catalysed GPF) has been reported to be an efficient and economy-friendly approach for PM abatement [40, 83, 84]. Similar to the design of DPF, GPF is generally a cylindrical honeycomb ceramic structure consisting of mutli-channels with porous substrates coated on the internal surface. The porous surface with small pores act as filter medium to physically trap PM, and a PM layer is subsequently formed on the GPF wall by the accumulated PM [85]. The collected PM will be burned by either passive or active regeneration approach. Although the design of GPF share similarity with DPF, there are some key differences because of the distinct gasoline exhaust characteristics. For example, gasoline exhaust generally has higher temperature and flow rate than diesel exhaust, which can potentially result in higher pressure drop across a wall-flow GPF; Also, the soot emissions from gasoline engines are much less than that from diesel engines, which was found to be related to the missed PM layer formation on GPF wall and associated lower particle filter efficiency [86]; In addition to the PM filtration, the GPF coated with noble metals can also provide

supplementary purification function to the TWC, and this coated type filter is generally called cGPF. Xia et al. reported the feasibility of employing cGPF on a GDI engine for NO_x control to meet the China 6 emission regulation [87].

2.5 Hydrogen effect on catalysts performance

Apart from the aforementioned approaches to improve the performance of aftertreatment catalytic converters (see section 2.4.1 and 2.4.2), the potential of using hydrogen to enhance the catalyst activity has been researched [6, 7, 10, 88-90]. It was found that the presence of hydrogen has been reported to be beneficial for CO, HC oxidation and NO_2 formation over the platinum (Pt), palladium (Pd) and Pt-Pd based catalysts [4-7, 88, 89] and NO_x reduction over certain types of catalysts (i.e. Pt/Al_2O_3, Ag/Al_2O_3) [8, 9, 70, 91, 92]. Some of the literatures will be briefly reviewed in the following section.

2.5.1 Hydrogen effect on catalytical oxidation of CO, HC, and NO

Muraki et al. (1991) evaluated the effect of hydrogen on the low temperature (< 200 ^oC) oxidation activity of CO over three alumina-supported Pt-, Pd-, and Rh-based catalysts respectively by varying the H_2 level in the feed gas mixture (CO, O_2, H_2 and N_2 as balance gas) [89]. Based on the experimental measurements, empirical power law rate expressions for CO oxidation were obtained for the cases with and without H_2 presence. It was shown that the presence of H_2 accelerates CO oxidation with reduced self-inhibition term of CO

and the H_2 enhancement effect is ranked in an increasing order as Pt>Pd>Rh. They believed that hydrogen was firstly oxidized to water over the catalysts, and the weakening of CO self-poisoning was induced by the water. Botas et al. (2001) suggested similar beneficial effect of water on moderating the CO self-inhibition, thereby releasing more free active sites for other species to be adsorbed and other reactions to commence which accelerated the CO and NO conversion simultaneously [93]. However, the research conducted by Salomons et al. (2006) presented a different argument regarding the underlying cause of the hydrogen effect [7]. They studied the interaction between CO and H_2 oxidation over a Pt-based diesel oxidation catalyst (DOC) using a flow reactor under simulated lean atmosphere. The hydrogen beneficial effect was observed as well, suggesting that hydrogen addition in small concentrations (i.e., 500 ppm) leads to significant reduction (22 ^oC) in CO light-off temperature compared to the condition without the presence of hydrogen . Only a minor marginal reduction (another 3 ^oC) was reached with higher hydrogen concentrations (2000 ppm). However, they reported that CO oxidation occurs first in the mixture of CO, H_2, and O_2 and the occurrence of H_2 oxidation was captured until CO was largely depleted. Consequently, they believed that the underlying cause of the hydrogen promotional effect cannot be attributed to hydrogen oxidation. Katare et al. (2009) studied the influence of hydrogen concentration in diesel exhaust on the DOC performance through flow reactor experiments using synthetic feed gas mixtures to simulate diesel engine exhaust under two extreme conditions: (1) with 257 ppm hydrogen; and (2) 0 ppm hydrogen [6]. They reported that the addition of 257

ppm H_2 into the feed gas is beneficial for CO and HC oxidation and NO_2 formation over a DOC, thereby advancing the DOC light-off by 20 ^oC compared to the condition without hydrogen in the feed gas. They stated that the reduction of the catalyst light-off temperature might result from the exotherm caused by hydrogen oxidation. It was estimated that the 20 ^oC reduction in this DOC light-off is equivalent to a reduction of 70 g/ft^3 in PGM loading with reference to Hepburn's work [94]. In addition to the experimental study, Katare et al. also investigated the hydrogen effect via simulation approach using a DOC model. Corresponding simulation results reported more significant hydrogen effect in improving the CO and HC conversions (up to 32% higher) than the experimental observation. Thereby, the importance of conducting tests using real engine exhaust was highlighted. Herreros et al. (2014) experimentally examined the impact of small amount hydrogen addition on a Pt only and a Pt-Pd based DOC using a single cylinder diesel research engine [10]. Various amounts of hydrogen (500, 1000, 2500, and 8000 ppm) were injected into diesel engine exhaust before entering the catalyst inlet. The hydrogen enhancement effect on improving CO and HC oxidation as well as NO_2 formation were noticed for both catalysts. They suggested that the hydrogen promotional effect results from a combination of different factors: the exothermic effect of hydrogen oxidation; the production of hydrogen containing intermediate species (like OH radical); and the chemical effect that hydrogen increases the oxidation reaction rate and promotes the species accessibility on the catalyst surface sites.

Apart from these experiment-based research studies, relevant modelling studies were

carried out to help elucidate the underlying causes of the hydrogen promotional effect. Bhatia et al. (2009) simulated the CO light-off behaviour with the presence of hydrogen over a Pt-based catalyst using both microkinetic and global mechanisms [95]. For both mechanisms, the hydrogen promoting effect on CO oxidation can be correctly explained by lowering the activation energy of CO desorption when there is hydrogen adsorbed. Salomons et al. [96] also performed a modelling study to examine the hydrogen promotional effect on CO light-off. A kinetic model, in which the activation energy of CO desorption is defined to be a decreasing function of hydrogen absorption, was found to be able to predict the hydrogen effect. Corresponding modelling results are consistent with their experimental findings, suggesting that the presence of hydrogen promotes CO light-off through affecting the CO desorption rate. Hauptmann et al. (2011) simulated the hydrogen promoting effect on CO light-off over a Pt-based catalyst using a microkinetic model, [97] and the model parameters were calibrated and validated based on the experimental data presented in Salomons's works [7, 96]. They stated that the hydrogen enhancement effect is chemically related so that the CO oxidation can be proceeded via an alternative pathway (carboxyl-path), in addition to its direct oxidation. With the addition of hydrogen, hydroxyl (OH radical) is formed and subsequently reacts with adsorbed CO to form carboxyl (COOH radical), thereby forming CO_2. It was also suggested that the carboxyl-path can be proceeded easier at low temperatures compared to the direction of the CO oxidation. Rankovic et al. (2011) [98] performed a detailed kinetic simulation study on the interaction between CO, H_2, with O_2 over a Pt-Al_2O_3 and

a Rh- Al_2O_3 based catalyst. They obtained some similar findings as Hauptmann, that hydrogen accelerates the CO light-off by providing an alternative pathway (CO-s with OH-s) for consuming the adsorbed CO on the catalyst surface site.

Accordingly, the following general explanations were derived to explain the underlying causes of the hydrogen promotional effects: (1) H_2 improves CO and HC light-off through the exotherm from hydrogen oxidation [5, 6]; (2) the H_2 enhancement effect on CO oxidation results from a chemical effect, which is associated with the formation of some intermediate reaction products like OH radical [97, 98]; (3) H_2 promotes the CO desorption from the catalytic surface site, thereby creating more free sites on the catalyst's surface for more oxidisation reactions to take place [95, 99, 100]. The first explanation contradicts the results of the experiments by Salomons et al. [7] as previously discussed. A more recent experimental study conducted by Stewart et al. (2018) reported that there are no thermal effects taking place in the hydrogen promotion phenomenon [101]. The combination of spatially resolved mass spectrometry (MS) and X-ray absorption spectroscopy (XAS) and temporal analysis of products (TAP) analysis suggested that the presence of hydrogen enhances the interaction of O with the Pd surface site, thereby promoting the proceed of CO oxidation. However, Stewart et al. reported that there is no direct evidence for the presence of OH during their laboratory observations. Therefore, the debate is continuing, and no definitive conclusions can be made based on the literature.

2.5.2 Hydrogen effect on NO_x reduction

The impact of hydrogen on catalysed NO_x reduction is also of great interest. Burch and Coleman (1999) studied the effect of reactant concentrations (i.e. NO and H_2) on NO reduction activity over a Pt/Al_2O_3 and a Pt/SiO_2 based catalyst in a lean atmosphere using a microreactor with different feed gas [70]. It was found that higher NO conversion efficiency can be achieved via increasing the H_2 concentration; while increasing the NO concentration was accompanied by the opposite effect for both catalysts. Over the Pt/Al_2O_3 catalyst, the low temperature (135 ^oC) NO conversion was largely improved from around 8% to over 80% by increasing the hydrogen level from 600 to 4700 ppm with the amount of NO contained in the feed gas unchanged. Similarly, NO conversion over the Pt/SiO_2 catalyst at 90 ^oC was enhanced from the previous 4% to over 35% when increasing the hydrogen level from 300 to 900 ppm. Nova et al. (2010) investigated the NO_x reduction by CO, H_2, and CO/H_2O mixture over a $Pt/Ba/Al_2O_3$ LNT catalyst through transient experiments using a flow reactor system and Fourier-transform infrared spectroscopy (FTIR) analysis [92]. Among those examined reductants, H_2 was observed to be the best reductant for NO_x in the temperature range of 200-350 ^oC compared to others with the mixture of CO/H_2O which exhibited better NO_x removal activity than pure CO. The superior NO_x reducing activity of H_2 is consistent with previous findings reported by Theis et al. [102]. It was suggested that hydrogen is likely to be formed via WGS reaction with the presence of water together with CO, yielding better NO_x reduction performance. Regarding the NO_x reduction by H_2, it was proposed that the reduction proceeds via a dual-steps mechanism: (1) NO_x is first reduced to NH_3; (2) the formed NH_3

further reacts with other nitrate species leading selectively to N_2. Apart from those Pt-based catalysts studies, research on the hydrogen promoting effect on NO_x reduction has been also examined for other types of catalysts, such as the Ag/Al_2O_3 based SCR catalyst, which will be discussed later.

2.5.3 Adding hydrogen to engine exhaust to enhance the catalyst activity

Regardless of the actual causes of the hydrogen effect, the addition of hydrogen is demonstrated to be beneficial for promoting catalysts activity. Therefore, the idea of adding hydrogen upstream of a catalyst to promote the catalytical reactions was inspired. Relevant study on the DOC was reported by Herreros et al. as discussed previously [10]. The potential influence of hydrogen addition on HC-SCR catalysts has also been researched [91, 103]. Sitshebo et al. (2009) studied the impact of hydrogen addition on NO_x removal performance over a Ag/Al_2O_3 based HC-SCR catalyst [91]. The laboratory investigation was conducted on a modified single-cylinder DI diesel engine with different quantities of hydrogen (from 700 to 5000 ppm) being injected upstream of the passive mode SCR. They reported that the addition of H_2 was able to strongly improve the NO_x conversion over the SCR at lower temperatures (< 250 ^oC, can be also referred to as lower loads condition) to different degrees. The effectivity of the hydrogen promoting effect on HC-NO_x reduction was closely dependent on several factors: such as the exhaust gas temperature (engine load) and space velocity (engine speed); the amount of hydrogen addition; and the HC: NO_x ratio. Besides that, they also examined the potential influence

of injecting the on-board generated reforming gas to engine exhaust on the NO_x reduction activity of the HC-SCR catalyst. The on-board fuel reforming was achieved by integrating a mini-scale partial and exhaust gas fuel reformer with the engine test bench. The corresponding results suggested that the fuel reformer was able to produce sufficient hydrogen for improving the catalytical NO_x conversion with approximately 60% of NO_x reduction efficiency being achieved (the baseline case without hydrogen or fuel reformate addition is below 10%). This study highlighted the feasibility of using an on-board fuel reformer to produce hydrogen to be used for improving the low-temperature activity of catalytical converters.

Regarding the investigation on the gasoline engine aftertreatment system, Heimrich et al. [88] and Viktor et al. [90] performed an experimental study on a gasoline engine equipped with TWCs. Heimrich et al. (2000) investigated the on-board hydrogen production using a water electrolyser on a gasoline-fuelled light-duty vehicle and the potential effect of injecting hydrogen and air upstream of a Pt-based TWC [88]. Extra air is injected to provide oxygen for hydrogen oxidisation. The experimental results indicated that the upstream hydrogen addition helped the catalyst to achieve rapid heating due to a large heat release from the catalytic combustion of the hydrogen, thus significantly reducing the HC and CO emissions during the cold start of the gasoline engine. Viktor et al. (2019) examined the impact of a small amount of hydrogen addition (500, 1500, and 2500 ppm) upstream of a Pt/Pd/Rh-based commercial TWC on its light-off activity [90]. Relevant catalyst light-off tests were performed on a four-cylinder DI-SI research engine under

stoichiometric operating condition. The corresponding results suggested that low-level hydrogen injection advanced the CO, THC, and NO_x light-off to different degrees, enhancing the TWC low-temperature performance. Although the hydrogen beneficial effect on gasoline aftertreatment catalysts has been previously reported by Heimrich et al. [88] and Viktor et al. [90], the associated experimental studies were performed under stoichiometric engine operation. While the hydrogen effect for lean-burn gasoline engine exhaust system has been little researched, according to the author's knowledge.

2.5.4 Using hydrogen-enriched reformate for LNT regeneration

As previously discussed, NO_x removal over an LNT catalyst is achieved by NO_x storage in a lean exhaust, and then NO_x release and subsequent NO_x reduction by different reductants in a rich atmosphere. A rich environment, which contains a considerable number of reductants, is required to initiate the NO_x release and reduction. The alternating lean/rich exhaust environment can be achieved by varying the engine lambda operation. However, periodically switching the engine operation from lean to rich can result in instability of engine combustion, reduced driving performance of the vehicle and worse fuel economy. Consequently, equipping the engine with an on-board fuel reformer to ensure the regeneration of the LNT is of great interest. Kong et al. (2004) experimentally assessed the potential of using an on-board generated hydrogen-rich reformate gas for LNT regeneration through the integrated system of a plasma fuel reformer and a diesel engine test bench [104]. The results showed that the hydrogen-rich reformate was able to

regenerate the LNT under a wide range of operation modes. Comparing the average NO_x conversion and fuel consumption obtained using hydrogen-rich reformate to the condition of using upstream diesel fuel injection for LNT regeneration, it was found that using hydrogen-rich reformate is more advantageous in terms of higher NO_x conversion and less fuel penalty. Park et al. (2010) also explored the feasibility of using a plasma reformer (with diesel fuel pulse injection) to supply H_2-enriched gas as NO_x reductants to the inlet of a Pt-based LNT catalyst, which was implemented in the aftertreatment system of a diesel research engine [105]. Alternation between a lean and rich exhaust environment was achieved using a dual-pass system mounted with two butterfly valves to control the supply of the reforming gas or actual exhaust gas to the LNT. It was found that the overall NO_x conversion efficiency was affected by several factors, including the amount of reductant supplied, the exhaust gas temperature, and the O_2/C ratio (the ratio of reforming oxidant to the reformed diesel fuel). Ngan et al. (2011) proposed an advanced aftertreatment system for diesel engines, which consists of a fuel reformer, an LNT, a DPF and an urea-SCR catalyst (see Figure 2-8) [106]. A fuel doser and vaporiser were employed to supply diesel fuel to the downstream reformer for on-board generation of hydrogen-rich reforming gas, which was subsequently passed downstream for LNT regeneration. It should be noted that NH_3 is generally formed as by-product by selective NOx reduction over the LNT catalyst, and those undesirable NH_3 slips was beneficial for the downstream SCR. The ammonia is stored and used for the second phase NO_x removal over the SCR catalyst; thereby eliminating the need for an extra urea storage tank. The

system's performance was examined under various engine operating modes, such as the nonroad transient cycle (NRTC). The corresponding results showed that an overall 89% NO_x conversion was achieved for the NRTC test with very low fuel penalty.

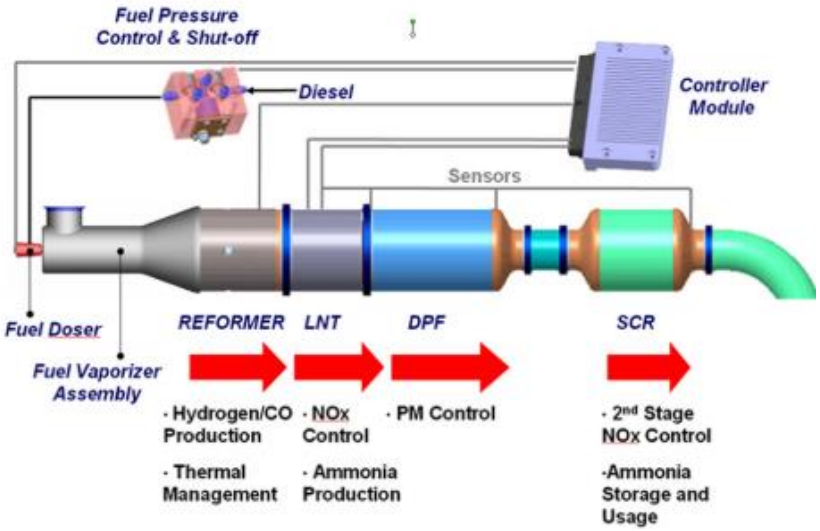

Figure 2-8. An advanced aftertreatment system layout (Adapted from Ngan et al., 2011) [106]

2.6 Hydrogen production

With the rapidly growing demand for fossil fuels worldwide and the resulting environmental problems (global warming and poor air quality) becoming increasingly serious, the development of a clean and sustainable energy system has been extensively researched. Among the applications of all those renewable energy sources, utilisation of hydrogen as an energy carrier is believed to be the cleanest way, providing a promising solution to reduce the dependency on traditional non-renewable resources and the corresponding environmental problems [107]. Generally, hydrogen can be employed in

different applications, including using hydrogen as the energy source for fuel cell applications [108-110], and adding hydrogen to enhance the combustion performance and efficiency of IC engines [111-113]. It was reported that a small fraction of hydrogen addition to gasoline engines can improve the gasoline engine performance in terms of improving the combustion stability, improving the thermal efficiency, and reducing the regulated pollutants (CO, THC, NO_x, PM) emissions. These advantages can be attributed to the characteristics of hydrogen combustion compared to gasoline, including the higher laminar flame speed, wider flammability limit, and smaller quenching distance [114]. Although the utilisation of hydrogen brings benefits, there are still some challenges involved in the hydrogen storage and transportation.

Generally, hydrogen can be stored via physical and materials-based storage methods. The physical storage approach includes the utilization of traditional storage techniques, like a compressed hydrogen gas cylinder, and liquified hydrogen. As for the materials-based storage, it involves the process of hydrogen being absorbed and desorbed from storage materials (generally metal hydrides, e.g., $LaNi_5$ or $NaAlH_4$) [115]. When selecting an appropriate method for hydrogen storage and transportation, it is necessary to consider the gravimetric capacity, volumetric capacity, efficiency and expense [116]. However, it can be seen that there are some inherent disadvantages associated with those approaches. For example, carrying hydrogen on board via pressurised vessels results in a large space penalty due to the relative low density of hydrogen gas, which is not a suitable solution for long-distance driving of automobiles. Using the liquid hydrogen tank is associated

with reduced energy efficiency caused by hydrogen liquefaction, and the inevitable hydrogen loss during the extended parking period [116]. Although hydrogen storage via metal hydrides has better gravimetric and volumetric capacity than the former two approaches, the decreasing hydrides life cycle as refuelling continues is a problem.

Hydrogen is largely available on the planet in the form of compounds (such as water and hydrocarbons). Generally, hydrogen can be produced from the electrolysis of water [117, 118], and the reforming of hydrocarbon fuels [119, 120]. Apart from the aforementioned traditional approaches of hydrogen storage, on-board hydrogen production can be achieved via exhaust gas fuel reforming technology. It utilises the engine exhaust heat, H_2O, CO_2, and additional injected fresh fuel (e.g., gasoline, ethanol) to produce hydrogen rich gaseous reformate. The following reactions are mainly involved in the exhaust gas fuel reforming process, including the steam reforming, dry reforming, partial oxidation reforming and water gas shift reaction (WGS). Generally, reformate consists of hydrogen, nitrogen, methane (CH_4), steam, carbon dioxide and various other hydrocarbons. It has been extensively studied and thus reported to be feasible to generate hydrogen on-board under GDI engine operating conditions [41, 55, 121-123]. Therefore, incorporating an exhaust gas fuel reformer upstream of the catalytic converter offers a viable solution for generating hydrogen to be used as a chemical promoter to improve the catalyst performance. It should be mentioned that the oxygen concentration contained in gasoline exhaust gas under lean-burn conditions is relatively high, which is similar to that for diesel reforming. Therefore, the studies related to diesel exhaust gas reforming might be

applicable to gasoline exhaust gas reforming under engine lean operations [124-126].

2.7 Catalytic converter modelling

2.7.1 General catalytic converter models

Computational modelling is generally regarded as a complementary tool to experimental studies since it can do parameter optimisation with lower time consumption and financial cost and can also obtain information which cannot be directly derived from traditional laboratory testing. In addition, simulation can provide insight into the fundamentals of physical and chemical processes taking place over the catalytic converter, offering a better understanding of the catalytic converter operation. With the rapid development of computer technology nowadays, the performance of computational models has been greatly improved, with the computational cost being reduced in the meanwhile. Therefore, catalytic converter modelling (validated with experimental results) is becoming an indispensable part of the design of reliable and advanced aftertreatment system.

The generally used catalytic converter models can be classified into , 1. single channel model, and 2. entire catalytic converter model. In the single channel model, as stated by the name, a single channel of the catalytic monolith is selected to represent the whole simulation domain. For this type of model, it is assumed that all channels give the same performance and the inter-channel interactions are neglectable. Also, the fluid flow in the

converter is assumed to be uniformly distributed. However, those assumptions are usually not valid during real catalytic converter operation. Similarly, a representative number of channels can be selected as the whole solution domain as well. In the work of Braun et al. (2002), the simulation of reactive flows in a representative number of monolith channels was performed through a 2D model [127]. As for the entire catalytic converter model, the real physical space of the entire catalytic converter is simulated, including thousands of monolith channels. Simulating this type of multichannel structure is highly time and computational consuming. Thus, a volume averaging process, which considers the solution domain as a continuous porous medium, is introduced. Although, the volume averaging process method presents some problems as well, for example, some micro-level details will be missed using this method.

Catalytic models are also classified as one-dimensional up to three-dimensional models. Among all those models, the one-dimensional (axial direction) catalytic converter model is the simplest. Several assumptions were made to simplify the model, for example, the radial gradients in the monolith channel are assumed to be ignored. Mukadi and Hayes (2002) reported that the 1D model is sufficient to capture the thermodynamic and fluid dynamic through comparing the simulation results obtained from both 1D and 2D models [128]. Chen et al. (1988) suggested that the flow mal-distribution can greatly affect the thermal gradients in the monolith and has a minor influence on the overall conversion performance. Generally, the 1D model is simple but can provide enough information regarding the transient phenomenon occurring over the catalyst surface with relatively

lower computational expense. Therefore, the 1D model is preferable for performing parameter studies and fast design evaluations.

In the late-1980s and 1990's, some researchers began developing more complex catalytic converter models to include the effect of the non-uniformity of flow distribution on the catalyst light-off. Among those, Zygourakis et al. (1989) studied the impact of flow maldistribution on CO light-off using a 2D reactor model [129]. The corresponding simulation results revealed that the flow maldistribution can substantially degrade the catalyst light-off activity, which is totally in contrast to the aforementioned Chen's opinion. Also, they suggested that the radial flow nonuniformity must be included in comprehensive catalytic converter models to ensure the models' reliability. As for the three-dimensional model, it became more and more popular the appearance of both the commercial and open-sources computational fluid dynamics (CFD) codes, such as ANSYS Fluent, COMSOL, AVL Fire, and OpenFOAM. Extensive studies were carried out using the 3D catalytic converter model to study the light-off activity of a three-way catalyst [130-133].

2.7.2 Modelling catalytic surface reactions

Simulation of realistic reaction kinetics is also a big challenge when modelling a catalytic converter. The chemical reactions over the monolith surface are sophisticated. In recent years, intensive studies have been carried out to develop comprehensive and reliable chemical kinetic models to describe the surface reactions occurring over the catalyst. Over

the catalyst surface, the chemical reactions can be significantly accelerated by either homogeneous or heterogeneous catalysis [134]. Two frequently used reaction mechanisms are used to describe the heterogeneous catalysis, which are the Langmuir-Hinshelwood (LH) and the Eley-Rideal (ER) mechanisms [135]. Basic steps involved in those two mechanisms are schematically illustrated in Figure 2-9. It can be seen that the LH mechanism proceeds via three steps including: (1) the two reacting species (A and B) are firstly chemisorbed on the catalyst surface site; (2) subsequently, the surface reaction between A(s) and B(s) takes place to form AB(s), where s means adsorbed; (3) AB(s) desorbed from the surface site and the final product C are generated. As for the ER mechanism, it is a totally different situation that one specie (B in gas phase) directly reacts with another chemisorbed specie A(s) to form the final product C.

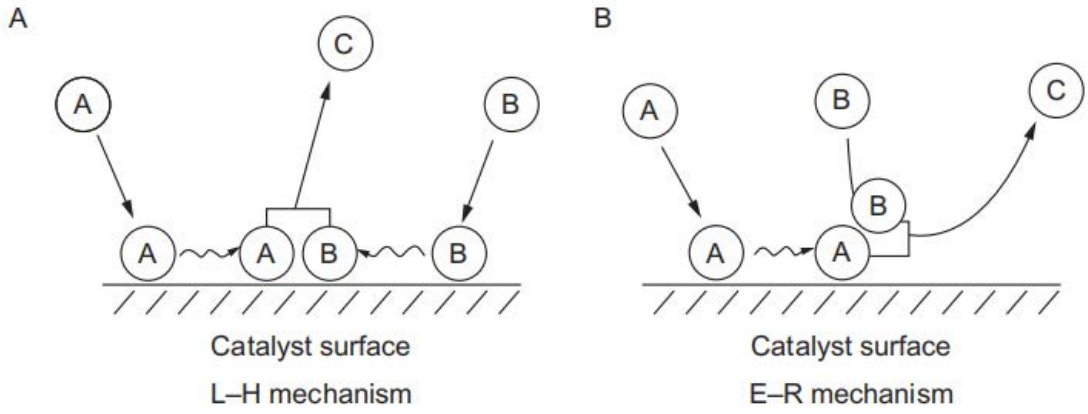

Figure 2-9. Schematic illustration of (a) LH and (b) ER mechanisms (Adapted from Misono, 2013) [136]

It has been reported that the majority of catalytical surface reactions proceed via the LH approach with fewer reactions proceeding via the ER approach [137-139]. Baxter and Hu (2002) [140] explained this phenomenon through study of the catalytic CO oxidation on

Pt (111) surface. The corresponding results suggested that the ER reaction path involves a specific channel where factors such as the titling of reactant atom (CO) and the activation of absorbed oxygen atom can greatly affect the reaction energy barrier and make it hard for the ER reaction mechanism to proceed. Accordingly, the LH approach is much more probable for the surface reaction to proceed. In the past decades, the LH approach was widely adopted in catalytic converter modelling, and the reaction rates were estimated well with modified activation energy and kinetic constants [141-144].

2.8 Summary

The present PhD research work is mainly focused on hydrogen effect on lean-burn gasoline engine aftertreatment systems, including a TWC and LNT catalyst. Therefore, several publications regarding the hydrogen influence on catalyst oxidizing and reducing activity were reviewed and discussed in this chapter. The hydrogen production technologies were also introduced, including both conventional compressed gas cylinder and on-board hydrogen production via fuel reforming. Based on existing literature, it is believed that the presence of hydrogen in the feed gas is beneficial for enhancing CO and HC conversion over the Pt, Pd, and Pt-Pd based catalysts and NO_x reduction over certain types of catalysts. However, it should be mentioned that the majority of aforementioned publication works are based on flow reactor experimental results using simulated gas rather than actual engine testing bench. Also, the hydrogen influence has been examined

over several DOCs. Thus, there is a lack of research about the hydrogen effect on TWCs and LNTs when employed in gasoline engine aftertreatment system. In present thesis, the impact of upstream hydrogen addition on TWC light-off and LNT performance were experimental evaluated using an actual GDI engine test bench.

Regarding the underlying causes of the hydrogen effect, there are three common explanations, including: (1) Oxidation of the extra added hydrogen results in a local temperature increment over the catalyst; (2) The presence of hydrogen is associated with the formation of hydrogen-containing intermediate species (like OH), which provides supplementary reaction pathways; (3) Hydrogen can moderate the CO's strong self-inhibition effect, thereby releasing more free active sites for other reactions to proceed. However, there is no definitive answer, and the debate is still continuing. In present work, simulation works were carried out to provide auxiliary information for exploring the underlying causes of the hydrogen effect on catalyst activity.

Since the majority of experimental works in present thesis were conducted via a GDI engine, the GDI engine combustion and emissions formation fundamentals were briefly introduced. Besides that, special attention was given to lean-NO_x abatement devices (LNT catalyst). Unlike the conventional TWC, NO_x is reduced over the LNT catalyst via NO_x storage under lean exhaust environment, and subsequent regeneration and reduction under rich exhaust environment. Effective regeneration and reduction can be controlled by many factors. Although there are several publications discussing about the NO_x storage and regeneration chemistry over LNT, those studies were mainly focused on diesel engine.

There is a lack of study for gasoline exhaust which generally has higher temperature than diesel. Moreover, the majority of research works were carried out using flow reactors and simulated exhaust gas to represent steady-state engine operations. In present thesis, the performance of TWC-LNT catalysts for a lean-burn gasoline engine under various conditions were examined, including complex engine operating conditions like cold start. Generally, the required rich exhaust environment for LNT regeneration is achieved by periodical in-cylinder fuel injection, namely engine rich operation. In present work, the feasibility of using periodical reductant (hydrogen) injection directly to the LNT inlet for purging the LNT catalyst was investigated.

Overall, although the reviewed literature has covered a range of works regarding the hydrogen effect on the catalyst activity, there are still certain unaddressed issues. In present work, the scientific gaps have been filled by experimental and modelling studies. It is believed that this could help with the design of more advanced aftertreatment system.

CHAPTER 3 METHODOLOGY

3.1 Introduction

In this chapter, the experimental approach and simulation methods used in the present study will be explained. Regarding the experimental section, the experimental set-up, details of the engine instrumentation, related measuring facilities, and data acquisition and post-processing system will be described. The engines were provided by Ford and the engine test cell developed by previous PhD students during their research studies at the University of Birmingham. For the modelling section, the governing equations solved in the CFD model will be first introduced, followed by the chemical kinetic mechanisms considered in the present study. Afterwards, the optimisation approach used to calibrate the surface reaction parameters based on corresponding experimental data, like activation energy, kinetic constants, and inhibition factors, will be explained.

3.2 Experimental set-up

The basic experimental set-up utilised in the present study is described, including the engine instrumentation set-up, the furnace, catalysts, relevant temperature recording facilities, and emissions measuring devices. The engine instrumentation set-up consists of a gasoline research engine, a dynamometer, engine control, data acquisition and

recording system. The experimental studies for the present research were performed on two gasoline engines. The research works of Chapter 4 were focused on a commercial TWC, so relevant experiments were performed using a four-cylinder, air-guided GDI engine. However, the study of Chapter 5 and 6 involved experimental investigation on the LNT catalysts, which required engine periodical lean/rich operation. Thus, a modern DI/PFI 3-cylinder gasoline engine was employed to enable leaner operation (i.e., $\lambda = 1.15$) for the LNT studies. Moreover, the utilisation of a more advanced gasoline research engine examined the potential of applying the hydrogen benefits to modern vehicles. During the author's PhD research, a hydrogen injection system was designed and built to allow precious and flexible hydrogen injection via either continuous or periodical mode. Also, the exhaust flow rate measuring system and the heating system for catalyst light-off study was updated.

3.2.1 Engine instrumentation

(1) The four-cylinder GDI engine

The 2L, four-stroke, four-cylinder turbocharged DISI gasoline research engine was provided by Ford as shown in Figure 3-1, and the details of the engine specification are listed in Table 3-1. The engine utilises an air-guided DI combustion system, which consists of a flat top piston and side-mounted, solenoid-actuated, and multi-hole fuel injector, as well as a centrally located spark plug. The engine has compact dual overhead camshafts (DOHC) with a dual, continuously variable, electro-hydraulic phasing function.

Another key component of the engine fuel system is a high-pressure pump (12V electric fuel pump), which is directly driven by one of the camshafts to feed the pressurised fuel to the fuel rail. Based on different engine operating conditions, the engine control unit (ECU) can control a solenoid valve that is integrated with the fuel pump assembly, thereby varying the fuel rail pressure. The coolant and oil temperatures will be elevated and then maintained at a fixed value during the experiment, as shown in Table 3-1. The air-stream temperature also needs to be maintained at a constant level to ensure less test-to-test variability.

Table 3-1- The four-cylinder GDI engine specifications

Engine specification	Value
Type	Four strokes
No. of cylinders	4
Swept volume (cc)	1999
Compression ratio	10:1
Bore x stroke (mm)	87.5 x 83.1
Turbocharger	Borg Warner k03
Injectors	Multi-holes, side-mounted, solenoid-actuated
Fuel system	High pressure fuel pump (up to 120 bar), camshaft driven, solenoid-actuated pressure control
Rated power (kW)	149@6000rpm
Rated torque (Nm)	300@1750-4500rpm
Coolant temperature (°C)	95 ± 0.5
Oil temperature (°C)	101 ± 2

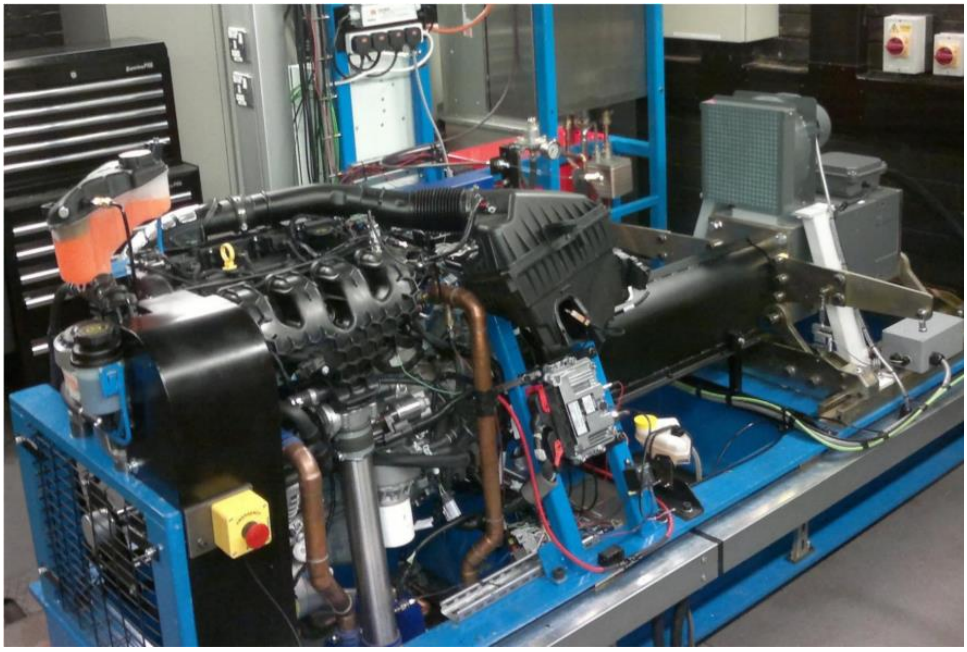

Figure 3-1. The four-cylinder GDI engine testing bench

(2) The three-cylinder DI/PFI gasoline engine

The 1.5 L, four-stroke, three-cylinder research gasoline engine was also supplied by Ford as shown in Figure 3-2. The engine has a dual injection mode: DI and PFI; and the DI mode was mainly used in the present study. The basic engine specifications are summarized in Table 3-2.

Table 3-2- The three-cylinder DI/PFI gasoline engine specifications

Engine specification	Value
Type	Four strokes
No. of cylinders	3
Swept volume (cc)	1497
Compression ratio	11:1
Injection system	DI and PFI
Rated power (kW)	134@6000rpm
Rated torque (Nm)	240@1600-4500rpm

Coolant temperature (°C)	90 ± 3
Oil temperature (°C)	93 ± 1

Figure 3-2. The three-cylinder DI/PFI gasoline engine testing bench

(3) Engine Dynamometer

Both engines use the same dyno. Either engine is connected to a 75-kW alternating current (AC) dynamometer and inverter drive, which can maintain the engine speed or load at a fixed value under motoring and firing conditions. During engine start-up, the dynamometer acts as a starting motor; when the engine is fired, the dynamometer is used as a generator for absorbing and regenerating power from the engine. A torque meter integrated into the dynamometer ensures its capability of delivering an accurate torque reading instantaneously.

(4) Fuel delivery system and flow rate measurement

For both engine set-up, fuel is delivered from the fuel tank which is pressurized by a low-pressure pump to the fuel pipeline. The fuel, which is gasoline in present study, subsequently pass the filter and being fed to the engine common rail via a high-pressure (HP) fuel pump at 150 bar. The mass flow rate of fuel supplied to the engine is measured by a Rheonik Coriolis fuel flow meter (RHM015) with a measuring range of 0.004 to 0.6 kg/min and an accuracy of $\pm 0.1\%$. The air flow rate to the engine is not directly measured but can be conveniently estimated using the fuel flow rate and the actual A/F ratio. Based on the stoichiometric A/F ratio and the $\boldsymbol{\lambda}$ value measured by a lambda sensor mounted after the turbocharger, the actual A/F ratio can be easily obtained. The exhaust gas flow rate (mass) can be calculated as the sum of the fuel flow rate (mass) and the air flow rate (mass), which could be subsequently converted into a volumetric base for exhaust analysis.

(5) In-cylinder pressure measurement

For the four-cylinder GDI engine, the in-cylinder pressure is measured by an AVL piezo-electric pressure transducer (model GM12D) with 0 to 200 bar measuring range (accuracy ±0.3%) and a resolution of 0.5 crank angle degree (CAD). The pressure transducer is directly mounted in the 4^{th} cylinder head and used in conjunction with relevant charge amplifier. As the in-cylinder pressure changes, the electrical charges proportional to the pressure are firstly deducted by the pressure transducer, and then amplified by the charge

amplifier; eventually the signals will be passed to the National Instruments data acquisition system. It should be mentioned that the pressure recorded by the AVL pressure sensor is not an absolute reading but a relative value in reference to the intake manifold pressure. It is assumed that the in-cylinder pressure equals to the intake manifold pressure at the bottom dead centre (BDC) of the intake stroke [145, 146]. Therefore, the intake manifold pressure recorded by another absolute pressure sensor is used as the reference point for the in-cylinder pressure measurement. The corresponding crankshaft position is recorded by a Baumer 720 pulse per revolution magnetic rotary encoder. The in-cylinder pressure trace is obtained with the combination of the crank shaft position and pressure sensor data.

As for the three-cylinder engine, the in-cylinder pressure transducer is a Kistler PiezoStar® water-cooled pressure sensor (Type 6045B-3-2), which is mounted in the head of the 1st cylinder. As for the shaft encoder, an AVL Rotary Encoder 366C was applied. The pressure sensor and shaft encoder follow the same working principle to obtain a real-time in-cylinder pressure measurement as previously mentioned.

(6) Engine control and data-acquisition system

An engine control and data-logging system was developed via an in-house programmed LabVIEW application with the utilisation of two National Instruments cards (model PCI-6251) for the four-cylinder GDI engine. The data-logging system was developed by previous research students at the University of Birmingham to ensure real-time

parameters adjustment and visualisation through the LabVIEW panel for our research engine under engine running conditions. As shown in Figure 3-3, the program will be triggered by the camshaft encoder and uses the camflag signals as inputs, thereby delivering corresponding output information, including the signals of injection, ignition and variable valve timing (VVT) control. The controllable engine parameters include the ignition angle and timing, the start of injection, the injector pulse width, the timing and angle of both intake valve open (IVO) and exhaust valve close (EVC). Whilst the engine is running, the real-time calculation and display of the engine running parameters can be also achieved through the LabVIEW program; those such as the indicated mean effective pressure (IMEP), the percentage coefficient of variation (% COV) of the IMEP, the peak pressure and its corresponding crank angle degree (CAD). Regarding the three-cylinder gasoline engine, AVL IndiCom rather than LabVIEW is used to monitor those engine operation parameters. Engine control and data-logging follows the same manner as the four-cylinder GDI engine.

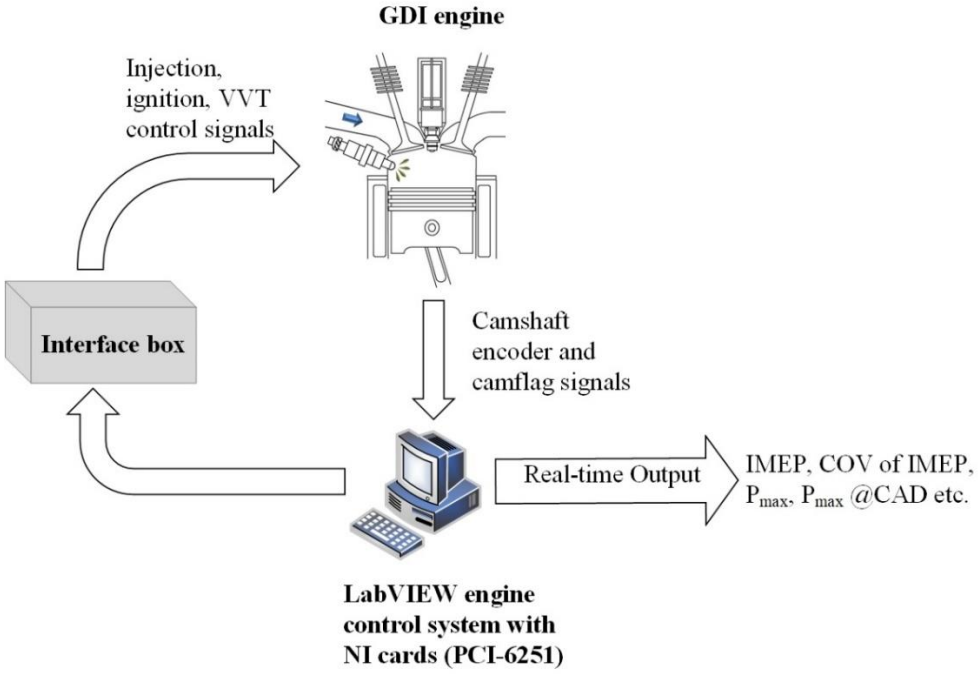

Figure 3-3. The LabVIEW engine control system

The data acquisition via NI cards enables the feasibility of both low frequency and high frequency data sampling. Engine combustion related data, such as the in-cylinder pressure, is acquired using a high-speed data acquisition (HSDAQ) programme via the LabVIEW system. For the data with a lower variation, they were recorded at a lower sampling speed, such as the exhaust emission data, the lambda, and throttle position. As for the data acquisition (DAQ) of other critical engine operation parameters, like engine speed and load, critical fluid temperatures and a variety of analogue and thermocouple inputs, this is accomplished via the CADET dynamometer control system.

An in-house written MATLAB script is used to analyse the data obtained from both the low and high speed DAQ system in the present study. Data from different channels will be firstly imported and time-aligned by the custom script. Afterwards, a related calculation will be performed to generate a summary file, which includes critical

information about the test conditions, data measurement, and parameter calculation.

3.2.2 Related experimental equipment

Relevant experimental instruments employed in the present study are briefly introduced as below, including the exhaust gas composition analysers, temperature measuring devices, and the hydrogen injection system. More details of the technical and control specifications can be found in Appendix B.

(1) Exhaust gas composition analysis

An MKS MultiGas^{TM} 2030 Fourier transform infrared (FTIR) spectroscopy-based gas analyser is employed to provide continuous and simultaneous measurement of engine exhaust gaseous species, including NO_x (NO and NO_2), CO, CO_2, H_2O, NH_3, N_2O, and various HC species, such as methane (CH_4), ethylene (C_2H_4), ethane (C_2H_6), propylene (C_3H_6), propane (C_3H_8). The measurement accuracy for different gaseous compositions is presented in Appendix Table B-2.The FTIR gas analyser is capable of detecting multiple gas samples in real time from 10 ppb to 100%. It analyses the concentrations of gas compositions based on the principle that different gas molecules will generate their own characteristic infra-red (IR) spectrum by absorbing the IR radiation at its characteristic frequency. Thereby, it is easy to identify different gas molecules utilising a reference spectrum. In the present study, a collection of spectra, which is specifically formulated for gasoline combustion products, is provided by the instrument manufacturer

and used as reference spectrum. As for the concentration of each gaseous species, it can be determined from the IR spectrum according to Beer's law, where the absorption strength (peak height in the plot) is considered to be proportional to the concentration. Prior to entering the analyser, the exhaust gas sample is firstly directed to a filter in the FTIR through a heated line, to prevent potential damage to the optical lenses of the equipment caused by PM. After that, the sample gas is pumped to the analyser through another heated line to avoid condensation of water and HCs. The heated lines are manually set as 191 ^{o}C. The FTIR analyser is calibrated by the manufacturer using calibration gases with known concentrations. On each testing day, prior to the experiments, pure nitrogen gas was used for purging, cleaning, and zeroing.

The hydrogen level contained in the exhaust is measured by a hydrogen and helium mass spectrometer (HSense) manufactured by V&F. The HSense analyser provides dynamic online measurement of H_2 volumetric concentration ranging from 0 to 50,000 ppm (accuracy $\pm 2\%$) according to the electron impact ionization mass spectrometer (EIMS) principle. An electron ion source is used to energise different gas ions in the exhaust sample and afterwards the excited ions will be focused and separated in a magnetic field; thus the hydrogen ions can be easily detected based on the location. Water or HCs condensation and particulates are eliminated by an internal fine filter ($< 2\ \mu m$) from the exhaust gas to prevent any potential contamination to the measurement unit. This device is calibrated every time prior to any measurement using pure hydrogen gas (certified 5%) with a tolerance of $\pm 2\%$.

As for the oxygen concentration in engine exhaust, a Testo flue gas analyser (model 340), which is equipped with an oxygen sensor, is utilised to provide a fast and reliable oxygen concentration measurement. It offers a wide measuring range from 0 to 25 vol.% with ±0.2 vol.% accuracy and 0.01 vol.% of resolution.

(2) Laboratory furnace

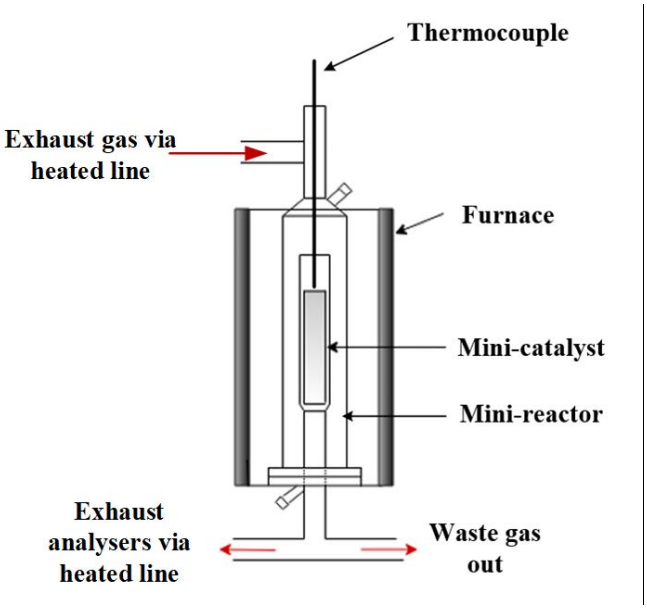

Figure 3-4. Schematic of the mini-reactor and furnace set-up

A tubular furnace (Carbolite Gero GVA 12/600) is used to heat up the catalyst in a specified temperature ramp to perform light-off test or to control the operating temperature at a fixed value for steady-state tests. Mini-scale monolith catalyst is loaded into a mini-reactor and placed in the furnace to control its operating temperature, as illustrated in Figure 3-4. The furnace is capable of rapid heating and the maximum working temperature can reach 1200 ºC, which covers all temperature ranges needed for present study. A pump is used to direct the sampling exhaust to pass through the furnace.

At the furnace outlet, a Platon flow meter is used to measure the mass flow rate of exhaust gas passing through the catalyst. A laboratory oven manufactured by Carbolite Gero is used for hydrothermally catalyst aging, prior to the experiment.

(3) Temperature measurement

Temperature measurements at various sampling points, such as the oil and coolant temperature, intake, and exhaust manifold temperatures, are accomplished by using K-type stainless steel thermocouples (steel sheath, 3 mm x 0.15 m) and a Pico TC-08 thermocouple data logger. Afterwards, the thermocouples outputs will be transmitted to the data acquisition system and will be used in further data analysis. As for the temperature measurement along the exhaust system, another K-type thermocouple was used to collect temperature data for both the exhaust gas and the catalysts brick upstream and downstream of the catalysts (see Figure 3-5). The thermocouples are placed inside the converter through the sampling ports and positioned perpendicular to the monolith channel with a penetration of approximately 50% of the catalyst diameter. It should be mentioned that for the brick temperature measurement the thermocouple closely attaches to the brick surface. While another thermocouple for gas temperature measurement is positioned in the radical direction of the converter and about 10 mm away from the catalyst brick.

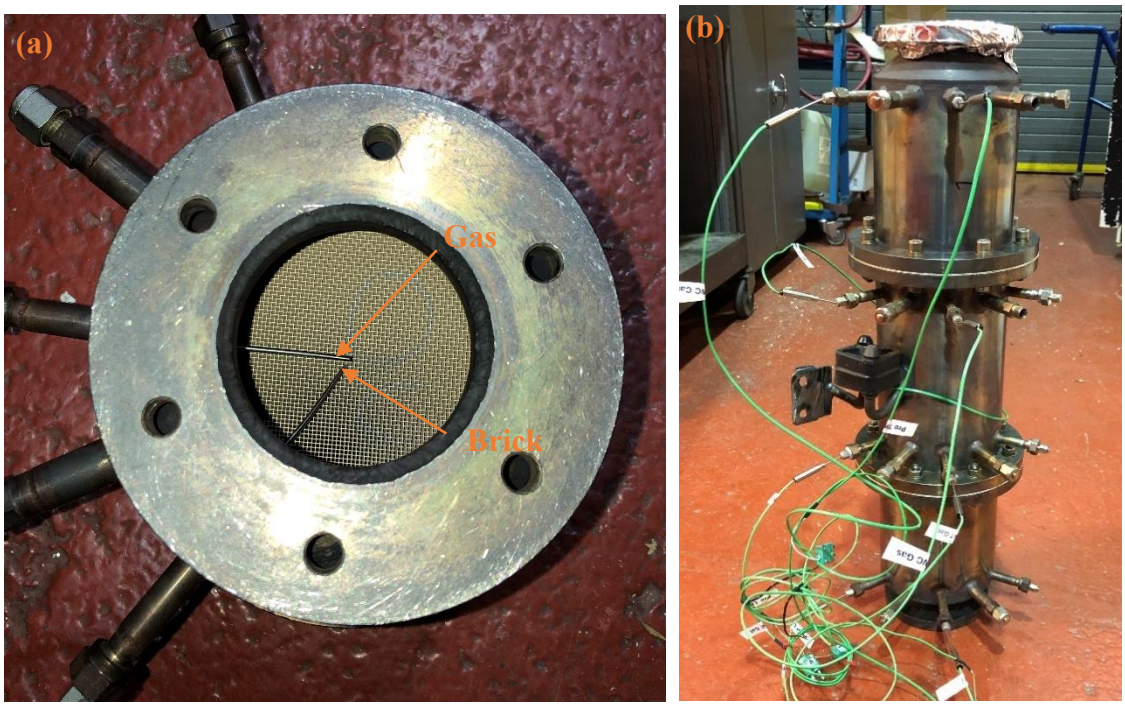

Figure 3-5. (a) Thermocouple location for gas and brick temperature measurement (b) Thermocouple layout of the aftertreatment system

(4) Hydrogen injection system

For the hydrogen addition upstream catalysts, an injection system was designed and implemented, which is shown in Figure 3-6. Pure H_2 from a compressed gas cylinder (pressurised at 4 bar) is injected at required locations (upstream of the catalysts) along the exhaust system. A Bronkhorst digital mass flow controller (model EL-FLOW *Select* F201-AV; accuracy ±0.5% for RD and ±0.1% for FS) is used to measure and control the H_2 injection flow rate, yielding the required amount of hydrogen injection. The injection duration and frequency can be achieved via user-configured scripts to ensure cycling injection. A one-way flow system with check valve (Swagelok®) is designed and adopted for the H_2 injection to prevent reverse flow from the exhaust pipeline to the H_2 injection

system. Since hydrogen is extremely flammable, a flashback arrestor (GCE SAEF-GUARD-3) is installed in the pipeline for safety reason to prevent any potential fire. The flashback arrestor contains a stainless-steel element with a large surface area which is able to quickly lower the temperature and extinguish the flame. Also, there is a temperature actuated cut-off valve contained in the flashback arrestor to shut down the pipeline before the internal temperature reaches a dangerous level.

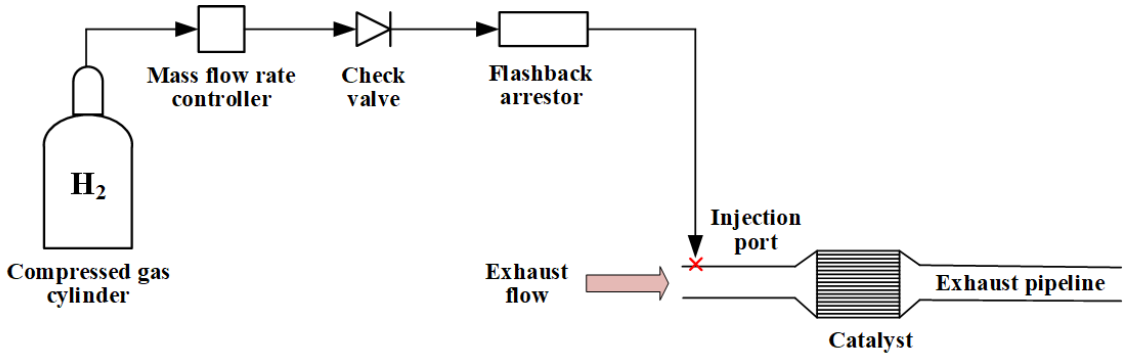

Figure 3-6. Schematic of the hydrogen injection set-up

3.2.3 Catalysts

All the catalysts tested in the present study are ceramic monolith catalysts provided by Johnson Matthey Plc, including a mini-TWC (studied in Chapter 4), a full-size TWC and LNT as well as a mini-LNT catalyst. The later three catalysts were involved in the study in Chapter 5 and 6. Basic dimensions of those catalysts are given by Table 3-3. It should be mentioned that the mini-TWC is originally provided by Johnson Matthey Plc; while the mini-LNT was manually cut from a fresh full-size LNT brick (see Figure 3-8).

Table 3-3- Specifications of tested catalysts

Catalyst	Diameter (mm)	Length (mm)	Volume (litre)	CPSI (1/inch^{-2})
Mini-TWC	25.4	110	0.0557	400
Full-TWC	118.5	110	1.2132	400
Full-LNT	118	101.6	1.1111	400
Mini-LNT	25.4	101.6	0.0515	400

Before assembling the catalysts into the exhaust canning, the monolith catalysts were wrapped with a special wrapping mat (made of low bio-persistent fibres supplied by Johnson Matthey Plc) to ensure it can be smoothly and properly fitted into the exhaust canning without causing any damage to the brick (see Figure 3-7). Also, the wrapping mat can be used for thermal insulation and preventing the exhaust gas from escaping. There are several different sampling ports located at the end of this canning (marked in red), which can be used for temperature measurement or extracting exhaust gas to the furnace or other gas composition analysers.

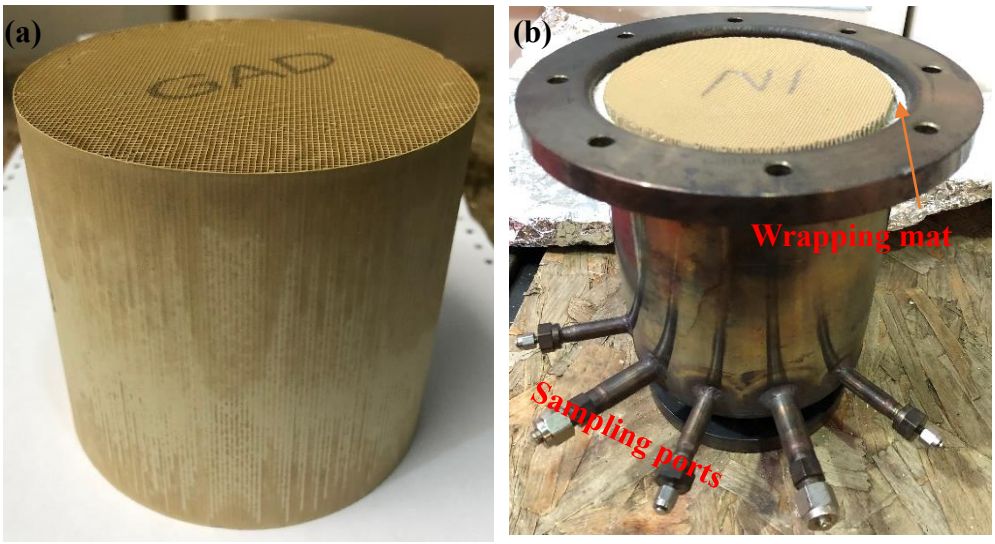

Figure 3-7. (a) TWC monolith (b) TWC fitted into the aftertreatment canning

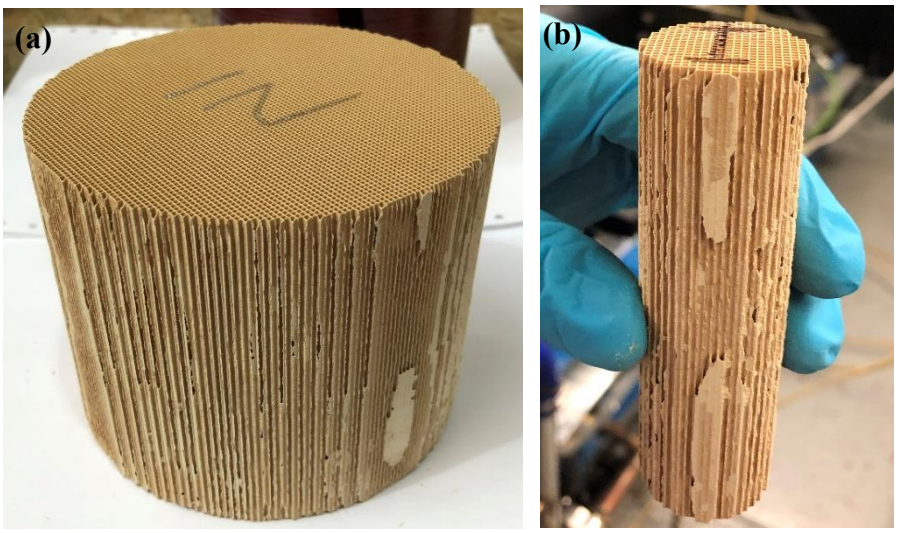

Figure 3-8. (a) Full-scale LNT catalyst, (b) Mini-scale LNT catalyst

3.2.4 General experimental procedure

Prior to every test, preparation works are performed to reduce experimental errors and ensure the quality and reliability of data, such as checking the accuracy of the emissions measurement instruments via calibration gases with known concentrations; cleaning the emissions analysers, catalyst canning, and exhaust sampling lines using nitrogen gas to remove condensed residuals. Also, the thermocouples will be checked to see whether it works properly under both room temperature and high temperature (e.g., engine exhaust temperature). Besides that, the local time of different analysers is calibrated every day to ensure correct data analysis. Both the compressed nitrogen and hydrogen gas cylinders are placed in a ventilated gas cupboard outside the building with cylinder regulators, pressure indicator, and flashback arrestors mounted for safety protection. Generally, the engine is started about one hour before any data measurement till the oil and coolant temperatures reach and stabilize at the target values (see Table 3-1 and Table 3-2), which

is considered to be the full warm-up of the engine. Afterwards, the torque and speed value are changed to the target operating condition. Throughout the test, the COVs (%) of IMEP and peak cylinder pressure are monitored via the ATI panel to record the combustion stability. For all tests in the present study, the COVs should be maintained below 5%. It should be mentioned that the 3-cylinder DI/PFI gasoline engine firstly ran with PFI injection during the whole cold-start period, until it was fully warmed-up, and then was switched to DI injection mode to ensure stable and smooth operation.

3.3 Model description

3.3.1 Computational fluid dynamics and thermodynamic model

For the present thesis, relevant simulation studies were carried out by developing a single-channel, 1-D model on the AVL Boost v2018 [147]. Previous studies have demonstrated the suitability of a 1-D model to simulate the catalytic converter performance, reporting reliable results compared to both 2-D and 3-D simulation [148]. A single-channel model is adopted to represent the catalytic monolith with the assumption that the variations and interactions between different channels can be ignored. In the Boost model, the conservation of the mass, momentum, and energy for both the gas phase and solid phase, and individual gas species were solved. The mass and heat transfer inside the catalytic monoliths are calculated from the empirical expressions for Sherwood and Nusselt numbers, respectively.

The continuity equation of the gas phase in the single-channel model is:

$$\frac{\partial \rho_g}{\partial t} = -\frac{\partial \rho_g \cdot v_g}{\partial z} \qquad \text{Equation 3-1}$$

Generally, the flow in the monolith channel is considered as laminar flow because of its low Reynolds number due to the small channel diameter [149]. Also, the Reynolds number for this case has been checked and it is below 2000. The volume averaging approach is used to consider the solution domain as a continuum porous medium. Thus, the momentum equation in the channel can be reduced to Darcy's equation [150]:

$$\frac{\partial p_g}{\partial z} = -K_D \cdot v_g \qquad \text{Equation 3-2}$$

K_D is the friction coefficient, and it is calculated according to Darcy's law in this study:

$$K_D = \varphi * \frac{v_g}{2} * \frac{\rho_g}{d_H} * \varsigma \qquad \text{Equation 3-3}$$

Where φ is the pipe channel shape factor, taking account of different shapes of the pipe cross section, 0.89 is used for the square cell catalyst; ς is a generic friction coefficient, and $\varsigma = \frac{64}{Re}$ is used to obtain the friction coefficient for laminar flow [151].

Assuming that the viscous dissipation is negligible, the conservation of energy for the gas phase can be expressed by Equation 3-4 in terms of temperature T_g:

$$\varepsilon_g \cdot \frac{\partial}{\partial t}(\rho_g \cdot \sum_j^S w_{j,g} h_j) = -\varepsilon_g \cdot \frac{\partial}{\partial z}(\rho_g \cdot \sum_j^S w_{j,g} h_j \, v_g) + \varepsilon_g \cdot \frac{\partial}{\partial z}\left(\lambda_g \cdot \frac{\partial T_g}{\partial z}\right) +$$

$$\sum_j^S \varepsilon_g \frac{\partial}{\partial z}(\rho_g D_{eff,j} \frac{\partial w_{j,g}}{\partial z} h_j) + A_{geo}\alpha(T_s - T_g) - \sum_i^R (\Delta h_i)\dot{r}_i \, (y_j^L, T_s) \qquad \text{Equation 3-4}$$

The first three terms on the right-hand side represent the gas phase conductive heat transfer, the heat transfer due to species diffusion, and the heat transfer between gas and channel wall respectively. While the last term stands for the heat release from the

homogeneous catalytic reaction, which is evaluated as a function of solid temperature T_s and the molar surface concentration of reactant j as shown in Equation 3-5.

$$A_{geo}\alpha(y_{j,g} - y_j^L) = \sum_i^R (\Delta\dot{h}_\iota) r_i \ (y_j^L, T_s) \qquad \text{Equation 3-5}$$

The energy balance equation of the solid phase is given by Equation 3-6. where $\dot{q}_l$ considers the heat loss to the surroundings.

$$\left(1-\varepsilon_g\right)\rho_s c_{p,s}\frac{\partial T_s}{\partial t} = \left(1-\varepsilon_g\right)\frac{\partial}{\partial z}\left(\lambda_g\frac{\partial T_g}{\partial t}\right) + \sum_i^R(\Delta h_i) r_i\left(y_j^L, T_s\right) - A_{geo}\alpha\left(T_s - T_g\right) + \dot{q}_l$$

Equation 3-6

The species conversation equation is written as follows:

$$\varepsilon_g \cdot \frac{\partial(\rho_g \cdot w_{j,g})}{\partial t} = -\varepsilon_g \cdot \frac{\partial(\rho_g \cdot w_{j,g} \cdot v_g)}{\partial z} + \varepsilon_g \cdot \frac{\partial}{\partial z}\left(\rho_g \cdot D_{eff,j} \cdot \frac{\partial w_{j,g}}{\partial z}\right) + M_{j,g} \cdot \sum_i^R \nu_{i,j} \cdot$$

$$r_i(y_j^L, T_s) \qquad \text{Equation 3-7}$$

The transfer coefficient of mass (k_m) and heat (k_h) inside the catalytic monoliths can be calculated from the empirical expressions for the Sherwood and Nusselt numbers respectively:

$$k_m = \frac{\mathrm{Sh} * D_{eff,j}}{d_H} \qquad \text{Equation 3-8}$$

$$k_h = \frac{\mathrm{Nu} * \lambda_g}{d_H} \qquad \text{Equation 3-9}$$

Various approaches are available to calculate the Sherwood and Nusselt numbers based on experimental investigations [152-154]. In the present study, the Sieder/Tate correlation is used to obtain the mass and heat transfer coefficients; [155] where Gz_{heat} and Gz_{mass} stands for the Graetz numbers for heat and mass transfer and can be calculated using Equation 3-12 and Equation 3-13 respectively; Pr and Sc is the Prandtl number and

Schmidt number, which are expressed by Equation 3-14 and Equation 3-15, respectively.

$$\mathrm{Sh} = 1.86 * (\mathrm{Gz}_{mass})^{1/3} \quad \text{Equation 3-10}$$

$$\mathrm{Nu} = 1.86 * (\mathrm{Gz}_{heat})^{1/3} \quad \text{Equation 3-11}$$

$$\mathrm{Gz}_{heat} = Re * Pr * \frac{d_H}{l} \quad \text{Equation 3-12}$$

$$\mathrm{Gz}_{mass} = Re * Sc * \frac{d_H}{l} \quad \text{Equation 3-13}$$

$$\mathrm{Pr} = \frac{c_p * \mu}{\lambda_g} \quad \text{Equation 3-14}$$

$$\mathrm{Sc} = \frac{\mu}{\rho * D_{eff,j}} \quad \text{Equation 3-15}$$

3.3.2 Chemical kinetics

The classical LH relation proposed by Voltz et al. is selected to calculate the kinetic rate expressions for CO, H_2, and C_3H_6 oxidation with the consideration of the self-inhibition effect of CO, C_3H_6 and O_2 in the present study [135]. As for the NO reduction by CO, Subramanian and Varma's research is considered to be the first source that provides the rate expressions in terms of CO oxidation and NO reduction modelling over a TWC [156]. For the catalytic surface reactions, oxidation of HC, H_2, and CO, NO reduction reaction, water-gas shift reaction and HC steam reforming reaction are taken into consideration. Propene (C_3H_6) was selected as the representative of hydrocarbons in the exhaust gas. Detailed expressions of catalytic surface reactions are listed in Table 3-4.

Table 3-4- Surface reaction over TWC

Reaction	Reaction enthalpy (J/mol)
(1) $CO + \frac{1}{2}O_2 \longrightarrow CO_2$	$\Delta H_1 = -2.83 \times 10^5$
(2) $H_2 + \frac{1}{2}O_2 \longrightarrow H_2O$	$\Delta H_2 = -2.42 \times 10^5$
(3) $2C_3H_6 + 9O_2 \longrightarrow 6CO_2 + 6H_2O$	$\Delta H_3 = -1.93 \times 10^6$
(4) $2NO + 2CO \longrightarrow 2CO_2 + N_2$	$\Delta H_4 = -3.74 \times 10^5$
(5) $2NO + 2H_2 \longrightarrow 2H_2O + N_2$	$\Delta H_5 = -3.32 \times 10^5$
(6) $9NO + C_3H_6 \longrightarrow 3CO_2 + 3H_2O + 4.5N_2$	$\Delta H_6 = -2.74 \times 10^6$
(7) $CO + H_2O \longrightarrow CO_2 + H_2$	$\Delta H_7 = -4.10 \times 10^4$
(8) $C_3H_6 + 3H_2O \longrightarrow 3CO + 6H_2$	$\Delta H_8 = 3.74 \times 10^5$

The catalytic reaction rates which were calculated based on the LH approach will be discussed below. For the oxidation reactions, the reaction rate of CO oxidation can be calculated by Equation 3-16 shown as below:

$$r_1 = \frac{k_1 Y_{CO} Y_{O_2}}{I^2} \qquad \text{Equation 3-16}$$

$$k_i(\mathrm{T}) = k_i^{573.15\,K} \exp\left(\frac{-E_i}{\mathrm{R}} \times \left(\frac{1}{T} - \frac{1}{573.15K}\right)\right) \quad \mathrm{i} = 1 \ldots 8 \qquad \text{Equation 3-17}$$

$$\mathrm{I}^2 = (1 + \mathrm{k}_{co}^{inh} Y_{\mathrm{CO}} + k_{C3H6}^{inh} Y_{C3H6} + k_{O2}^{inh} Y_{O2})^2 \qquad \text{Equation 3-18}$$

$$\mathrm{k}_j^{inh}(\mathrm{T}) = k_j^{573.15\,K,inh} \exp\left(\frac{-E_j^{inh}}{\mathrm{R}} \times \left(\frac{1}{T} - \frac{1}{573.15K}\right)\right),\ j = \mathrm{CO}, C_3H_6, O_2 \qquad \text{Equation 3-19}$$

Where: Y_i means the molar concentration of gaseous reactants; k_1 is the temperature dependent reaction pre-exponential factor and can be described by an Arrhenius type equation (see Equation 3-17); $k_i^{573.15\,K}$ is the kinetic constant, and the value is generally obtained from previous literature; E_i is the reaction activation energy. R is the universal gas constant and equals 8.314 kJ/ (kmol K); I^2 describes the promotion/inhibition effect

of CO, C_3H_6 and O_2 and is calculated as shown in Equation 3-18; $k_j^{inh}(T)$ is the reaction pre-exponential factor for the inhibition term and can be calculated based on Equation 3-19 similar to k_1.

Similarly, the reaction rate of H_2, and C_3H_6 oxidation and the NO reduction reaction by CO, H_2, and C_3H_6 can be calculated using Equation 3-20; where: m and n denote the reactants.

$$r_i = \frac{k_i Y_m Y_n}{I^2}, i = 2 \dots 6 \qquad \text{Equation 3-20}$$

The water-gas shift and hydrocarbon steam reforming reaction rates are calculated as below:

$$r_7 = \frac{k_7 Y_{CO} Y_{H_2O}}{I} \qquad \text{Equation 3-21}$$

$$r_8 = \frac{k_8 Y_{C_3H_6} Y_{H_2O}}{I}\left(1 - \frac{Y_{CO}^3 Y_{H_2}^6}{Y_{C_3H_6} Y_{H_2O}^3 k_{C_3H_6,H_2O}^{eq}}\right) \qquad \text{Equation 3-22}$$

3.3.3 Model calibration and parameter optimisation

Regarding the simulation of a commerical TWC presented in Chapter 4, the aforementioned 1-D Boost model was applied (see Figure 3-9). ATB1 and ATB2 represents the inlet and outlet of the catalyst in the model. Relevant experimental data were imported into the model as initial boundary conditions. General physical properties of the catalyst monolith can be found in Table 3-3. The cell structure of the monolith is described as squared cells. The value of geometric surface area (GSA) of the catalyst is internally calculated by the model via the formula of $A_{geo} = \frac{4*d_H}{(d_H+d_W)^2}$. d_W and d_H

represents the wall thickness (0.2 mm) and the channel's hydraulic diameter which is calculated internally based on the input catalyst dimensions. A mass flux of 0.766 kg/hr was inputed, corresponding to the GHSV of 25,000 h^{-1}. Mole gas fraction of key species (CO, H_2, O_2, C_3H_6, CO_2, H_2O, and NO) at catalyst inlet are calculated and inputed based on the measurements shown in Table 4-2. The temporal profile of inlet gas temperature collected via thermocouples was imported into the model inlet to describe the catalyst light-off performance during the furnace temperature ramp-up process. Transient simulation was performed with a total simulation duration of 3000 s and a time step of 1s. In the 1-D model, the radial effects inside the channel are considered to be of minor importance and assumed to be neglected. Thereby, only the conservation equations in the axial direction are calculated, and 50 grid points were defined in the axial direction for the discretization. The grid shape factor was defined as 0.8 to produce more dense grid points at the boundaries of the model. Figure 3-10 gives an example of several grid points locations in the axial direction of a grid shape factor of 0.8 in the 1D Boost model. A specific solver method named 'Office', which was in-built in the Boost model, was utilised to calculate the conservation equations.

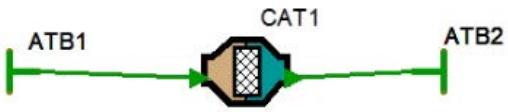

Figure 3-9. Schematic diagram of the catalyst model in AVL Boost

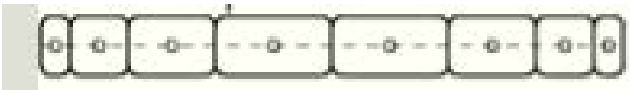

Figure 3-10. Example of mesh grid points in the axial direction of a grid shape factor of

0.8 in the 1D Boost model

The developed AVL Boost catalyst model has been calibrated based on relevant experimental data and the general calibration procedure is illustrated in Figure 3-11. It can be seen that the thermal calibration will be performed first using the exhaust temperature data recorded by K-type thermocouples. Afterwards, calibration on the chemical reaction sector will be carried out based on corresponding exhaust gas compositions measurement by FTIR and HSense analysers. The whole process was iterated to minimise the difference between model predictions and actual measurements.

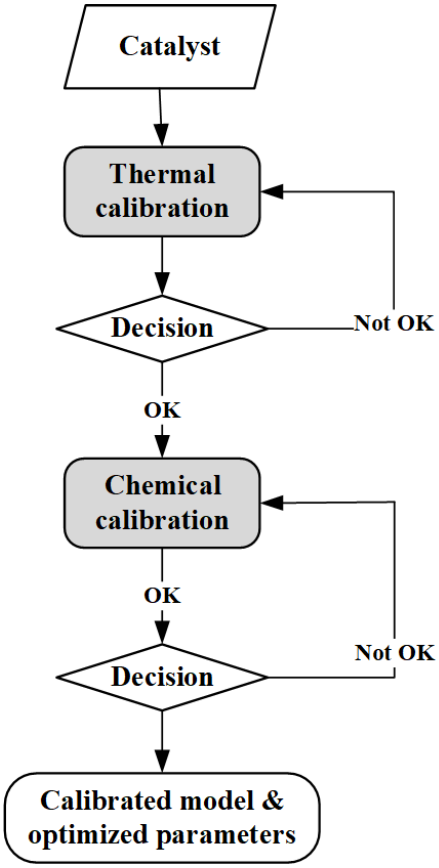

Figure 3-11. General calibration procedure for the Boost catalyst model

For the thermal calibration, the values of thermal conductivity and specific heat capacity were manually tuned to match the model's output with the practically measured outlet

exhaust temperatures. As for the chemical reaction sector, the kinetic parameters from Brinkmeier's work [157] were employed as preliminary values for TWC simulation and further parameter optimisation is conducted based on experimentally obtained light-off data. An optimisation technique was used to calibrate the reaction factors with high accuracy and efficiency rather than manual calibration. Therefore, an optimisation function was defined and calculated using a genetic algorithm (GA) approach to minimise the sum of the integral mean of squares of error between the measured and predicted data for CO, HC, NO and H_2. This function is as follows:

$$\text{Optimisation function} = min \sum_i^4 \int \overline{\left(Y_{sim} - Y_{exp}\right)^2} dx \qquad \text{Equation 3-23}$$

Where Y_{sim} and Y_{exp} are the predicted and experimental conversion efficiency for each species respectively; i denotes the chemical species (CO, HC, NO, and H_2); and x is time. Both the activation energy and reaction constant for all reactions along with the inhibition term will be calibrated. The optimisation process was coupled with the catalyst model via AVL Design Explorer (DE). History plot obtained from a random iteration of DE chemical optimization is given in Figure 3-12. In the plot, the objective represents $\sum_i^4 \int \overline{\left(Y_{sim} - Y_{exp}\right)^2} dx$ in Equation 3-23 and the optimisation process targets to minimise the objective value. It can be seen that the objective value drops from 350 to lower level (around 200) after hundreds of runs. For each run, random values (within the pre-defined range) will be assigned to variables based on the GA method. For example, the activation energy and parameter constant of CO oxidation which are shown as E1_CO and K1_CO in the plot, were assigned to different values for each run and the corresponding objective

value was calculated. After several iterations, the objective value reduced to an acceptable level and then the parameters are well estimated.

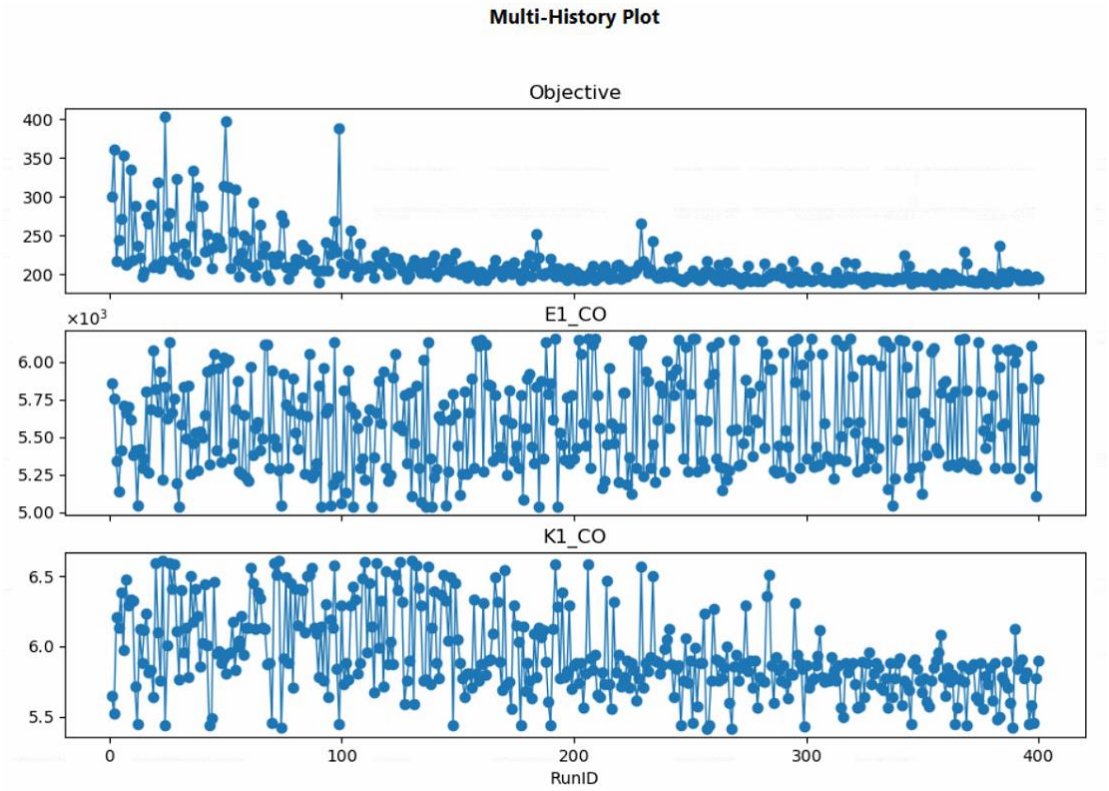

Figure 3-12. History plot of the variables and objective values of the chemical calibration

3.4 Analytical approach

3.4.1 Engine performance evaluation

During the tests, the engine IMEP and COV of IMEP (%) were calculated and displayed by the LabVIEW programme using Equation 3-24 and Equation 3-26. And the engine displaced volume is described by Equation 3-25. The COV of IMEP (%) for 200 consecutive engine cycles was closely monitored and maintained below 5% during the

test to ensure combustion stability and minimised cycle-to-cycle variability.

$$\text{IMEP} = \frac{Indicated\ Work\ per\ Cycle}{Displaced\ Volume} = \frac{\oint pdV}{V_d} \quad \text{Equation 3-24}$$

$$V_d = \frac{1}{4} * \pi * Bore^2 * Storke \quad \text{Equation 3-25}$$

$$\text{COV of IMEP (\%)} = \frac{Standard\ deviation\ of\ IEMP}{Mean\ of\ IMEP} \quad \text{Equation 3-26}$$

Besides that, fuel consumption was closely monitored, and brake specific fuel consumption (BSFC) was quantified. The BSFC (g/Wh) calculation is presented as below.

$$\text{P} = T * \frac{2\pi * n}{60} \quad \text{Equation 3-27}$$

$$\text{BSFC} = \frac{\dot{m}}{P} \quad \text{Equation 3-28}$$

Where: $\dot{m}$ is the fuel mass flow rate (g/hr); P represents the engine brake power (W); T is engine brake torque (Nm); and n stands for engine speed (rpm).

3.4.2 Lambda calculation

It is believed that adding hydrogen to the exhaust gas upstream of the catalyst will slightly shift the lambda of the exhaust. Therefore, the corresponding lambda calculation is performed before and after hydrogen injection to evaluate the lambda shift. Many equations have been developed by researchers to calculate the AFR of engine operation based on exhaust gas concentrations measurements [158, 159]. Although the information used for different methods might slightly vary depending on the availability of the exhaust data measurements, they follow the same combustion theory. In the present study, the

equation from Germann's work [158] was applied for calculating the engine lambda (see Equation 3-29).

$$\lambda = \frac{2y_{O_2}+2y_{CO_2}+y_{H_2O}+y_{CO}+y_{NO_x}}{2y_{CO}+y_{H_2}+4y_{THC}+2y_{CO_2}+y_{H_2O}} \quad \text{Equation 3-29}$$

Where: y stands for the concentration of different gaseous species.

3.4.3 Key performance variables calculation for catalysts

The gas hourly space velocity (GHSV) of exhaust gas is an important parameter that needs to be monitored during study of the catalyst light-off. The GHSV (h^{-1}) is calculated as the volumetric flow rate of the exhaust ($\dot{V}_{exhaust}$) divided by the catalyst monolith volume ($V_{catalyst}$), as given by Equation 3-30. Since the catalyst monoliths used in the present study are all cylindrical, the catalyst volume (cm^3) can be easily obtained. It should be mentioned that the exhaust flow rates measured using the flow meters (both the Platon and Rheonik) are mass-based and need to be converted to volumetric-based first for GHSV estimation. The gas density could be estimated based on the ideal gas law using Equation 3-31.

$$\text{GHSV} = \frac{\dot{V}_{exhaust}}{V_{catalyst}} = \frac{\dot{m}_{exhaust}/\rho}{\pi*\left(\frac{1}{2}D\right)^2*L} \quad \text{Equation 3-30}$$

$$\rho = \frac{P}{R_{air}*T} \quad \text{Equation 3-31}$$

Where: D and L is the diameter and length of the catalyst; R_{air} is the ideal gas constant of 287.057 (unit: J/(kgK)); P and T are the measured exhaust gas pressure and temperature. The conversion efficiency of target exhaust species (HC, CO, NO, and H_2) over the TWC

converter can be calculated using Equation 3-32, based on the concentration measurement. This equation is exemplified using CO. The calculation for the other species follows the same manner; where: $[CO]_{in}$ and $[CO]_{out}$ means the volumetric concentration of CO measured at pre- and post-TWC.

$$\eta_{CO} = \frac{[CO]_{in} - [CO]_{out}}{[CO]_{in}} \quad \text{Equation 3-32}$$

The light-off temperature at which the species conversion efficiency reaches 50% will be denoted by T_{50_x} (x stands for CO, NO, H_2, and HC) in this thesis.

During the tests involve LNT catalyst, several key variables are of interest to evaluate the catalyst performance, including the average conversion of CO, THC, NO_x, and the NO_x reduction selectivity to NH_3, N_2O, and N_2. The cycle averaged species conversion efficiency is calculated based on the accumulated emissions at pre- and post-catalyst via Equation 3-33 for CO, THC and NO_x, respectively; where: $Y_{species}$ denotes the cycle averaged species conversion efficiency. $X_{species_{in}}$ and $X_{species_{out}}$ (unit: ppm) are the accumulated species emissions obtained at the inlet and out of the catalyst over the specific cycles of observation.

$$Y_{species} = \frac{X_{species_{in}} - X_{species_{out}}}{X_{species_{in}}} \quad species = CO, THC, NOx \quad \text{Equation 3-33}$$

The yield and selectivity of NH_3 and N_2O is calculated using Equation 3-34 to Equation 3-37; where: y_{NH_3} and y_{N_2O} denotes for yield; s_{NH_3} and s_{N_2O} denotes for selectivity; $NH_3\ out$ means the total amount of NH_3 measured at the catalyst outlet within the observation window; while $NO_X\ in$ is the total amount of NO_x recorded at the catalyst

inlet within certain cycles. The N_2O calculation follows a similar fashion as NH_3. The FTIR analyser is not able to measure the N_2 concentration, thereby the N_2 selectivity is calculated based on mass balance theory (see Equation 3-38), assuming that the NO_x reduction will only form those three N-containing products. For all those key variables' calculation, the 'in' and 'out' means inlet and outlet of the LNT if we are calculating the conversion over the LNT. A similar theory can be applied for the TWC and the TWC-LNT system.

$$y_{NH_3} = \frac{NH_3\ out}{NO_X\ in} \quad \text{Equation 3-34}$$

$$s_{NH_3} = y_{NH_3}/\mathrm{Y_{NO_X}} \quad \text{Equation 3-35}$$

$$y_{N_2O} = \frac{2*N_2O\ out}{NO_X\ in} \quad \text{Equation 3-36}$$

$$s_{N_2O} = y_{N_2O}/\mathrm{Y_{NO_X}} \quad \text{Equation 3-37}$$

$$s_{N_2} = 1 - s_{NH_3} - s_{N_2O} \quad \text{Equation 3-38}$$

3.5 Experimental errors and uncertainty analysis

It should be mentioned that certain degrees of errors or uncertainty are undeniable for experimental data collection during laboratorial tests. In this section, the calibration information of relevant experimental instruments will be introduced. Regarding the measurement accuracy of various instruments, it has been discussed in Chapter 3.2 and more details can be found in Appendix B. To minimise any measurement errors,

experiments were only allowed to be started if all the required instruments were fully warmed-up and calibrated. Associated calibration works of the measuring devices were generally conducted on a daily basis. For instance, a certified 5% hydrogen gas (with ±2% tolerance) was used to calibrate the hydrogen analyser (HSense).

During the experimental studies, several testing points were repeated to ensure the repeatability and reproducibility of measurements. Also, it should be mentioned that all the data regarding steady-state species concentrations measurements included in the present thesis are the average of multiple measurements. An example will be discussed here to show good repeatability of the experimental results. Ten sets of repeated measurements were conducted on both the same and different days to collect the engine out species levels under steady-state engine operation at the speed of 2100 rpm, BMEP of 1.68 bar, and λ of 0.9962 with DI mode using the 3-cylinder gasoline research engine. Each measurement was averaged for a constant duration of 120 s. In addition, the fuel consumption was also monitored during the tests. Statistical analysis of part of the results obtained from the repeated experiments is given by Table 3-5 and Figure 3-13 with error bars plotted as reference. It was noticed that the standard deviations (SD) are at a very low level for all parameters, showing a good repeatability of the experimental measurements.

Table 3-5- Statistical analysis of parameters measurements for random error experiments (2100 rpm, 1.68 bar BMEP, and λ=0.9962)

Parameter	CO	THC	NO_x	H_2	Fuel*
Unit	ppm	ppm	ppm	ppm	kg/h

Average	7334.22	1604.46	1179.42	2748.33	1.6740
SD (±)	34.22	39.34	13.86	14.50	0.0018

Fuel* represents fuel consumption rate.

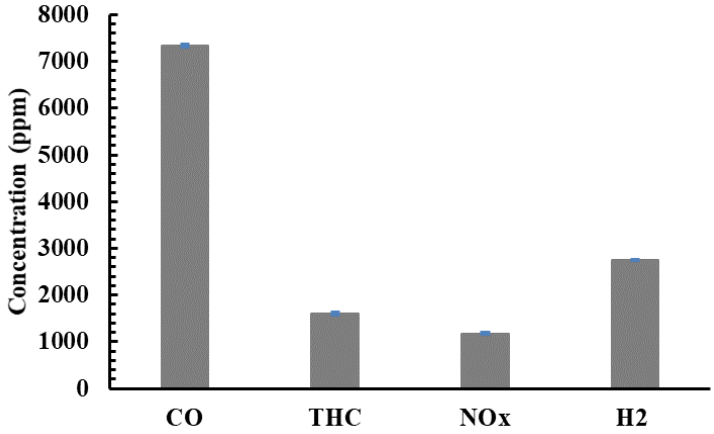

Figure 3-13. Gaseous species concentrations measured at engine-out for random error experiments with error bars plotted

CHAPTER 4 EFFECT OF HYDROGEN (H_2) ADDITION ON THE LIGHT-OFF PERFORMANCE OF A TWC

4.1 Introduction

In the Literature Review Chapter, it was revealed by several previous publications that the presence of hydrogen in the feed gas (synthetic gas mixture) is beneficial for catalyst oxidizing and reducing activity. Therefore, the potential impact of hydrogen addition over a TWC under real engine operating conditions is investigated in this chapter. For this purpose, light-off experiments were performed using an integrated system of consisting an engine test bench and a heated catalytic reactor with different levels of hydrogen injection upstream of a mini-TWC. In addition, simulation approach was utilised to provide auxiliary information to better the understanding of the underlying chemical mechanisms. Detailed chemical reactions occurring over the TWC were simulated through a one-dimensional catalytic converter model with kinetic parameters being adjusted respectively for different hydrogen levels based on the experimental data. The corresponding simulation results show how the hydrogen promotional effect can be numerically revealed.

4.2 Experiment design and basic testing procedures

Related experiments were performed on the four-cylinder GDI engine test bench. Each testing point was examined under both stoichiometric ($\lambda = 1$) and lean condition ($\lambda = 1.08$) at the low engine load of 2.2 bar BMEP and 2100 rpm engine speed. Although the hydrogen studied in present work is injected from a compressed gas cylinder, it is believed that an on-board fuel reformer can be implemented into the aftertreatment system to provide hydrogen. According to experimental studies on exhaust fuel reforming conducted by other PhD students in the research group using this GDI engine test bench, the required amount of hydrogen (1000 to 5000 ppm) can be successfully produced under this specific engine operating condition. The schematic of the experimental set-up is shown in Figure 4-1. A mini-scale ceramic Pd/Pt/Rh based TWC was used, and details can be found in Table 3-3. As shown in Figure 4-1, the mini TWC was placed in a reactor, and was heated up by a tubular furnace (from 120 ^{o}C to 340 ^{o}C with a temperature ramp of 7 ^{o}C/min under a GHSV of 25,000 h^{-1}. The fuel used was European unleaded gasoline with a research octane number of 95, specification EN228.

Pure H_2 from a gas cylinder was injected at the required flow rates to ensure 0 (without hydrogen addition, baseline condition), 1000, 5000 ppm hydrogen addition to the engine out hydrogen concentrations. The hydrogen concentrations were measured at each testing point by the HSense at the inlet of the TWC. As shown in Figure 4-1, the dotted lines represent three different sampling points: (1) engine out; (2) TWC inlet (after hydrogen

injection); (3) TWC outlet. The measurement of the exhaust gas composition was conducted at these three sample points in sequence. The concentrations of gaseous species at the TWC inlet without hydrogen addition are listed in Table 4-2.

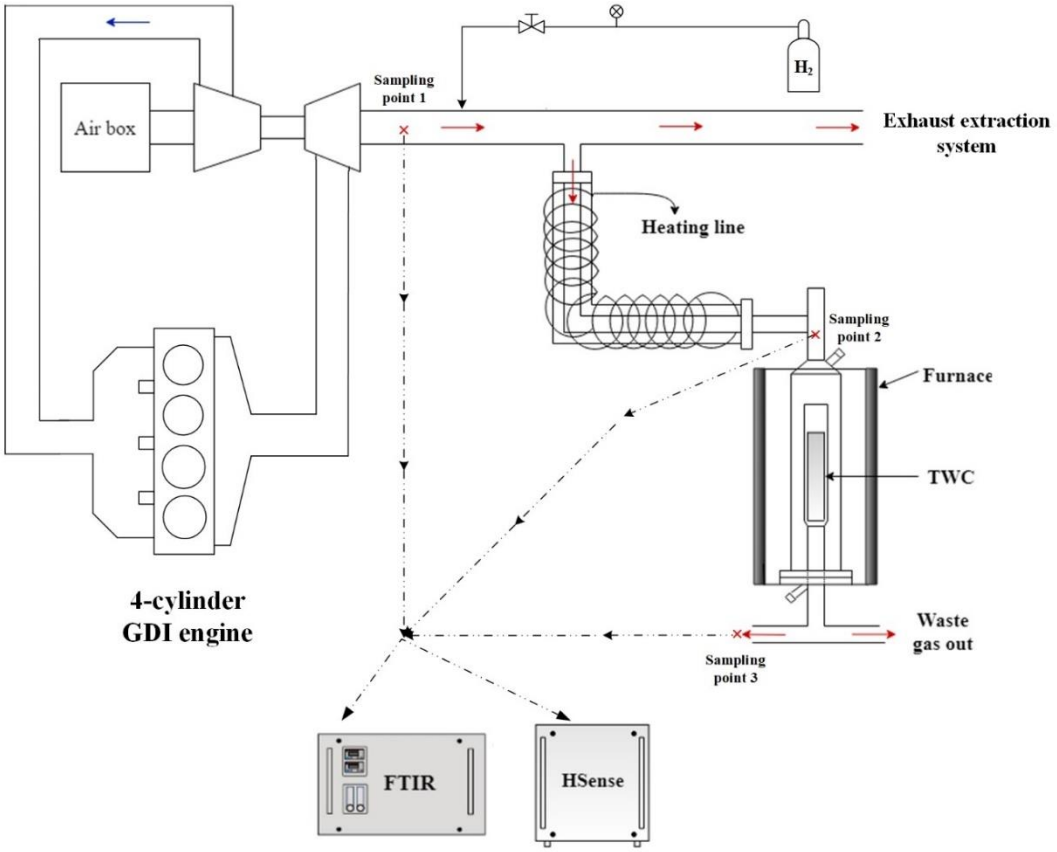

Figure 4-1. Schematic of the experimental set-up (FTIR: exhaust gas composition analyser; HSense: hydrogen analyser; Dotted lines: different sampling points)

4.3 Results and discussion

The lambda of exhaust gas after hydrogen injection is calculated using Equation 3-29. The lambda shift caused by hydrogen addition under different engine operating conditions are summarised in Table 4-1. As it can be noticed the lambda shift is below 1.5%, even with 5000 ppm of hydrogen injection. Moreover, the BSFC during the tests was analysed

for both conditions using Equation 3-28. A reduction of 3.61% in fuel consumption was obtained when running the engine under lean condition compared to the stoichiometric case.

Table 4-1- Lambda shift caused by hydrogen addition under different conditions

	Stoichiometric		Lean	
	λ_{cal} (-)	$\Delta\lambda$ (%)	λ_{cal} (-)	$\Delta\lambda$ (%)
Baseline (0 ppm)	1.009	-	1.089	-
1000 ppm	1.008	0.120	1.088	0.146
5000 ppm	0.997	1.242	1.076	1.238

Table 4-2- TWC inlet emissions concentration for the baseline under stoichiometric and lean conditions

Gas species	Stoichiometric	Lean
O_2 (%)	0.76	1.780
CO (ppm)	5925	1525
NO (ppm)	2269	2695
HC (ppm)	1396	851
H_2 (ppm)	2350	374

4.3.1 Light-off experiments

Figure 4-2 and Figure 4-3 show the hydrogen addition effect on CO and H_2 light-off performance under both engine stoichiometric and lean operations, respectively. As shown in Figure 4-2, adding more hydrogen improved the CO conversion at low temperatures under both stoichiometric and lean conditions. This is in line with the results of some studies on Pt/Pd based catalysts under conditions resembling the diesel engine exhaust [6, 10]. Under the stoichiometric conditions, 5000 ppm of hydrogen introduction

to the exhaust feed was observed to be detrimental for the maximum CO conversion efficiency. Similar phenomenon can also be found in Viktor and Hellier's work [90]. The negative effect on CO overall conversion is considered to be related to two possible reasons. Firstly, unlike the lean exhaust, there is no excess oxygen contained in the engine out exhaust under stoichiometric condition; when introducing more hydrogen upstream the TWC, the competition for oxygen between H_2 and CO is facilitated, and CO is inferior to hydrogen. Additionally, it was previously reported that H_2 is more effective than CO in reducing NO [81]. Therefore, NO was actively consumed by H_2, which resulted in the deficiency of NO. As we can notice in the 5000 ppm case, NO has been completely consumed at T >250 ºC, see Figure 4-7 (a), and therefore no NO-CO reduction reaction is taking place afterwards. The slow increase in CO conversion after 250 ºC could be attributed to the WGS reaction (see Figure 4-3 (a)).

Under the lean conditions, for the baseline case without extra hydrogen addition, the CO conversion was initiated at 200 ºC and achieved the total conversion at around 270 ºC. When adding 1000 ppm of hydrogen into the exhaust, the CO conversion curve can be divided into three regions based on the inlet gas temperature:

(1) T < 180 ºC; With 1000 ppm of hydrogen addition, the CO's low temperature conversion was promoted and initiated shortly after 130 ºC. It is known that CO consumption over the TWC is generally proceeded via three reaction pathways, including CO oxidation, reduction with NO, and WGS reaction. Botas et al. reported that the CO-NO reduction reaction over a Pt-based TWC was of extreme low activity at temperatures

below 425 ºC due to the strong self-poisoning effect of CO, and CO preferentially reacted with oxygen at low temperatures. They also suggested that the addition of water (gas) or hydrogen into the feed gas mixture can enhance both the NO and CO conversion rates [93]. Other researchers suggested that the hydrogen beneficial effect on the CO conversion could result from the fact that hydrogen weakens CO adsorption strength over the catalyst's surface site (see section 2.5.1) [89, 95]. Therefore, it is believed that the CO desorption was promoted by the hydrogen addition, thereby creating more active sites for CO-O_2 and CO-NO reactions to take place at low temperatures.

(2) When the temperature was between 180 and 220 ºC, a stabilisation region was observed. From Figure 4-3(b), H_2 was totally depleted after 180 ºC, and the CO conversion was observed to be stagnated, forming a plateau region between 180 to 220 ºC. Without the presence of hydrogen, it is assumed that the CO self-inhibition effect is still preventing CO from being consumed within this temperature range. Similar stabilisation region could be found for the 5000 ppm case.

(3) T>220 ºC. As the furnace was continuously heated up, the strong CO self-inhibition effect was vanished with sufficient energy being accumulated over the catalyst surface site. Therefore, CO was consumed rapidly to achieve its light-off at 245 ºC and be totally converted soon after 290 ºC. However, the CO light-off was slightly delayed by 13 ºC compared to the baseline condition. This is believed to be related to the fact that small amount of hydrogen addition to lean exhaust accelerates the depletion of hydrogen, thereby resulting in a short stagnation region where there is no hydrogen acting as

promoter for the CO conversion and the exotherm is not sufficient for CO desorption.

When the concentration of hydrogen added to the exhaust increases to 5000 ppm, the CO low temperature conversion is greatly enhanced and the light-off is significantly promoted with a reduction in T_{50_CO} of 67 ºC compared to the corresponding baseline condition. Likewise, a stabilisation region was formed between 170 and 200 ºC, which occurred and ended earlier than the 1000 ppm case (180 to 220 ºC). It is worth noting that the hydrogen was totally converted at 170 ºC, and the CO conversion stagnation period immediately appeared with the depletion of the hydrogen. It is believed that the hydrogen beneficial effect on moderating the CO adsorption disappeared at 170 ºC. As can be seen from the ΔT figure (see Figure 4-4 (b)), for the 1000 ppm and 5000 ppm case, when the inlet temperature was 220 and 200 ºC respectively, the outlet temperature was observed to be the same- 280 ºC. This is because the 5000 ppm hydrogen addition resulted in more heat release than the 1000 ppm case. Accordingly, it is believed that when the catalyst surface site temperature exceeds the threshold (close to 280 ºC), the strongly adsorbed CO was released from the surface, thereby creating more active sites for other reactions to take place.

Generally speaking, hydrogen addition to the gasoline exhaust under oxidising environment promotes the CO low temperature conversion, which is believed to be attributed to the hydrogen beneficial effect on weakening the CO self-inhibition. Additionally, the heat release caused by the hydrogen addition increased the temperature of the catalyst surface site, and consequently advanced the CO light-off to some extent.

However, with the extra hydrogen addition, the depletion of the hydrogen is accelerated as well. This early depletion might result in a delay of CO light-off compared to the baseline condition, because there is a certain period where the local temperature is not sufficient for the adsorbed CO to be released and the promoter – hydrogen is absent. Whether the delay will occur depends on the temperature increment caused by the hydrogen addition, namely, the amount of hydrogen addition. Overall, it can be concluded that the hydrogen improvement effect results from many factors, including both the exothermic effect of hydrogen oxidation and the weakening of CO self-inhibition by hydrogen, which will be further discussed in section 4.3.3.

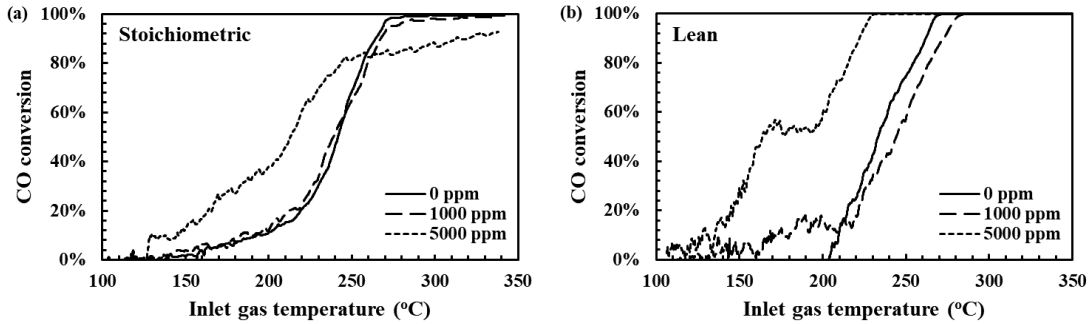

Figure 4-2. Impact of H_2 addition on CO light-off performance over the TWC under (a) stoichiometric and (b) lean conditions

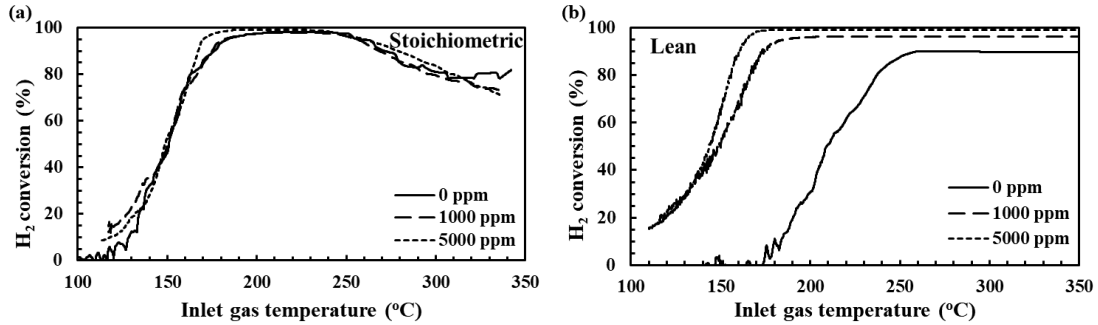

Figure 4-3. Impact of H_2 addition on H_2 light-off performance over the TWC under (a) stoichiometric and (b) lean conditions.

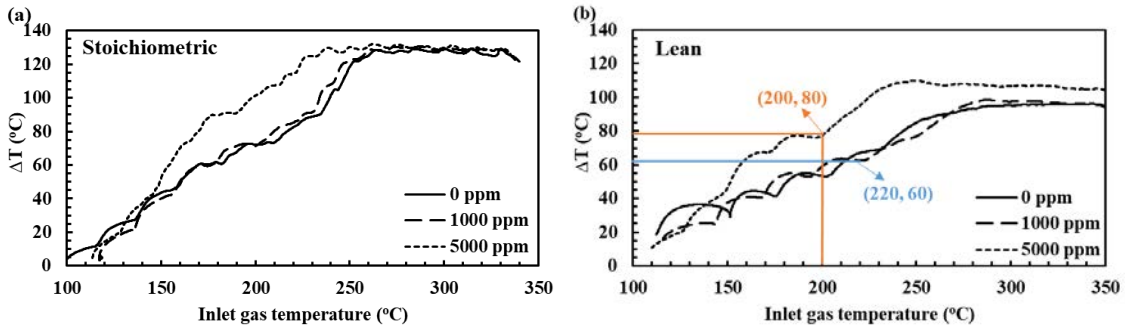

Figure 4-4. Temperature increment measured along TWC with different concentrations of H_2 injection under (a) stoichiometric and (b) lean conditions

The influence of the hydrogen addition on HC light-off is presented in Figure 4-5. In the case of stoichiometric air-fuel mixture, the addition of hydrogen promoted the HC low temperature conversion (below 240 °C); while negative influence on the total conversion of HC was also accompanied with the hydrogen addition at higher temperatures. With more hydrogen being added, the maximum HC conversion was suppressed to a larger extent. This phenomenon can be explained using similar competitive theory as for CO. When extra hydrogen was introduced into the stoichiometric engine exhaust, a competitive oxidation between HC and H_2 was triggered, and oxygen preferentially reacted with H_2. As the temperature is elevated, oxygen is practically depleted, the HC oxidation is in an inferior position to CO and H_2 in the competition, thereby suppressing the overall HC conversion.

For the case of lean air-fuel mixture, with 5000 ppm hydrogen addition upstream of the TWC, the HC light-off was considerably promoted with 38 °C decrease in T_{50_HC} compared to the baseline condition. Similar to the CO conversion curve, a slight delay in HC light-off was observed with 1000 ppm hydrogen addition. As previously discussed,

the extra hydrogen addition accelerated the hydrogen consumption rate. This fast depletion of hydrogen created a specific period (without the hydrogen beneficial effect) where certain amounts of CO were strongly adsorbed on the catalyst surface site and blocked the sites for other species to be adsorbed and other reactions to occur. Therefore, adding 1000 ppm of hydrogen exacerbated the competition between H_2 and HC for the limited free active sites, and HC was at a disadvantage. However, adding more hydrogen (5000 ppm) upstream of the TWC has different impact on the HC conversion compared to the 1000 ppm case, because of the exothermic effect of hydrogen. As can be noticed from the ΔT plot, the temperature increment along the TWC with the 5000 ppm H_2 addition is obviously higher than the baseline and the 1000 ppm conditions.

The concentrations of hydrocarbon species were also monitored both upstream and downstream of the TWC during the light-off tests. Figure 4-6 shows the comparison between the concentrations of representative hydrocarbon compositions measured before TWC and after TWC at 200 /250 /350 ºC under lean conditions with 0 and 5000 ppm H_2 addition, respectively. These three temperature points are selected because the hydrocarbon starts to convert at around 200 ºC and 350 ºC is the upper limit temperature in the present study. Saturated (e.g., methane (CH_4), propane (C_3H_8), dodecane ($C_{12}H_{26}$)) and unsaturated (e.g., acetylene (C_2H_2), ethylene (C_2H_4), propylene (C_3H_6), toluene (C_7H_8)) hydrocarbons conversions are improved with hydrogen addition, but the level of improvement differs depending on the species. At 200 ºC, the hydrogen addition shows beneficial effect for the removal of the longer chain saturated HC (dodecane and propane),

acetylene, and toluene. As the temperature increases to 250 °C, the majority of hydrocarbons are converted, and the unsaturated hydrocarbons are fully removed, benefiting from the hydrogen promoting effect. However, the TWC conversion efficiency of the low reactivity HC, such as CH_4, is not improved with hydrogen addition within the temperature range studied. For the case without hydrogen addition, there are some unsaturated hydrocarbons remaining at 250 °C.

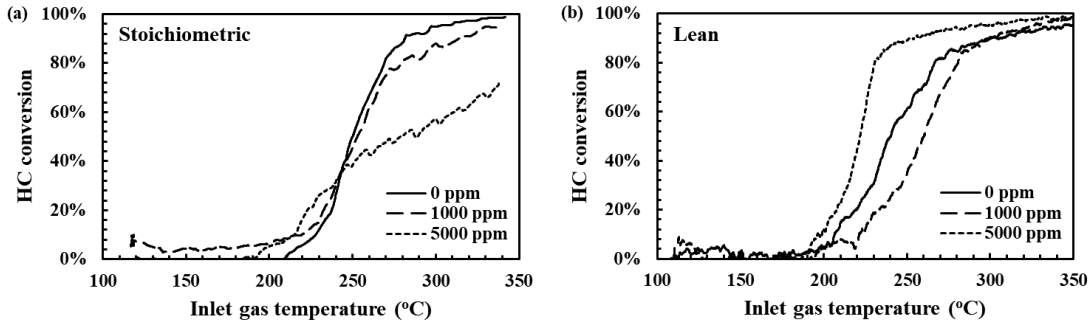

Figure 4-5. Impact of H_2 addition on HC light-off performance over the TWC under (a) stoichiometric and (b) lean conditions

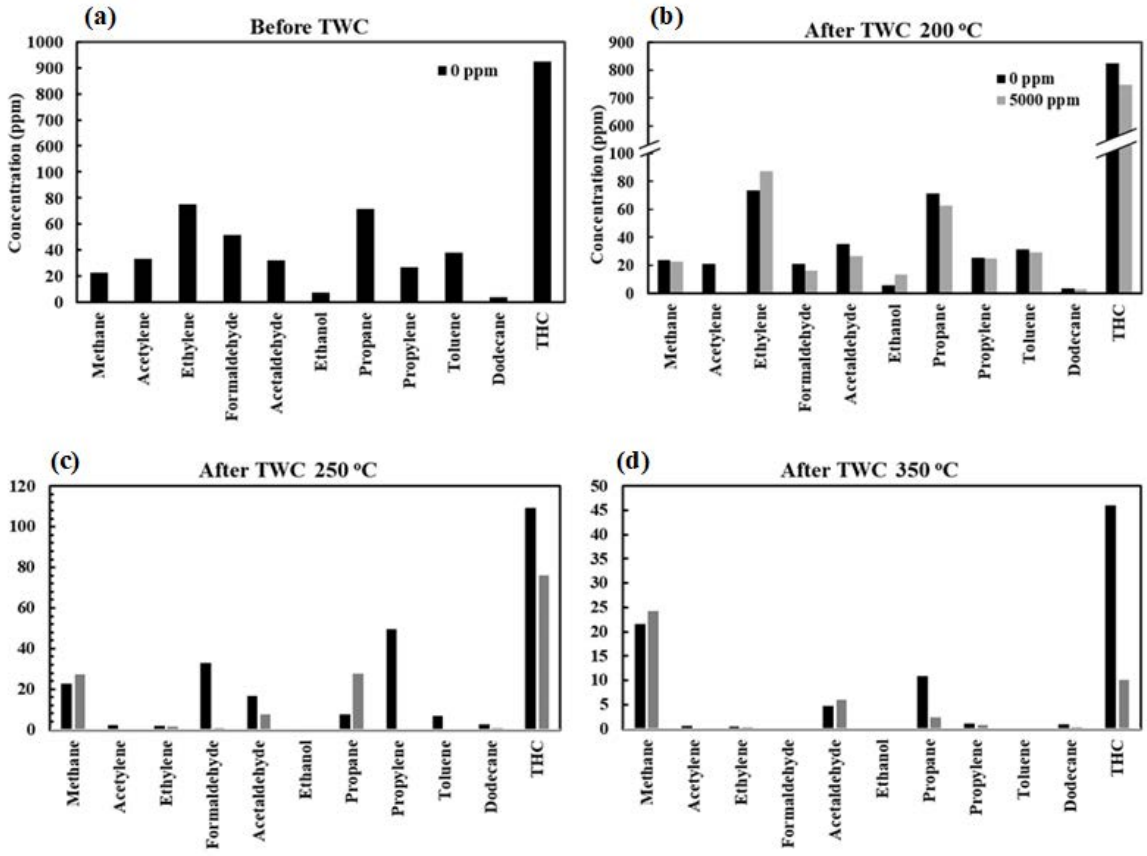

Figure 4-6. Concentration of hydrocarbon species measured (a) before TWC, (b) after TWC at 200 °C, (c) after TWC at 250 °C, (d) after TWC at 350 °C under lean condition with 0 and 5000 ppm hydrogen addition respectively

In Figure 4-7, the impact of hydrogen on NO light-off under the stoichiometric and lean conditions is presented. Apart from NO_x (NO and NO_2), the concentrations of NH_3 and N_2O were also studied. Even though the level of N_2O was low, it should be investigated because it is not only a greenhouse gas which promotes global warming but is also an ozone destroyer as well. Under stoichiometric condition, the NO_2 level is negligible, so only lean condition NO_2 production is included in Figure 4-10. Overall, the NO light-off and reduction rates were significantly enhanced for both conditions with the presence of extra hydrogen, particularly for the lean condition. The more hydrogen added, the more enhancement effect can be achieved.

For the stoichiometric condition, 1000 ppm H_2 addition results in an approximate 18 ºC reduction in NO light-off temperature compared to the baseline case; while the T_{50_NO} for 5000 ppm H_2 is almost 100 ºC advanced compared to the baseline condition. It was previously reported by Abduhamid [81], DiGiulio [80], and Nova et al. [92] that hydrogen shows best NO reducing activity compared to other reductants, like CO and HC. Forzatti et al. [78] also suggested that the NO-CO reduction did not take place at temperatures below 180 ºC. Therefore, it is suggested that the significant improvement in low temperature NO conversion was attributed to the fact that hydrogen was acting as a direct reducing agent for NO and exhibiting superior reducing activity. Additionally, as previously discussed for CO and HC light-off, hydrogen addition to the exhaust stream enhanced the competition for O_2, thereby promoting the NO-CO and NO-HC reduction reactions.

As it is known that the TWC is ineffective in NO_x removal under lean exhaust environment. Therefore, the hydrogen addition effect under lean condition will be discussed in detail here. For the baseline condition, NO conversion starts around 210 ºC. The overall NO conversion efficiency is very low with the maximum of approximately 10%, which is a characteristic for TWCs under lean conditions. When adding 1000 ppm of hydrogen to the exhaust stream, the NO reduction is initiated at very low temperature. It is noted that hydrogen addition upstream of the TWC promotes this low temperature NO reduction and the total NO conversion. Figure 4-7 indicates that nearly 55% of NO can be converted when the temperature reaches 160 ºC with 5000 ppm hydrogen addition.

For this case, two peaks can be observed for both NO and N_2O profiles (marked on Figure 4-7 and Figure 4-8). This dual-peaks feature can be explained by the transformation of the primary NO reduction pathway from NO-H_2 to NO-CO and NO-HC as the temperature increases. The first and second peaks occurred at around 160 ^oC and 230 ^oC, which is in accordance with the H_2 and CO profiles that the majority of hydrogen and CO was depleted at around 160 ^oC and 230 ^oC (see Figure 4-2 and Figure 4-3). Similar dual-peaks trend of NO_x light-off curve can be found in the study by Botas et al. [93] and Mejía-Centeno et al. [160].

Although the hydrogen addition leads to the formation of NH_3 and N_2O, which are not desirable products, it should be mentioned that the NH_3 produced over the TWC can be subsequently stored by a downstream NO_x removal urea-SCR. This can help solve the NH_3 slip issue of the TWC and reduce the expense of carrying an additional urea storage tank for the SCR. Additionally, N_2O was reported to be beneficial for soot removal. Davies et al. experimentally studied the catalysed chemistry of simultaneous soot oxidation and NO_x reduction over a silver-based catalyst, suggesting that the oxidation of trapped soot can be effectively initiated by N_2O which is formed via non-selective NO_x reduction by NH_3 at low exhaust gas temperature [63]. This finding can inspire the idea of designing an aftertreatment system composed of a commercial TWC brick, and a filter coated with the silver-based catalyst to utilise the N_2O and NH_3 generated over the first brick for the *in situ* soot oxidation over the downstream filter. Therefore, such an aftertreatment system could help remove both gaseous and particles emissions from the

fuel-efficient lean burn GDI engines.

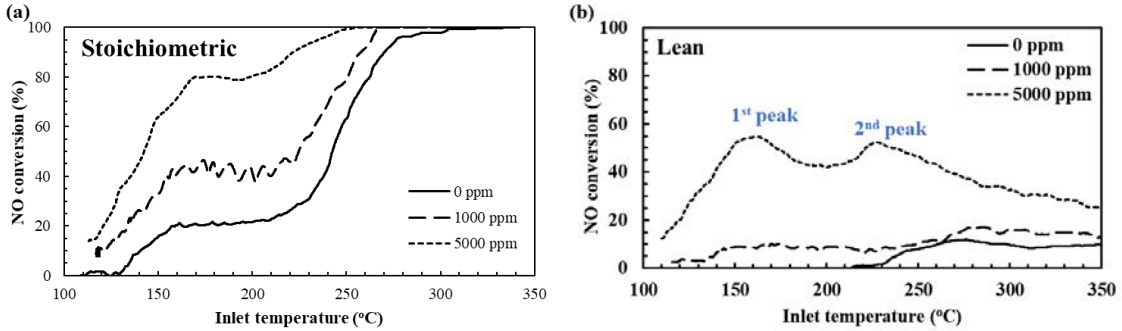

Figure 4-7. Impact of H_2 addition on NO light-off performance over the TWC under (a) stoichiometric and (b) lean conditions

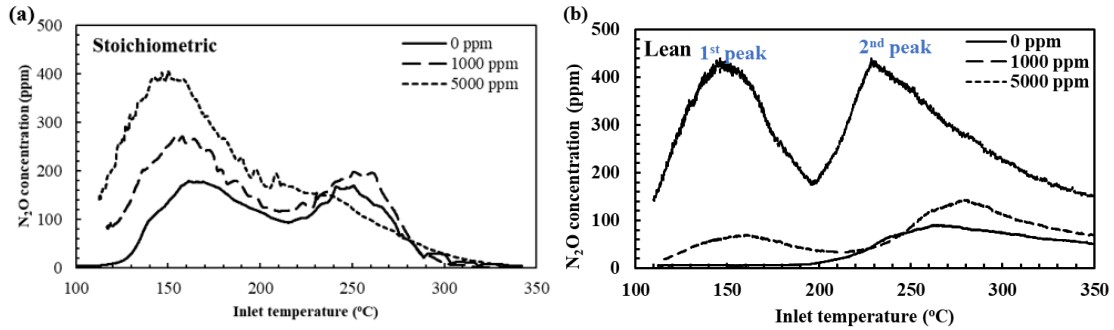

Figure 4-8. N_2O production with different concentrations of H_2 injection under (a) stoichiometric and (b) lean conditions

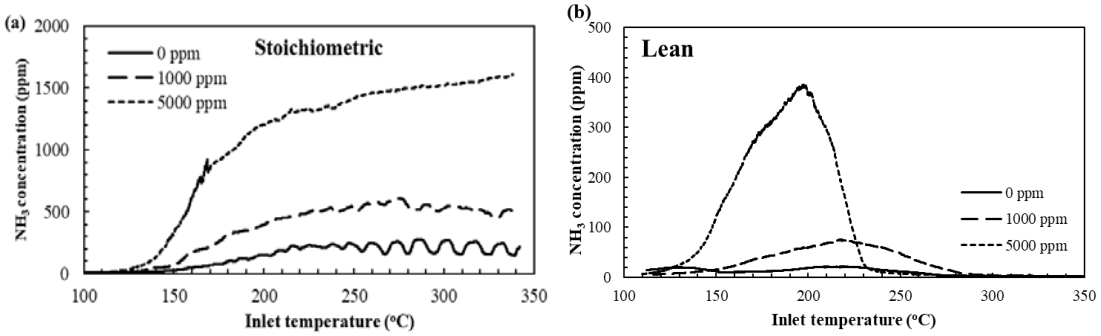

Figure 4-9. NH_3 production with different concentrations of H_2 injection under (a) stoichiometric and (b) lean conditions

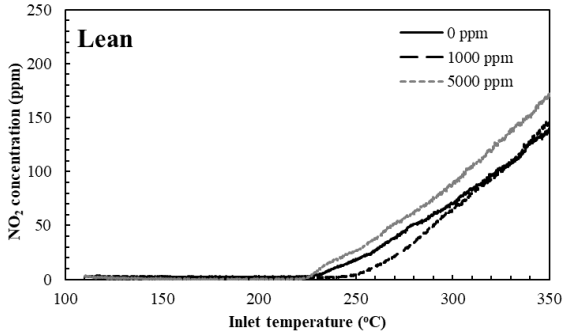

Figure 4-10. NO_2 production with different concentrations of H_2 injection under lean condition

4.3.2 Light-off modelling

Based on the light-off data, corresponding parameters tuning was performed to minimise the difference between the model prediction and the experimental data. As previously discussed in section 4.3.1, hydrogen addition under lean condition is more beneficial to the TWC light-off in terms of CO, HC and NO_x conversion. Therefore, the simulation of the TWC light-off in the following paragraphs will be only focused on lean conditions. Firstly, the activation energy and rate constants were estimated based on light-off data obtained from the baseline condition following the parameter optimization process as described in section 3.3. As indicated by Figure 4-11, good agreement between experimental data and model prediction was achieved. It is of note that the light-off temperature of the CO and HC can be successfully calculated by the model, and the overall conversion trend of the NO and H_2 can be well captured.

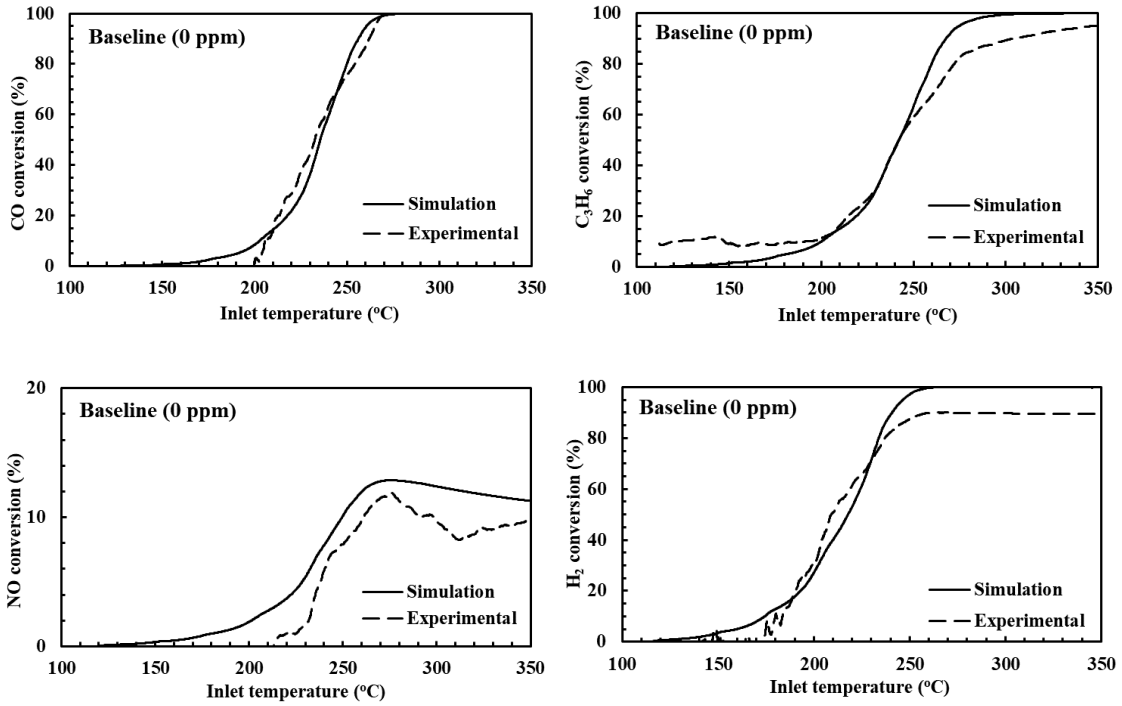

Figure 4-11. Experimental and modelling light-off curves of CO, C_3H_6, NO and H_2 for the baseline and lean condition (0 ppm hydrogen addition)

To model the cases with H_2 addition (1000 and 5000 ppm conditions), the kinetic parameters obtained from the baseline condition were used. Figure 4-12 compares the conversion curves of CO, C_3H_6, NO and H_2 obtained from the simulation and experiment for those two conditions. The comparison implies that using the parameters calibrated based on the baseline case cannot correctly predict the TWC performance with extra H_2 addition to the feed gas (engine-out exhaust). For NO conversion curves with both 1000 and 5000 ppm hydrogen addition, two peaks can be observed in the experimental light-off curves, while there is only one peak for the simulation prediction. On the simulated light-off curve (5000 ppm), the peak occurs at approximately the same temperature (around 235 ^oC) as the second peak of the experimental curve. As previously discussed in section 4.3.1, NO reduction at lower temperatures is substantially enhanced by H_2

addition; however, this low temperature improvement effect is not shown in the simulation results. In addition, the experimental data indicates larger improvements in the overall NO conversion than the modelling results. As mentioned in section 3.3, the heat release from catalytic reactions contributes as an important term for solving the gas-phase energy conservation equation (see Equation 3-4). The exothermic hydrogen oxidation is included in the model. Therefore, it can be hypothesised that there are other reasons (e.g., chemical effect as mentioned earlier) for the observed enhancements due to the H_2 addition rather than only the exothermic effect. Similar hypothesis can be made by comparing the experimental and simulation CO light-off results for the 5000 ppm H_2 addition case. This will be further discussed in section 4.3.3.

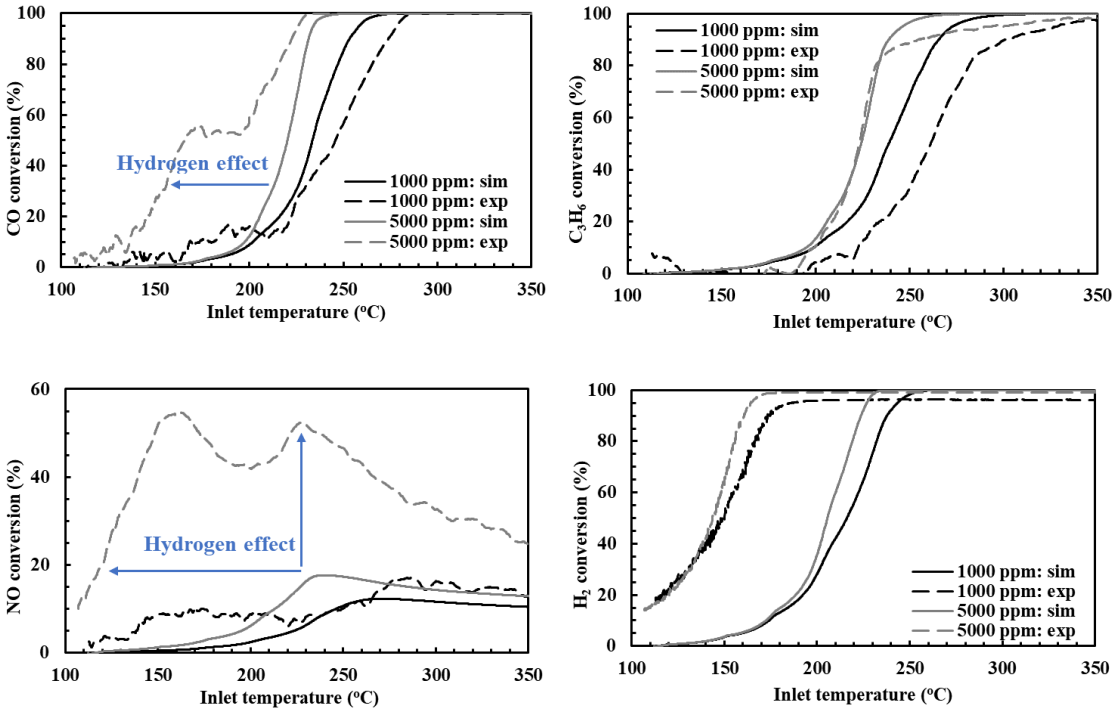

Figure 4-12. Comparison of experimental and modelling light-off curves of CO, C_3H_6, NO and H_2 for 1000 and 5000 ppm hydrogen addition lean conditions. Previously obtained reaction activation energy and rate constants (estimation based on baseline condition) are used. (Solid line: simulation; dashed line: experiment)

4.3.3 Kinetic parameters tuning for hydrogen addition cases

The activation energy and pre-exponential factor for each reaction under 1000 and 5000 ppm H_2 addition conditions were estimated via the parameter tuning process described in section 3.3. The comparison between the simulation (using the tuned parameters) and the measured TWC light-off curves for the 1000 and 5000 ppm hydrogen addition cases is presented in Figure 4-13. It can be seen that the simulation light-off curves match with the experimental curves well. Therefore, the kinetic parameters estimated for different conditions are reliable to some extent and some conclusions can be made from analysing the data. The derived parameter values are summarised in Table 4-3. According to the Arrhenius equation for calculating the chemical reaction rate (see Equation 3-17), the reaction rate is dependent on the values of the corresponding rate constant and activation energy. Once the reaction proceeds (passing the activation energy), the reaction rate will be mainly controlled by this rate constant, and an increase of the rate constant leads to a consequent increment of the reaction rate.

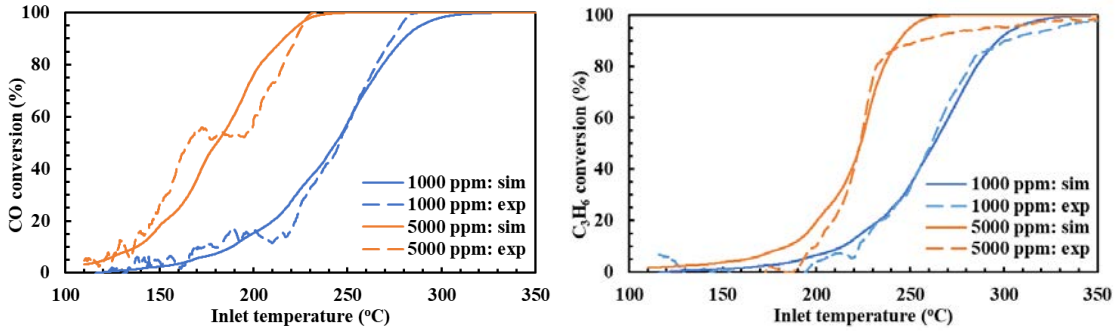

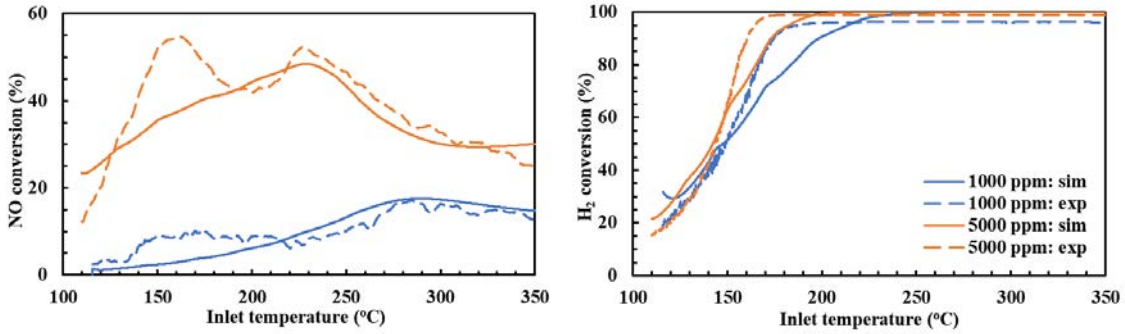

Figure 4-13. Comparison of experimental and modelling light-off curves of CO, C_3H_6, NO and H_2 for 1000 & 5000 ppm hydrogen addition cases under lean condition. Modified reaction activation energy and kinetic constants (separate estimation based on 1000 and 5000 ppm condition) are used.

Some researchers have reported that H_2 can effectively promote CO oxidation by modifying the catalyst surface and moderating the self-inhibition of CO. Consequently, more free active sites are released, which enables oxygen absorption and then reaction with CO [89, 161]. Based on Table 4-3, it can be seen that the activation energy for CO oxidation (E1) was largely reduced with the hydrogen addition from the baseline 9.39E+03 to 5.25 E+03 and 4.89 E+03 for the 1000 and 5000 ppm hydrogen addition cases. Thereby, it is suggested that the hydrogen addition can significantly reduce the activation energy for CO oxidation and suppress the CO self-inhibition effect, thereby enhancing the CO low temperature oxidation activity which is in line with the experimental results discussed in section 2.5.1 and the researchers' statements. A larger reduction can be detected for a higher hydrogen concentration condition. As for the NO reduction, the activation energy of the NO-CO, NO-H_2, and NO-C_3H_6 reduction is decreased simultaneously, resulting in a combination effect for advancing the NO light-off and promoting its overall conversion performance. As for NO reduction reactions (R4

to R6), it is noted that the initial activation energy of NO reduction by H_2 (E5) is at the lowest level compared to that for NO-CO and NO-C_3H_6 reduction, indicating that the NO-H_2 reduction reaction is the most affected reaction pathway among those over the catalyst. This is in agreement with findings reported by Abdulhamid et al. [81] where H_2 shows superior activity in reducing NO compared to other reducing agents, such as CO and C_3H_6. Additionally, the value of K5 increases and E5 decreases more effectively when the hydrogen addition amount increases to a higher level (from 1000 to 5000 ppm). The modelling results stated above provides better understanding of the hydrogen effect on the catalyst light-off performance from the perspective of chemical kinetics.

Table 4-3- Optimised kinetic parameters based on experiments data under lean condition. (The units of rate constants and activation energy are kmol/(m^2s) and kJ/kmol respectively)

Parameter		0 ppm	1000 ppm	5000 ppm
R1 ($CO+O_2$)	K1	21.8	9.61	11.9
	E1	9.39E+03	5.25E+03	4.89E+03
R2 (H_2+O_2)	K2	49.3	79.4	52.4
	E2	8.04E+03	2.81E+03	4.95E+03
R3 ($C_3H_6+O_2$)	K3	11.4	5.68	2.80
	E3	6.98E+03	6.51E+03	1.06E+04
R4 (CO+NO)	K4	11.8	12.5	14.0
	E4	9.00E+03	5.10E+03	8.98E+03
R5 (H_2+NO)	K5	6.64	12.7	17.0
	E5	4.72E+03	3.30E+03	1.51E+03
R6 (C_3H_6+NO)	K6	1.95	1.79	3.45
	E6	5.72E+03	1.30E+03	1.69E+03
R7 (WGS)	K7	9.96E-07	1.54E-06	1.10E-06

	E7	9.33E+03	5.76E+03	1.42E+04
R8 (C_3H_6 SR)	K8	9.55E-10	1.67E-09	1.48E-09
	E8	1.49E+04	1.85E+04	2.14E+04
CO inhibition term	K_{CO}	1.70E+03	8.34E+02	1.35E+03
	E_{CO}	53.08	40.77	47.51
C_3H_6 inhibition term	K_{HC}	3.33E+03	3.14E+03	4.25E+03
	E_{HC}	77.52	133.68	111.44
O_2 inhibition term	K_{O2}	2.39E+03	2.53E+03	1.55E+03
	E_{O2}	423.37	901.93	483.62

4.4 Summary

The effect of upstream hydrogen addition over a TWC under both stoichiometric and lean engine operating conditions were experimentally studied. A catalytic reaction model was developed to provide information for understanding the mechanisms involved in the hydrogen effect on the catalyst light-off activity.

Overall, the upstream hydrogen addition enhances the TWC low temperature activity under both stoichiometric and lean GDI engine operations, especially lean conditions where the CO and HC light-off were significantly advanced towards lower temperatures (by up to 67 ºC) with 5000 ppm hydrogen addition. The TWC's poor lean NO_x removal efficiency was also enhanced from approximately 10% (for the baseline lean condition with 0 ppm H_2 addition) to 55% and occurred at a considerably lower temperature.

However, it should be mentioned that the CO and HC light-off under engine lean condition might be slightly retarded with small amount of hydrogen addition (i.e., 500 or 1000 ppm) compared to the baseline case (without hydrogen addition), because the hydrogen addition accelerated the depletion rate of hydrogen. This created a certain region at lower temperatures where there was no hydrogen (for the baseline case, there was still a certain amount of hydrogen observed which was originally contained in the engine exhaust) acting as a promoter and the temperature of the catalyst active sites was not high enough for the strong CO self-poisoning effect to disappear. Regarding the 5000 ppm hydrogen addition case, this certain region was not captured due to the significant temperature increment caused by the hydrogen addition. Therefore, it is critical to find out the threshold and optimal value of the hydrogen addition amount. Also, it is noticed that the total conversion efficiency of CO was negatively affected by extra hydrogen addition under engine stoichiometric operation, which can be explained by the facilitated competition for oxygen between CO and the extra hydrogen.

The exhaust gas temperature measurements aligned with the species light-off analysis helped to reveal the underlying causes of the hydrogen promotional effect. It is suggested that the hydrogen beneficial effect can be attributed to different factors, including the exothermic effect where hydrogen oxidation leads to a temperature increment over the surface sites, and chemical reasons that hydrogen weakens the strong CO self-inhibition effect, which was also verified by the simulation study. According to the comparison of the experimental and model predicted light-off curves (considering the surface reactions

occurring over the TWC), it is noticed that the hydrogen addition affects the TWC performance through multiple mechanism rather than only the exothermic effect of hydrogen oxidation. Based on the estimated kinetic parameters for individual conditions, it is hypothesised that the hydrogen addition can effectively decrease the activation energy of CO oxidation and NO reduction, in addition to the kinetic constant of the CO self-inhibition term.

Although some amounts of NH_3 and N_2O were formed over the TWC with more hydrogen addition, the slip issue could be solved by designing a hybrid zoned TWC that utilises NH_3 and N_2O in NO_x reduction and *in situ* soot oxidation, respectively. Such an integrated hybrid zoned TWC can abate both gaseous and particle emissions from a fuel-efficient lean-burn GDI engine, and therefore help simultaneously obtain a higher fuel economy and lower emissions.

CHAPTER 5 STUDY OF A TWC-LNT SYSTEM PERFORMANCE ON A GASOLINE ENGINE

5.1 Introduction

In the present chapter, the performance of a TWC-LNT catalysts system was experimentally investigated. As discussed in Chapter 4, adding hydrogen upstream the TWC effectively improves its low temperature activity in converting CO and HC, while the lean NO_x removal performance is only marginally improved. Since the lean NO_x abatement is a focal point for lean-burn gasoline engine research, thus a downstream LNT catalyst is implemented in the aftertreatment system to provide supplementary NO_x reduction. The TWC-LNT catalysts system was experimentally studied in terms of the conversion efficiency of major pollutants (CO, THC, NO_x), the NO_x reduction selectivity, and the exhaust chemistry over the system. Different types of tests were conducted to explore the LNT performance under various conditions, including the cold start tests, transient lean/rich tests, and different operating temperature tests. For this purpose, two catalysts set-ups were developed and tested using the three-cylinder DI/PFI gasoline engine, including: (1) Full-scale set-up: TWC and a downstream LNT assembled on the exhaust system; (2) Small-scale set-up: TWC assembled on the exhaust canning and a mini-LNT placed downstream in a heated reactor to allow temperature adjustment by a

furnace.

5.2 Experiment design and basic testing procedures

5.2.1 Experimental set-up

In the present chapter, all experiments were conducted on the DI/PFI 3-cylinder Ford gasoline research engine. Apart from the cold start experiments, the remaining experiments were examined at 1.68 bar BMEP and 2100 rpm engine speed using DI mode with engine cycling lean/rich operation (50 s lean phase at λ = 1.15 and 10 s rich phase at λ = 0.9), unless otherwise stated.

(1) Full-scale testing bench set-up

The full-scale system experimental set-up schematic is shown in Figure 5-1. The aftertreatment system consists of an upstream TWC and an LNT, and both catalysts are full-size. More details can be found in Table 3-3. Prior to the experiment, the TWC and LNT catalysts have been thermally aged for 5 hrs using the laboratory oven at 600 and 400 ^{o}C, respectively. As shown in Figure 5-1, raw engine exhaust gas was sampled and analysed by related instruments at engine out, TWC-out, and LNT-out respectively. Exhaust gas temperature data were measured at both before and after the TWC and LNT.

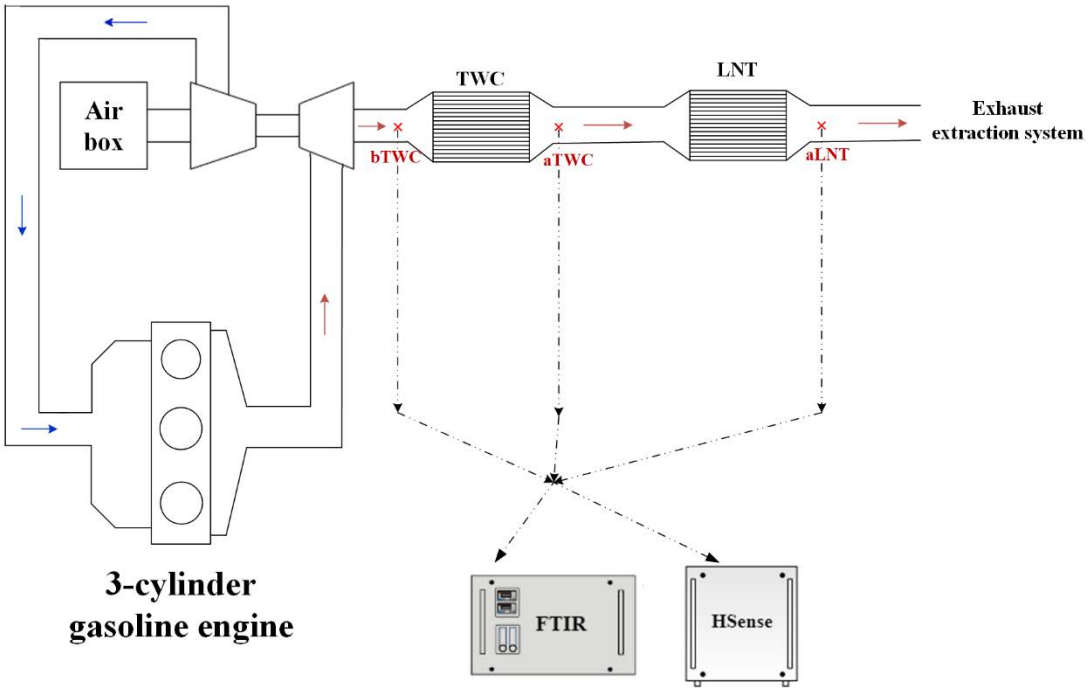

Figure 5-1. Schematic of the full-scale system experimental set-up. Dotted lines (three different sampling points): engine out, TWC-out, and LNT-out.

(2) Small-scale testing bench set-up

Schematic of the small-scale system is shown in Figure 5-2. The majority of this set-up is the same as the full-scale one, including the same engine, TWC, and exhaust species analysers. The only difference is the LNT which is of mini-scale and placed in a reactor heated by a tubular furnace. The furnace is connected to the full-scale TWC out via a heated line at 191 ºC. The operating temperature of LNT will be controlled by the furnace at fixed temperature (e.g., 150, 200, and 250 ºC). The sampling lines, connections, and basic testing procedures follow the same fashion as the full-scale tests.

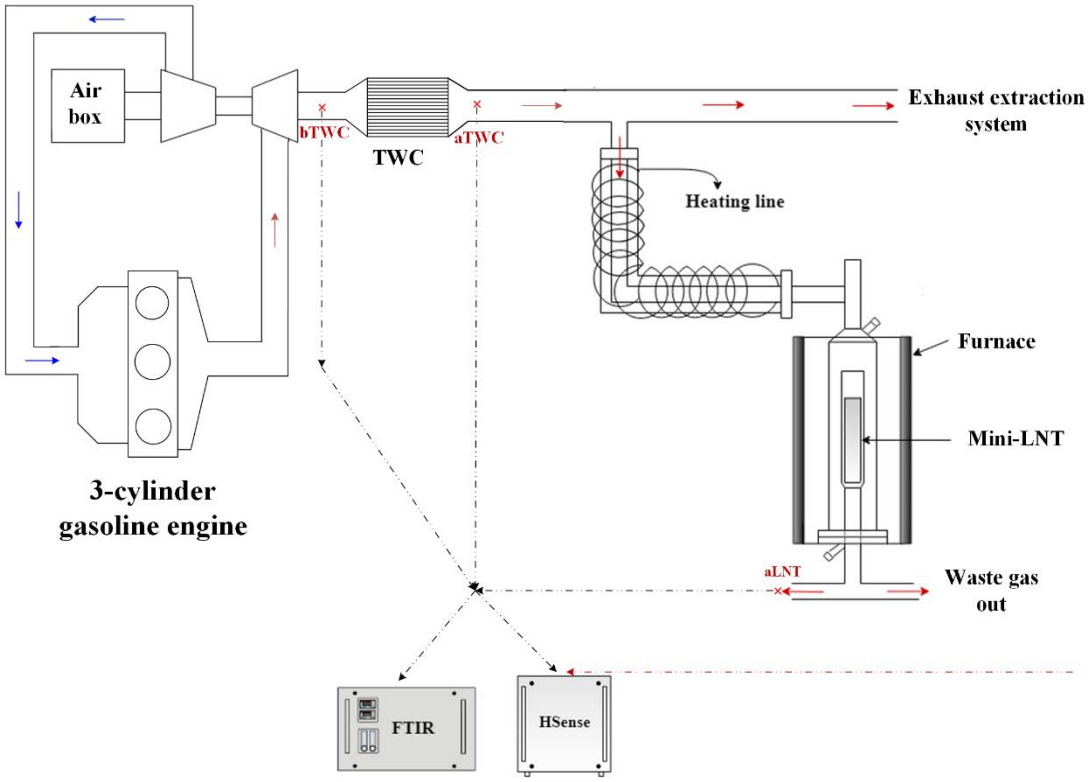

Figure 5-2. Schematic of the small-scale system experimental set-up. Dotted lines (three different sampling points): engine out, TWC-out, and LNT-out.

5.2.2 Experiment design

(1) Screening test

Screening tests were conducted to better understand the NO_x storage and regeneration phenomenon over the LNT catalyst under different conditions. It was observed that the NO_x concentration measured at LNT-out is not only dependent on the operating conditions (e.g., temperature and engine operation) but also affected by the exhaust condition that the LNT was previously exposed to. This can be explained by the LNT NO_x storage memory phenomenon. Therefore, not only the operating parameters but also the beforehand engine operation need to keep the same to minimize the experimental

errors and ensure the reliability and comparability of recorded data during the tests. Additionally, the LNT performance was examined under different engine lean/rich cycling operations, including 50 s/10 s cycle at $\boldsymbol{\lambda}$ = 1.15&0.9, 50 s/10 s cycle at $\boldsymbol{\lambda}$ = 1.2&0.9, 50 s/10 s cycle at $\boldsymbol{\lambda}$ = 1.15&0.925, 55 s/5 s cycle at $\boldsymbol{\lambda}$ = 1.15&0.9. Comparing the engine's operational stability and LNT performance observed under those conditions, the lean/rich cycle of 50 s/10 s duration at lambda value of 1.15&0.9 was employed as a default engine cycle for the following study. Details of these screening tests can be found in Appendix A.

(2) Cold start test

Engine cold-start emissions have always been a major issue. Understanding the aftertreatment system performance at low temperatures is significant for short distance driving where the time is insufficient for the engine and aftertreatment system to be warmed up. Moreover, it can help with the design and optimisation of hybrid electric vehicles (HEV) emissions control system as they have frequent starts and stops. Cold start performance of the TWC-LNT catalysts under both stoichiometric and lean conditions are of our interest; while starting engine directly with lean operation might lead to poor combustion stability and low reliability of results. Accordingly, a special 'lean' cold start test, where engine was running at stoichiometric in the first 170s to ensure stable engine operation and then switched to lean operation ($\boldsymbol{\lambda}$ = 1.15), was designed and performed. The temporal profiles of those two cold start tests are shown in Figure 5-3. Both tests

were carried out using the full-scale set-up. During both tests, engine was started from ambient temperature (15 ± 2 °C) and operated with PFI mode to ensure smooth operation. According to preliminary studies, a specific engine operation cycle (named as 'dragon cycle') was designed and operated for engine cold start to ensure the COVs being controlled at a satisfactory level (below 5%). During the tests, engine torque and speed were recorded by CADET (see Figure 5-3 (a)). For both tests, repeated experiments were conducted on separate days to enable the emissions data collection at engine out, TWC out and LNT out. Discussions on relevant experimental results are presented in Chapter 5.3.1 (1).

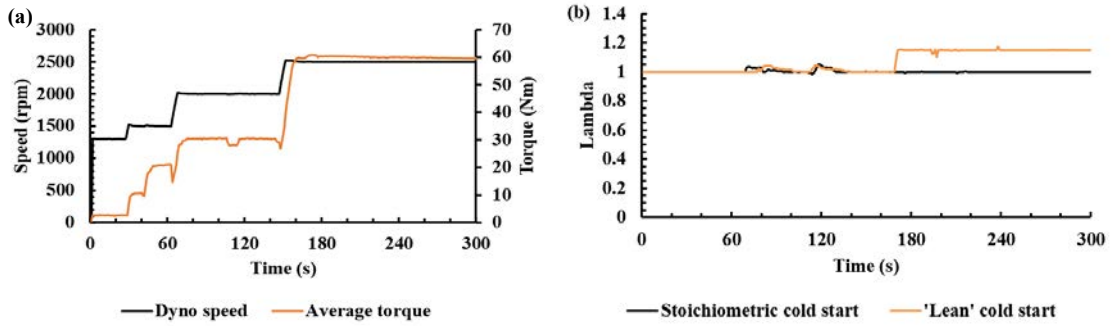

Figure 5-3. (a) Engine speed and brake torque during cold start, (b) Lambda value for two cold start tests

(3) Lean and rich cycling test

Transient lean/rich cycle is required for NO_x storage and regeneration over the LNT catalyst. Generally, the duration of lean period is 30-600 s and the rich period lasts for 1-10 s [162]. Based on screening tests results, the engine lean/rich cycle of 50 s at λ = 1.15 and 10s at λ = 0.9 was employed (see Figure 5-4). Relevant experiments were conducted using the full-scale testing bench. During the tests, emissions data was recorded at engine

out, TWC out and LNT out to help understanding the real engine exhaust condition over the TWC-LNT system. The cycle-averaged results were analysed based on the last 5 cycles (300 s) of measurement for each case after reaching a cyclic steady-state to reduce the influence of beforehand exhaust condition on LNT-out NO_x levels as previously mentioned. Corresponding results will be discussed in Chapter 5.3.1 (2).

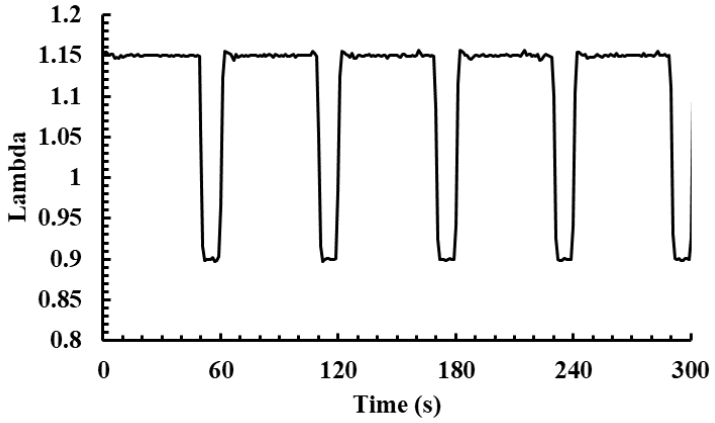

Figure 5-4. Lambda profile for the engine lean/rich cyclic operation

(4) Effect of LNT operating temperature test

It is known that the LNT activity is largely affected by the operating temperature. To explore the temperature dependence of LNT, relevant experiments were conducted via the small-scale testing bench. During the tests, LNT operating temperature was fixed by the furnace at 150, 200, and 250 ^{o}C, respectively under constant GHSV of 25,000 h^{-1}. Likewise, the engine was operated under lean/rich cycle as illustrated in Figure 5-4. It should be mentioned that the TWC operating temperature was not controlled by the furnace and will only be affected by changing the engine operating conditions in present study. Data analysis and results discussion are included in section 5.3.2.

(4) No upstream TWC test

Apart from the operating temperature and the lean/rich phase duration, effective regeneration of LNT will be also affected by the reductant chemistry, namely, concentrations of the major reductants (H_2, CO, THC, and NH_3). It is noted that the upstream TWC can directly alter the reductants' concentrations in the exhaust feed to LNT via various catalytical reactions. Accordingly, relevant experiments were performed to examine the reductant chemistry and the overall performance of a LNT catalyst when removing the upstream TWC. This can be conveniently conducted on the small-scale testing bench by connecting the furnace directly to engine out (see Figure 5-5). The remaining settings are kept the same as the original small-scale LNT experimental set-up. The LNT operating temperature was fixed by the furnace at 200 ºC under constant GHSV of 25,000 h^{-1} (See Chapter 5.3.3 for results discussion).

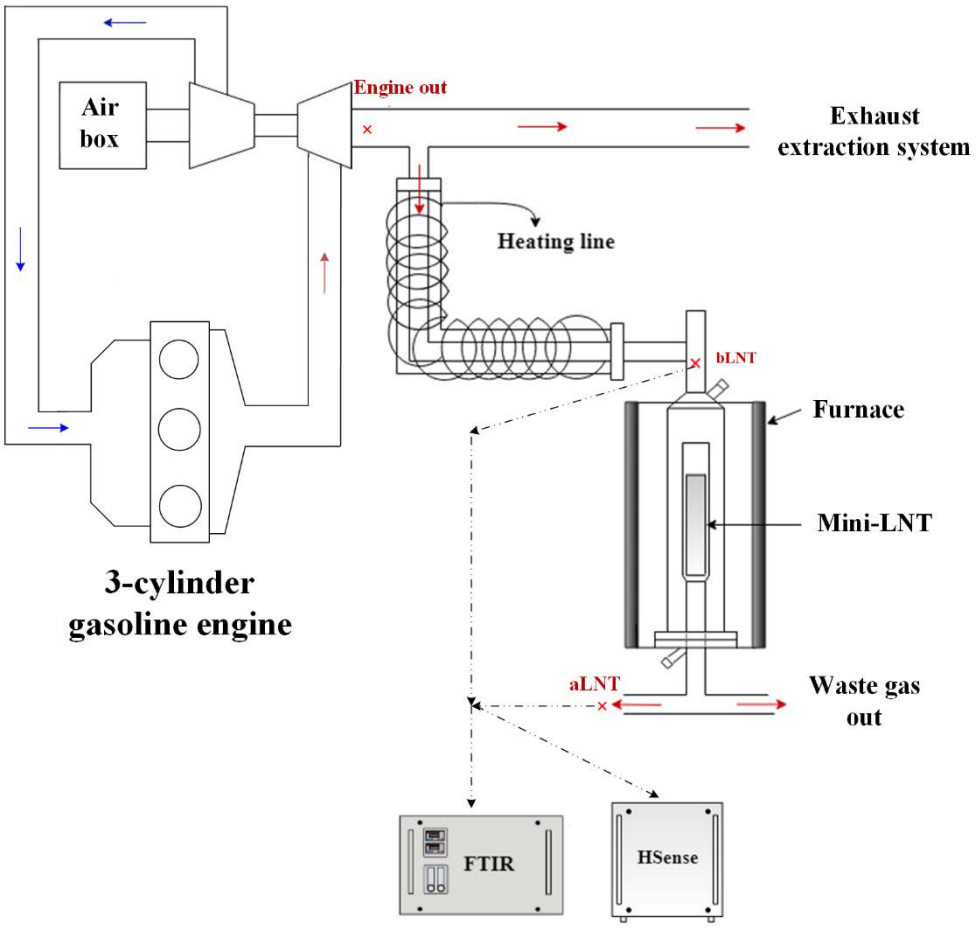

Figure 5-5. Schematic of the small-scale LNT experimental set up without the upstream TWC

5.3 Results and discussion

5.3.1 Evaluation of TWC-LNT performance under a set of various scenarios

(1) During engine cold start

Stoichiometric cold start test was firstly conducted. The exhaust gas temperatures measured at different locations along the aftertreatment system are presented in Figure

5-6. Figure 5-7 shows the concentration profiles of CO, THC and NO_x measured at engine out, TWC out and LNT out. In the first 100 s, the TWC and LNT operating temperature is below 150 ºC where the activities for both catalysts are low, resulting in certain amount of CO, THC and NO_x slips. As engine is warming up, the exhaust gas temperature gradually climbs to the range of 500-600 ºC and then stabilizes after 400 s. Meanwhile, the TWC and LNT is activated with the increasing temperature and the emissions can be fully reduced. It should be mentioned that the spike observed in THC profile at LNT out (see Figure 5-7) is caused by transition of engine torque and speed during cold start test. To help understanding the function of TWC and LNT, the accumulated emissions in the first 300 s are calculated and corresponding profiles are shown in Figure 5-8. Comparing the accumulated emissions at LNT out to TWC out, it is noticed that the CO and THC emissions at LNT out are effectively lower than that at TWC out. Thereby, it is suggested that the LNT acts as a 'secondary TWC' to provide additional conversion of CO and THC under engine stoichiometric operation. As for NO_x, the accumulated emissions recorded at LNT out are slightly lower than TWC out. According to Figure 5-7 (a), in the first 120 s when the aftertreatment system is at lower operating temperature, the LNT shows better NO_x reduction performance than the upstream TWC. As the exhaust system is gradually warmed up (after 120 s), the TWC is triggered and therefore NO_x is gradually removed over the TWC. In the first 300 s of the cold start under engine stoichiometric operation, it is calculated that 69.83% of engine-out NO_x emissions are removed over the TWC and another 4.09% are reduced over the downstream LNT, yielding an overall NO_x reduction

of 73.92% over the TWC-LNT. Overall, approximate 54.24%, 32.44% and 73.92% of engine out CO, THC and NO_x emissions are reduced over the catalysts during the first 300 s of cold start period when the operating temperature is relatively low.

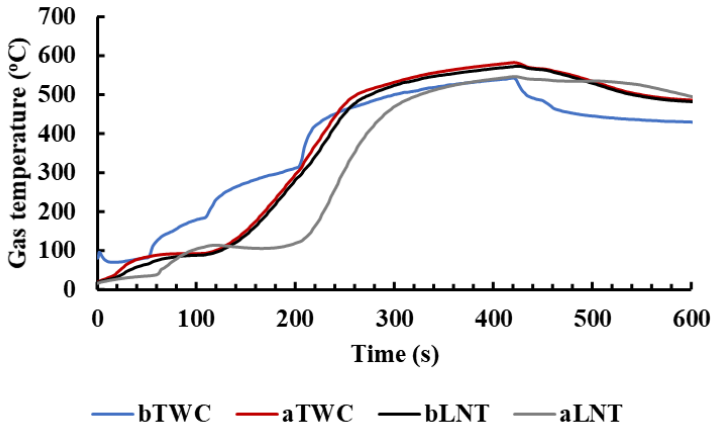

Figure 5-6. Exhaust gas temperature measured at various locations during the stoichiometric engine cold start test

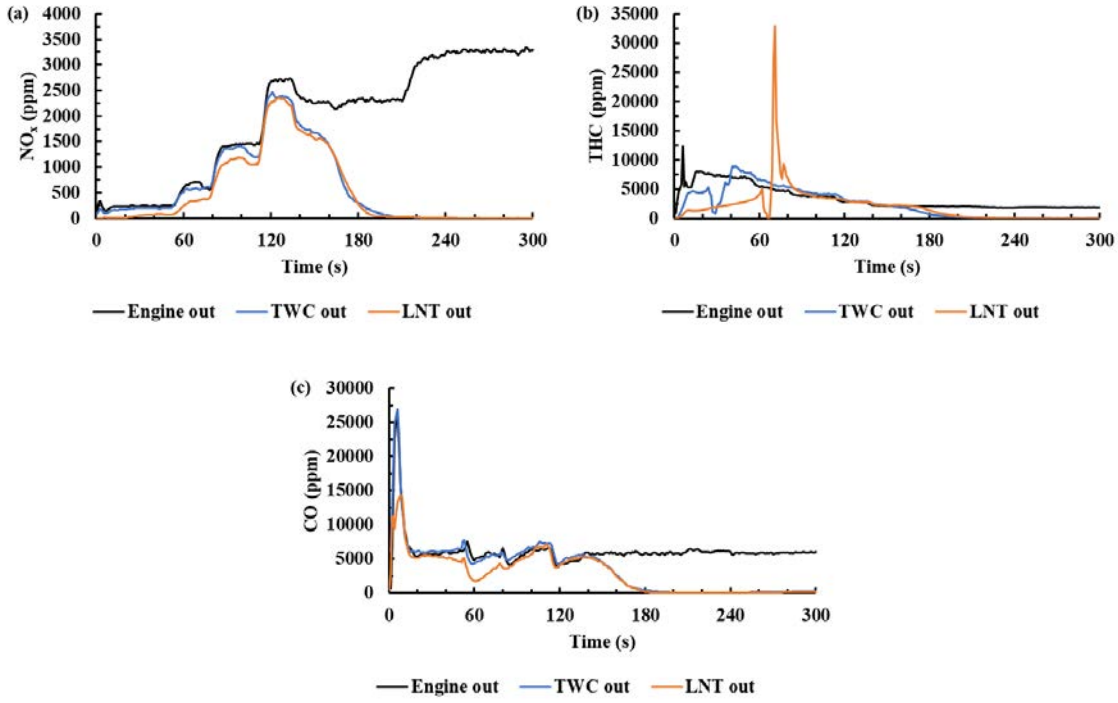

Figure 5-7. Temporal profile of the three major pollutants concentrations (a-NO_x, b-THC, c-CO) at engine out, TWC out and LNT out during stoichiometric engine cold start test

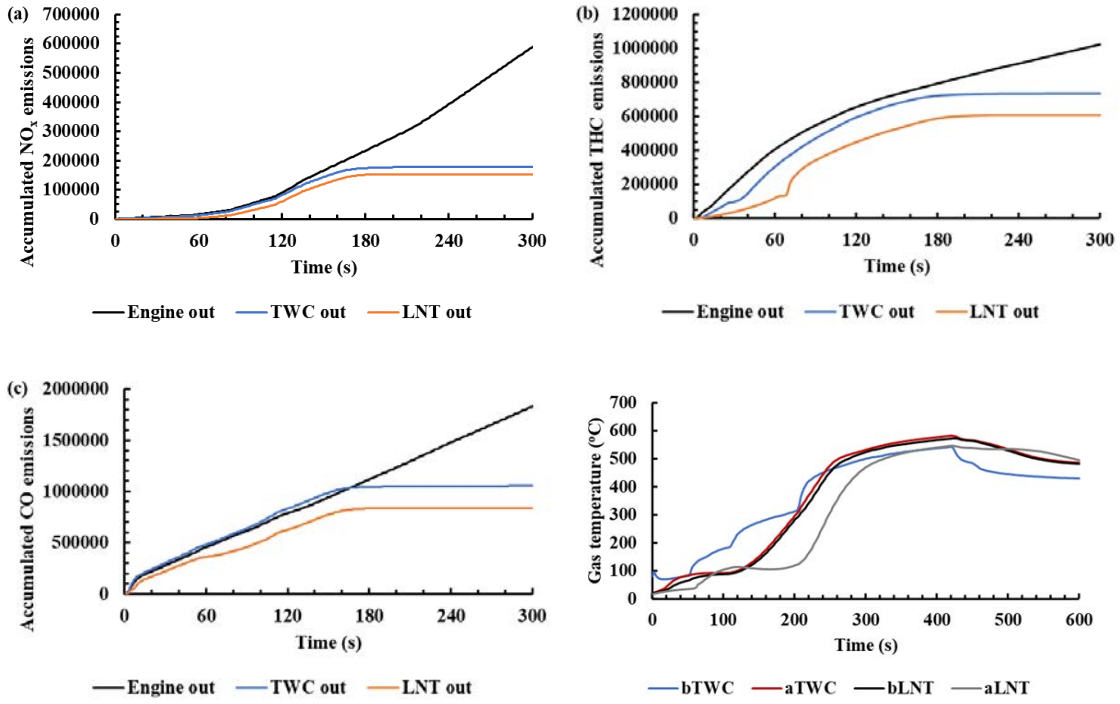

Figure 5-8. Accumulated emissions of (a-NO_x, b-THC, c-CO, in ppm) measured at engine out, TWC out and LNT out during stoichiometric engine cold start test

In addition to the stoichiometric cold start test, the TWC-LNT catalysts cold start performance under engine lean operation was also examined. Details of the lean cold start engine operation are given by Figure 5-3. Figure 5-9 compares the accumulated emissions at engine out, TWC out and LNT out recorded in the first 300 s. It is noticed that nearly no NO_x reduction is taking place over the TWC during the lean engine cold start. In the first 170 s, the exhaust gas temperature is low and TWC exhibits very low activity in reducing NO_x. According to the works presented in Chapter 4, it is believed that adding hydrogen upstream the TWC can strongly promote its low temperature activity, thus reducing the accumulated tailpipe emissions during engine cold start. Afterwards, although the aftertreatment system is gradually warmed-up, the TWC performance in NO_x reduction is limited by the lean exhaust chemistry. Under lean operating condition,

the LNT plays an important role in removing NO_x.

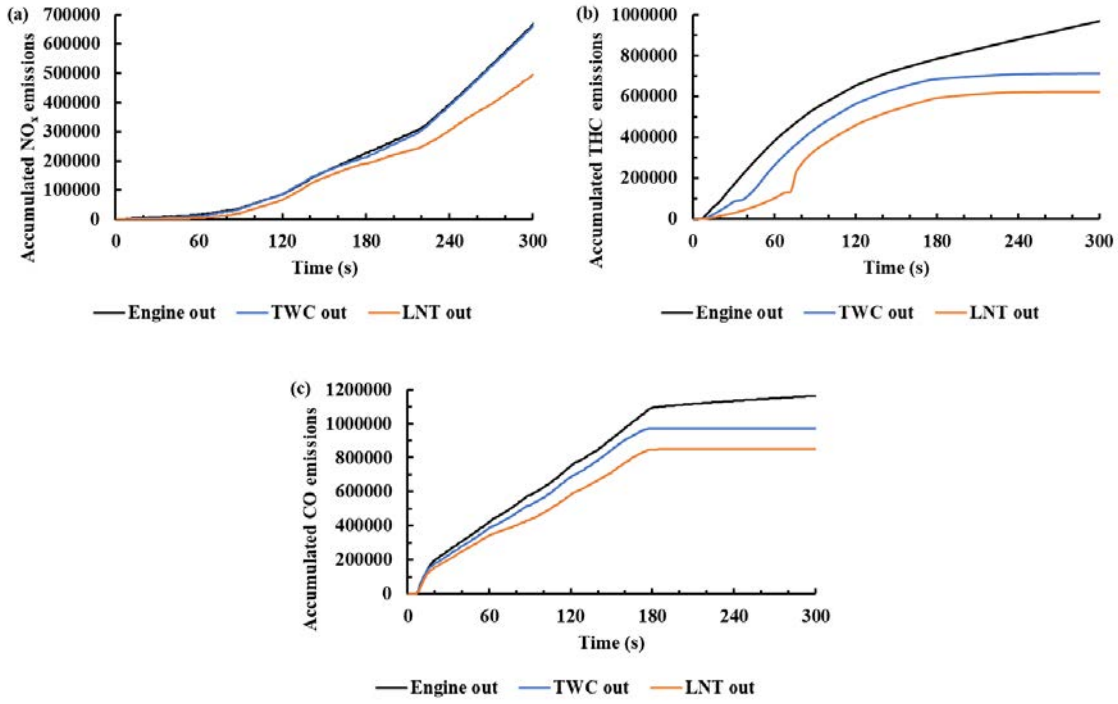

Figure 5-9. Accumulated emissions of (a- NO_x, b-THC, c-CO, in ppm) measured at engine out, TWC out and LNT out during engine cold start under 'lean' operation

(2) Under transient lean/rich cycling operation

NO_x storage and regeneration over LNT has been extensively studied for diesel exhaust; [163-165] while there is a lack of study for gasoline exhaust which generally has higher temperature than diesel. To better understand the LNT's storage and regeneration activity at relatively higher temperature, the transient lean/rich cycling test was performed using the full-scale set-up. Figure 5-10 shows the temporal profiles of exhaust gas temperature at various locations of the catalysts system. It can be seen that the exhaust gas temperature at TWC out is higher than that at TWC inlet, implying that exothermic reactions are taking place over the TWC, like the oxidation of CO, THC, and H_2. Referring to Figure 5-4, it

can be seen that during lean phase, the gas temperature at LNT out is lower than the inlet; while during rich phase, it is higher than the inlet. This implies that NO_x is stored on the LNT storage site under lean and the adsorption process is endothermic. Subsequently, the LNT catalyst is regenerated by engine rich operation. NO_x is released and then reduced by several reductants, thereby increasing the LNT-out gas temperature.

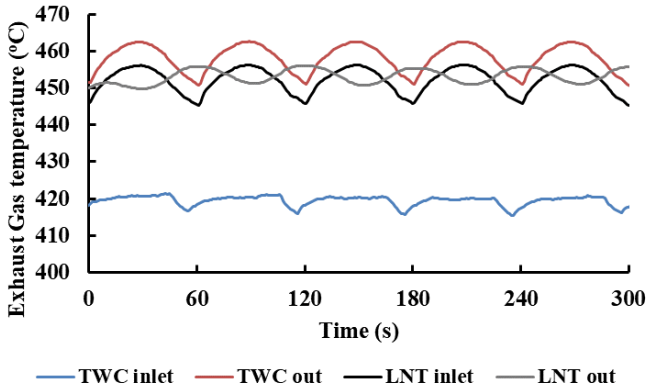

Figure 5-10. Exhaust gas temperature measured at various locations along the aftertreatment system under engine lean/rich cycling operation (50 s at λ = 1.15 and 10 s at λ = 0.9)

Figure 5-11 shows the temporal profiles of NO_x, CO, and THC concentrations measured downstream the exhaust system. With the alternating lean/rich engine operation, engine out NO_x emission level is slightly fluctuated in the range of 800-1000 ppm. Referring to the lambda profile in Figure 5-4, it can be seen that significant NO_x slips over TWC in the lean phase due to the TWC's poor lean NO_x removal performance. Subsequently, the majority of NO_x was stored on the LNT storage sites in the form of $Ba(NO_3)_2$ or $Ba(NO_2)_2$. When engine operation switching to rich, the LNT regeneration was triggered, certain amount of NO_x was released unreduced over LNT. The NO_x slips over LNT are considered to be resulted from two reasons: 1) NO_x slips during lean phase because the large amount of NO_x emitted exceed the storage capacity of this LNT catalyst; 2) NO_x

released unreduced during the regeneration period. As for the CO profile, it was noticed that the majority of CO was removed over the upstream TWC, and the remaining amount was completely converted over the LNT. Similar trend can be observed for the THC profile.

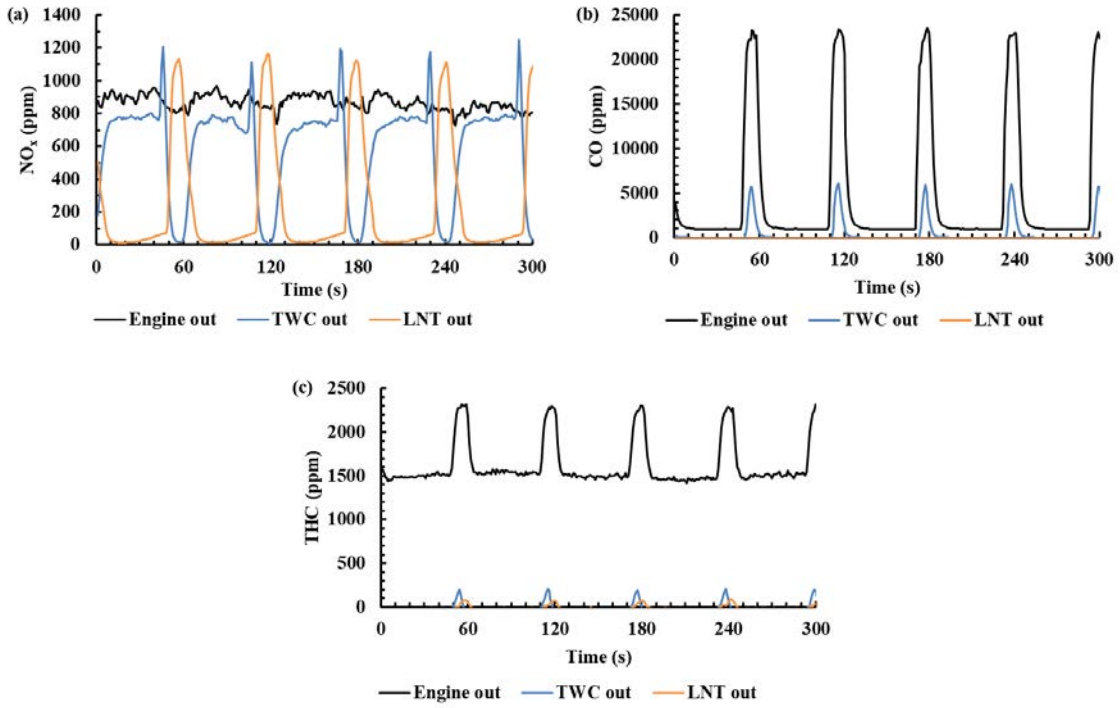

Figure 5-11. (a) NO_x and (b) CO, and (c) THC concentration as a function of time at engine out, TWC out, and LNT out under engine lean/rich cycling operation (50 s at λ = 1.15 and 10 s at λ = 0.9)

The cycle averaged conversion of NO_x, CO, and THC over TWC and the TWC-LNT system were calculated using Equation 3-33 to better quantify the TWC and LNT performance under the engine lean/rich cycle operation (50 s/10 s at λ = 1.15 and 0.9). Calculated results are presented in Figure 5-12. Overall speaking, 100% conversion of THC and CO could be reached over the TWC-LNT catalysts system. Regarding the total conversion efficiency of NO_x, 73.86% was achieved which is believed to be resulted from

the reduced $Ba(NO_3)_2$ stability over the LNT catalyst at relatively higher operating temperature. Regarding the separate role of TWC and LNT, it can be seen that the upstream TWC removed 100% and 87.95% of engine out THC and CO emissions, and the remaining fraction of CO (12.05%) was completely removed by the downstream LNT. As for NO_x, only 32.70% of engine out NO_x emissions could be consumed over the TWC, and a majority was removed by the downstream LNT. Therefore, it is suggested that under engine lean/rich cycling operation, the TWC is playing a major role in converting CO and THC, and the LNT catalyst is mainly functioning in reducing NO_x. Additionally, the LNT provides supplementary conversion for CO slips over the upstream TWC.

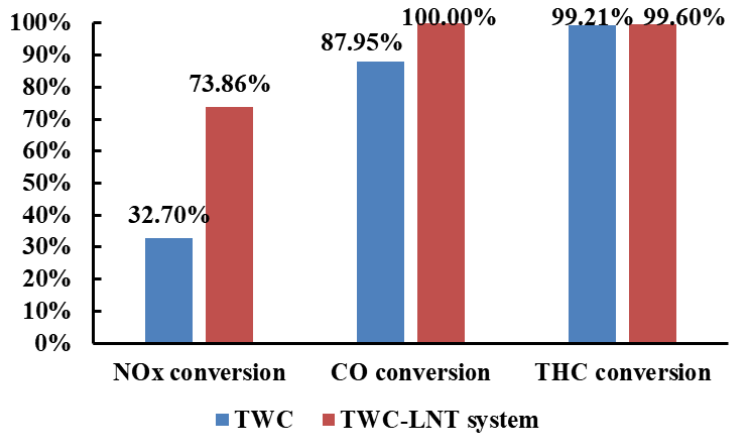

Figure 5-12. Cycle averaged NO_x, CO and THC conversion efficiency for TWC and the TWC-LNT system under engine lean/rich cycling operation (50 s at $\boldsymbol{\lambda}$ = 1.15 and 10 s at $\boldsymbol{\lambda}$ = 0.9)

Apart from NO and NO_2, the N_2O and NH_3 emissions are also a major concern since they can be formed as undesirable by-products via NO_x reduction over the catalysts. The cycle averaged selectivity of NH_3, N_2O and N_2 were calculated for TWC, LNT, and the TWC-LNT catalysts system respectively using Equation 3-34 to Equation 3-38. Corresponding results are summarized in Table 5-1. It can be seen that the NO_x reduction selectivity to

NH_3 and N_2O for TWC is 24.13% and 2.04%, suggesting that NH_3 is more favourably to be formed over the TWC; While different results were obtained for the LNT, the selectivity to NH_3 and N_2O are both very low (0.21% and 2.70%) at high temperature (around 450 ^oC). Overall speaking, the majority of NO_x (98.38%) was reduced to N_2 with only a minor fraction being converted into NH_3 and N_2O over the TWC-LNT system under the engine lean/rich cycling operation at relatively high operating temperature.

Table 5-1- Cycle averaged selectivity of NH_3, N_2O and N_2 calculated for TWC, LNT, and the TWC-LNT system under engine lean/rich cycling operation (50 s at λ = 1.15 and 10 s at λ = 0.9)

	NH_3	N_2O	N_2
TWC	24.13%	2.04%	73.83%
LNT	0.21%	2.70%	97.09%
TWC-LNT (Overall)	0.12%	1.50%	98.38%

5.3.2 Investigation of the temperature dependency of LNT performance

The LNT activity and NO_x reduction selectivity are sensitive to the operating temperature. Therefore, constant temperature study of 150, 200, and 250 ^oC was conducted using the small-scale set-up. Relevant data obtained for the full-scale LNT are also presented for reference, which will be denoted as 450 ^oC in following section. Figure 5-13 reveals the effect of operating temperature on LNT performance in terms of CO, THC and NO_x conversion. It should be mentioned that the cycle averaged species conversion efficiency presented in Figure 5-13 was calculated for the LNT based on accumulated species

emissions collected at the inlet and outlet of LNT within specific engine cycles. Large amount of CO slips (159535 ppm) was observed over the upstream TWC within the measurement engine cycles, but nearly all the CO escape from TWC can be converted over the LNT at all temperatures, even at 150 ºC. However, at temperature below 200 ºC, there is nearly no THC conversion taking place over the LNT. When temperature rises, more THC get converted with the average conversion efficiencies of 19.10% and 49.18% obtained for 250 and 450 ºC (full-scale), respectively. It should be mentioned that the majority of engine out THC emissions have been already removed over the upstream TWC. Therefore, though the THC conversion of LNT is not very high, the THC slips over LNT are not significant. As for the average NO_x conversion, it can be seen that the high temperature result (450 ºC) is relatively lower than the low temperature results. The NO_x adsorption on LNT catalyst is very sensitive to the operating temperature. It was reported that the NO_x adsorption activity is inhibited at lower temperature and the $Ba(NO_3)_2$ is not stable at higher temperature [79]. The NO_x conversion profile exhibits similar feature to the 'bell curve'. In other words, the LNT catalyst presents optimum NO_x removal performance at a specific temperature and the performance decreases when the operating temperature is either below or above this specific value. As shown in Figure 5-13 (c), the obtained NO_x conversion for 150, 200, and 250 ºC are close at around 80%, and the value for 450 ºC is around 60%. According to the reported 'bell curve' feature, it is assumed that the optimum temperature for this LNT catalyst should be in the range of 200-250 ºC. DiGiulio et al. [80] examined the temperature dependent performance of a

commercial LNT catalyst and reported that the NO_x conversion at lower inlet temperature is fairly low with the conversion efficiency observed to be around 5%, 25%, and 60% for 150, 200, and 250 ^oC, respectively. Li et al. performed relevant simulation studies on the impact of the inlet temperature on NO_x adsorption over a Pt/Ba/ Al_2O_3 based LNT catalyst. They reported that the simulated maximum site fraction of $Ba(NO_3)_2$ on the LNT at 200 ^oC is only 0.1%, implying that almost no NO_x adsorption is processing at that temperature [79]. Comparing to the literatures, the LNT catalyst studied in this thesis yield relatively higher NO_x conversion efficiency at low inlet temperature and lower value at high temperature, indicating that this specific LNT catalyst has better low temperature NO_x adsorption performance but lower stability of $Ba(NO_3)_2$ at high temperature.

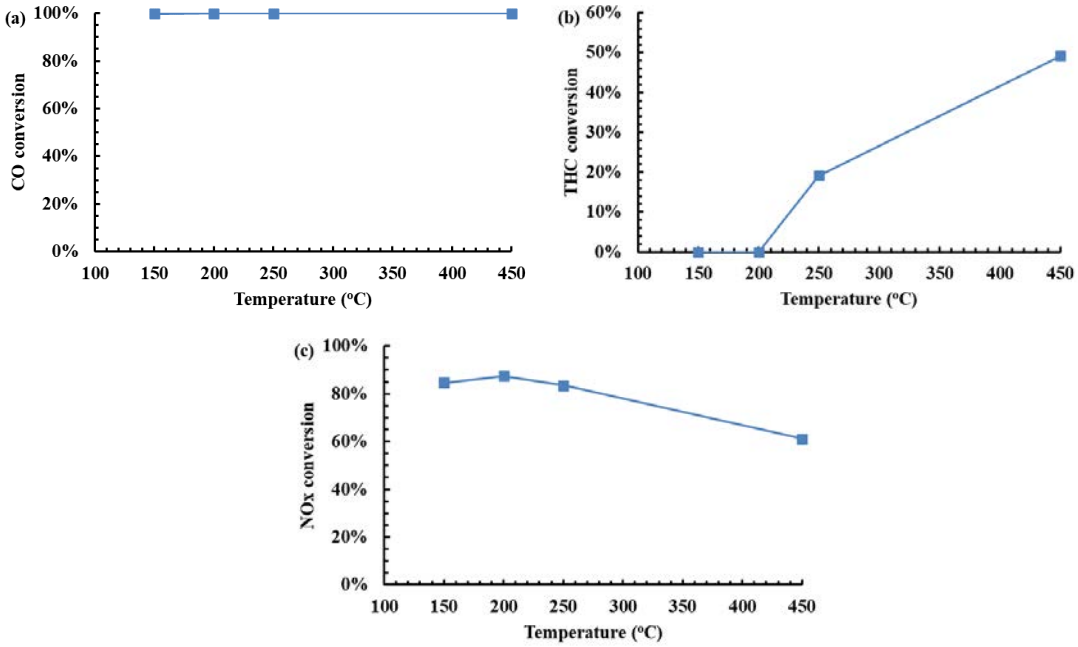

Figure 5-13. Cycle averaged (a) CO, (b) THC, and (c) NO_x conversion efficiency calculated for the LNT as a function of temperature under engine lean/rich cycling operation (50 s at λ = 1.15 and 10 s at λ = 0.9)

Corresponding results of N-containing products (N_2O, NH_3 and N_2) distribution as a

function of temperature are shown in Figure 5-14. It can be seen that the selectivity to N_2 is increasing as temperature increases. At 150 °C, the N_2 selectivity is low at around 40.72%; while for the 450 °C case, the N_2 selectivity is significantly lifted to 97.09%. It can be seen that the selectivity to N_2O and NH_3 are both dependent on temperature with the lowest value being observed at the highest temperature. This phenomenon is in line with other researchers' works [80, 166]. Overall speaking, the selectivity to NH_3 is very low at all temperatures with the maximum value below 1.2%. Comparing to NH_3, the N_2O selectivity is observed to be much higher, and the value drops monotonically with the temperature rises. It can be seen that the N_2O selectivity reaches its highest level at 150 °C or even lower which is beyond the temperature window examined in the present study. It is thereby suggested that N_2O is more favourably to be formed over this LNT catalyst rather than NH_3.

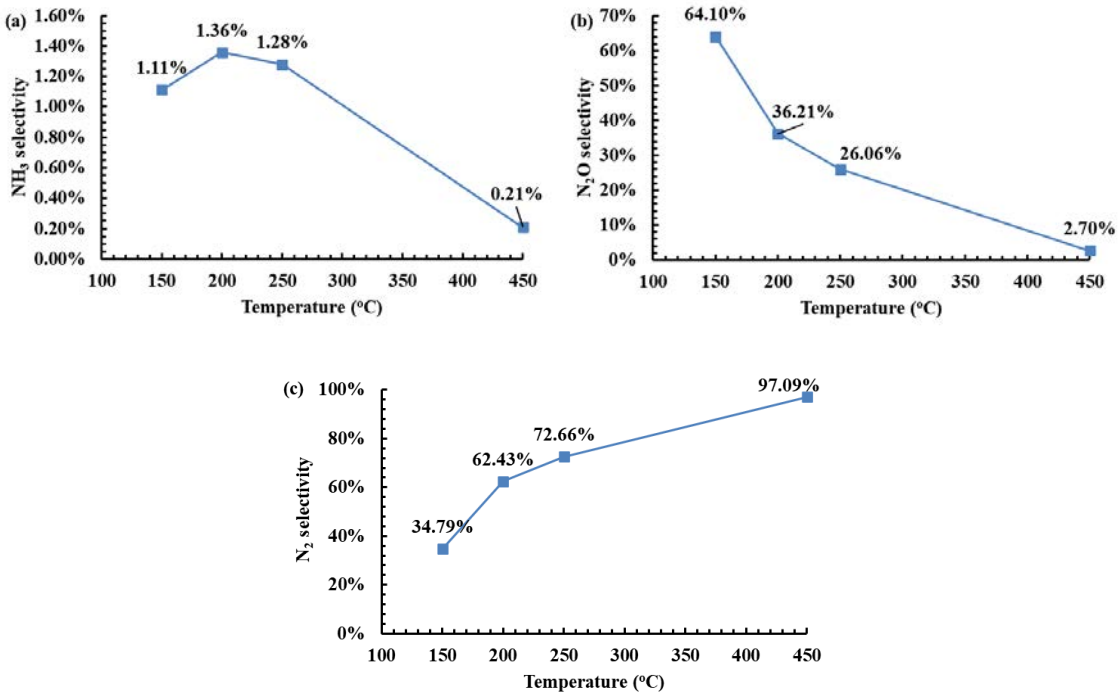

Figure 5-14. Cycle averaged selectivity of (a) NH_3, (b) N_2O, and (c) N_2 selectivity calculated for the LNT as a function of temperature under engine lean/rich cycling operation (50 s at λ = 1.15 and 10 s at λ = 0.9)

5.3.3 Study of the reductant chemistry during LNT storage and regeneration

(1) With the presence of upstream TWC

The reductants concentrations can greatly affect the LNT NO_x conversion performance. Figure 5-15 presents the temporal profiles of those major reductants measured at LNT inlet under engine lean/rich cycling operation (50 s at λ = 1.15 and 10 s at λ = 0.9). It should be mentioned that the H_2 is plotted on a percentage basis and CO is using ppm basis for better visualization. Clearly, H_2 and CO are found to be at levels of several orders of magnitude higher than THC and NH_3. H_2 was shown at the highest level with the peaks in rich phase reaching approximate 3.4%. As for CO, the peaks value during rich period is about 0.6% (6000 ppm). The THC and NH_3 levels are significantly lower with the peaks below 400 ppm. Overall, the temporal shape of those major reductants' concentration is very similar to each other, and the occurrence of the spikes are consistent with the regeneration event.

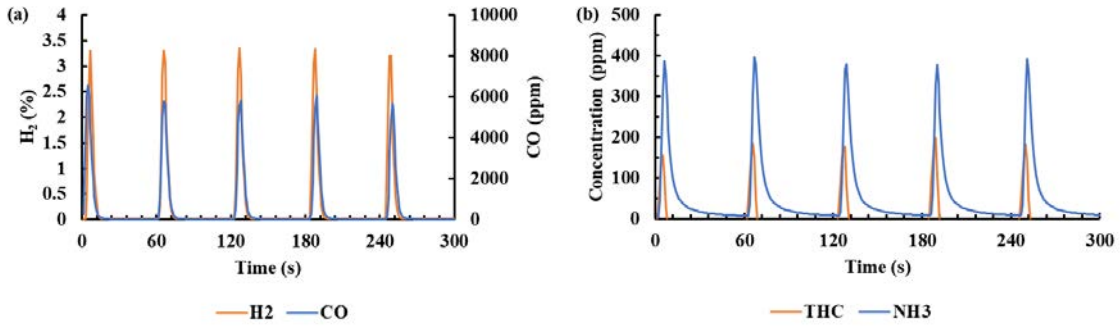

Figure 5-15. Concentrations of (a) H_2 and CO (b) THC and NH_3 as a function of time at LNT-inlet under engine lean/rich cycling operation (50 s at λ = 1.15 and 10 s at λ = 0.9)

It is believed that the upstream TWC will affect the reductant chemistry of the LNT catalyst. Therefore, the concentrations of those species were measured both upstream and downstream of the TWC. Over the observation window (300 s: 5 cycles), the cycle averaged species concentrations at TWC inlet and LNT inlet are summarized in Table 5-2. Changes in reductants levels over the TWC are also presented. It is clearly shown that the CO and THC levels are largely decreased over the TWC. While conversely, the H_2 and NH_3 concentrations are increased. Apart from the oxidation of CO and THC over the TWC, the CO and THC are also consumed via the WGS reaction and HC steam reforming reaction respectively, thereby forming certain amount of hydrogen. As previously discussed about the NO_x reduction selectivity, NH_3 is a typical and favourable by-product of NO_x reduction over the TWC under the examined condition, thereby leading to an increment of NH_3 concentration over the TWC (see Table 5-1).

Table 5-2- Changes in reductant chemistry monitored over the TWC under the baseline engine cycle operation

Cycle-averaged emissions (ppm)	CO	H_2	NH_3	THC
Pre-TWC	264864	133725	135	97033
Pre-LNT	31907	160970	4107	764
Change	−	+	+	−

(2) Without the presence of upstream TWC

For better understanding the effect of upstream TWC on LNT NO_x removal performance, relevant experiments were conducted using the small-scale set-up (but connect the LNT directly to engine out, see Figure 5-5) under engine lean/rich cycling operation. The LNT operating temperature was fixed at 200 ^oC by furnace. The cycle-averaged conversion of CO, THC, and NO_x as well as the NO_x reduction selectivity were calculated for the LNT catalyst and shown in Figure 5-16. Corresponding results obtained for the LNT from the case with an upstream TWC at 200 ^oC under the same engine cycle were provided for comparison, which is denoted as baseline case. It can be seen that the LNT's conversion efficiency for CO, THC, and NO_x is 85%, 84% and 95%. When removing the upstream TWC, the conversion efficiency for CO decreased from previous 100% to 85% . Regarding the THC conversion, it increased from previous zero level to 84%. It should be mentioned that the majority of engine out THC emissions were removed over the TWC for the baseline case, thereby resulting in limited amount of THC slips over the downstream LNT even the LNT's THC conversion efficiency is low; while for the case

without an upstream TWC, 16% of unconverted engine out THC emissions were emitted over the LNT catalyst, and this is a large quantity. Overall, it is suggested that the LNT catalyst solely is not able to completely convert the engine out CO and THC emissions. Interestingly, the overall NO_x conversion is slightly increased to 95% in the absence of TWC. As the upstream TWC is removed, the reductant concentrations at LNT inlet changed to engine-out levels, thereby leading to the variation of NO_x removal performance. Temporal profiles of the concentrations of the major NO_x reductants at pre-LNT in the absence of upstream TWC are shown in Figure 5-17. The levels of those four reductants can be ranked from highest to lowest as CO > H_2 > THC > NH_3; while for the case with a TWC upstream, it is H_2 > CO > THC > NH_3. As previously discussed, relevant reactions are taking place over the TWC (i.e., oxidation, WGS, and SR reactions), thereby altering the exhaust chemistry of the feed gas to the downstream LNT catalyst. Without the upstream TWC, the overall selectivity to NH_3 increases from previously negligible level (below 2%) to 18.85% with slight decrease being observed for the N_2O selectivity, thereby resulting in a reduction of N_2 selectivity from 62.43% to 53.65%. Although the NO_x reduction performance is improved when there is no TWC upstream, the negative influence on CO and THC conversion as well as the undesired NH_3 production cannot be neglected. Therefore, it is concluded that the upstream TWC is needed to ensure complete conversion of CO and THC emissions.

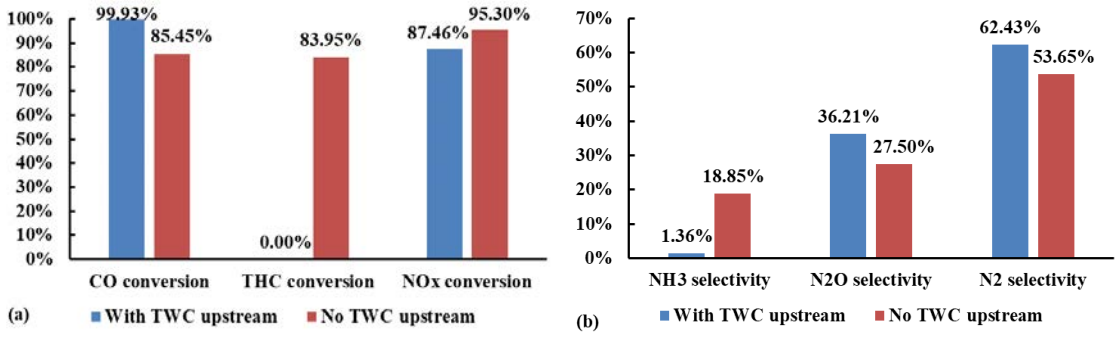

Figure 5-16. Comparison of the LNT performance for the case without an upstream TWC to the baseline case (with TWC upstream) under engine lean/rich cycling operation (50 s at λ = 1.15 and 10 s at λ = 0.9; LNT operating temperature is 200 °C for both cases)

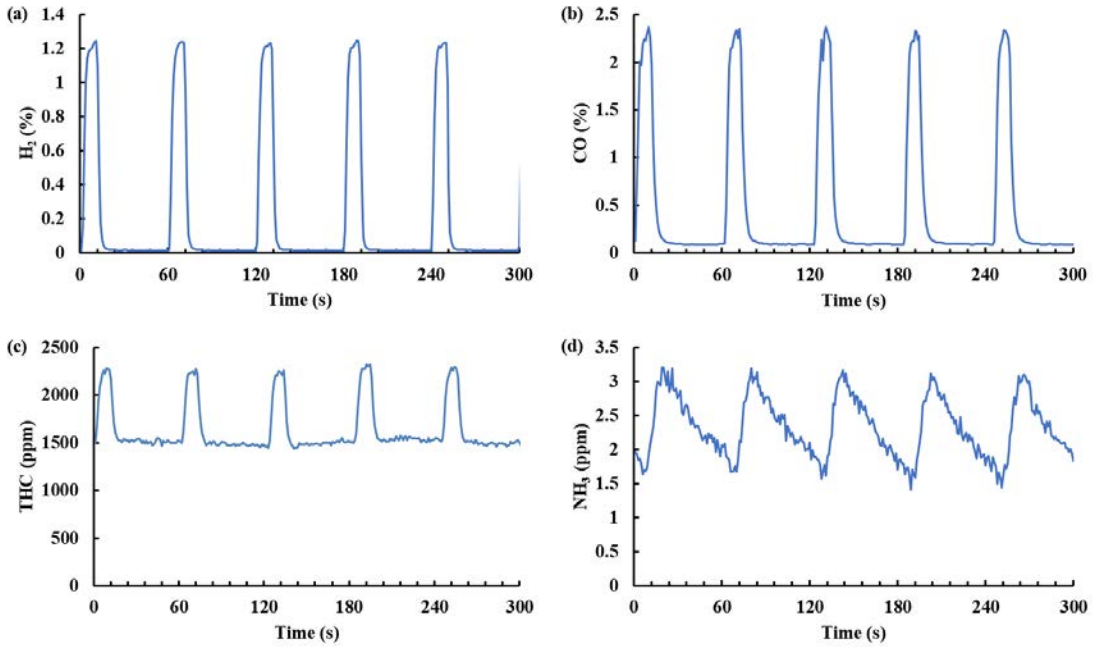

Figure 5-17. Concentrations of (a) H_2, (b) CO, (c) THC and (d) NH_3 as a function of time at pre-LNT under the baseline engine cycle

5.4 Summary

In present chapter, the performance of a gasoline engine aftertreatment catalysts system consisting of an upstream TWC and a LNT catalyst is experimentally studied under

various conditions. Although NO_x storage and regeneration over LNT has been extensively studied for diesel exhaust; while there is a lack of study for gasoline exhaust which generally has higher temperature than diesel. Moreover, it should be mentioned that corresponding experimental results were collected using actual engine testing bench rather than synthetic gas, which provides more practical and comprehensive understanding of the catalysts activity under different conditions.

During engine cold start, the upstream TWC plays as a major role in converting CO, THC and NO_x into harmless products, and the LNT is functioning as a 'secondary TWC' which provides auxiliary conversion for those species. Overall, there is still certain amount of CO, THC and NO_x escape over the TWC-LNT system due to the poor activity at low temperature.

The catalysts performance under engine lean/rich cycle operation (50 s/10 s at λ = 1.15 and 0.9) was also examined. Results indicate that the CO and THC emissions can be completely converted over the TWC-LNT and approximate 73.86% of NO_x conversion is achieved when the exhaust gas is around 450 ^{o}C. The majority of NO_x are stored on LNT surface site during lean period, and the stored NO_x are released and subsequently reduced by reductants when engine is switching to rich operation. But there are still NO_x slips over the LNT, which is believed to be related to the fact that the NO_x emissions are over the LNT storage capacity. Regarding the NO_x reduction selectivity at relative high exhaust temperature, it is observed that NH_3 is more favourably to be formed over the TWC than N_2O; while the selectivity to both species is very low over the LNT. Overall

speaking, most of the NO_x (98.38%) are converted into N_2. It is also found that the LNT performance can be greatly affected by the reductant chemistry. Therefore, the impact of upstream TWC on the reductant chemistry was also evaluated. Corresponding results indicate that H_2 and CO are the major reductants for NO_x removal during the rich regeneration period with THC and NH_3 at levels of several orders of magnitude lower. The concentrations of those reducing agents are significantly affected by the upstream TWC through catalytical reactions, including oxidation, WGS reaction, and hydrocarbon SR reactions. When removing the upstream TWC, the NO_x conversion efficiency over the LNT is slightly increased compared to the baseline case with the presence of TWC. While the negative side is the unsatisfactory level of CO and THC conversion efficiencies and more undesired NH_3 production.

The LNT performance was found to be affected by several factors, including the lean/rich cycle duration, operating temperature, and the exhaust chemistry which is strongly dependent on the upstream TWC. According to the experiments, it was observed that the LNT performance is primarily dependent on its operating temperature. The CO conversion over the LNT reaches 100% at all examined temperatures. As for the THC, very limited THC conversion occurs at temperature below 200 ^oC, and the THC conversion efficiency increases as the temperature rises. The NO_x removal efficiency as a function of temperature can be described as a 'bell curve'. Relative higher NO_x conversion efficiency was obtained at low temperature (150 ^oC) than high temperature (450 ^oC), suggesting that this specific LNT catalyst has better low temperature NO_x

adsorption performance but lower stability of $Ba(NO_3)_2$ at high temperature. The NO_x reduction selectivity was also found to be largely affected by the temperature. N_2O is more favourable to be formed rather than NH_3 at all examined temperatures over this LNT catalyst. Relative high selectivity to N_2O (64.1%) was noticed at 150 ºC and the value drops monotonically with the temperature increases.

CHAPTER 6 EFFECT OF HYDROGEN (H_2) ADDITION ON THE PERFORMANCE OF A LNT CATALYST

6.1 Introduction

Although the implementation of a LNT catalyst to the aftertreatment system of a lean-burn gasoline engine is shown to be helpful, NO_x slips can be still observed during the rich period as previously discussed in Chapter 5. Additionally, it can be observed that the periodical engine rich operation for LNT regeneration is associated with extra fuel penalty. Therefore, the idea of using upstream hydrogen addition to eliminate the NO_x slips was inspired, and the potential benefit of hydrogen addition upstream the LNT catalyst on its performance was investigated in the present chapter. For this purpose, relevant experiments were performed using an integrated engine test bench and aftertreatment catalysts system, with different levels of H_2 addition upstream of the LNT catalyst. Different sets of experiments were designed and conducted, including constant hydrogen injection experiments and cyclic hydrogen injection experiments. For the former one, engine is operating under standard LNT operating condition - transient lean/rich cycle, the potential of adding hydrogen upstream to improve the LNT performance was

examined. For the later one, engine is running lean and the concept of adding hydrogen to regenerate the LNT instead of periodic rich operation was explored.

6.2 Experiment design and basic testing procedures

As previously introduced in Chapter 5, two different experimental schematics (full-scale and small-scale) were developed and assembled. The same experimental configurations with additional integration with hydrogen injection system were used in the present chapter. H_2 is injected at TWC-out to ensure a good mixing between the added hydrogen and exhaust gas before entering the LNT. The amount of hydrogen injection is controlled by a digital mass flow controller (see section 3.2.2). After injection, the hydrogen levels were measured at each testing point by HSense at LNT inlet. To explore the possible influence of hydrogen addition on the LNT performance under different conditions, two sets of experiments were designed and conducted. Details are given as below. According to research works on exhaust fuel reforming conducted by other PhD students in the research group, it is noticed that the required amount of hydrogen can be successfully generated using an on-board fuel reformer under engine operating condition of 1.68 bar BMEP and 2100 rpm speed. Consequently, this specific testing condition was employed for both sets.

(1) Constant H_2 injection test

As it was discussed, the NO_x removal efficiency over LNT catalyst is not very satisfactory (below 85%) under engine lean/rich cycling operation with certain amount of NO_x slips over the LNT being observed during the rich period. It was previously reported by several researchers that H_2 shows superior activity in reducing NO_x compared to other reducing agents, like CO and C_3H_6 [81, 92, 167]. Therefore, the potential of injecting hydrogen upstream the LNT to enhance its performance was investigated. Engine was running with lean/rich cycle (50 s at λ = 1.15 and 10 s at λ = 0.9), and various amount of hydrogen was constantly added into the exhaust feed to LNT inlet at different operating temperatures. Details of each examined condition can be found in Table 6-1. For each temperature, a baseline case without any hydrogen addition was tested for reference. Both the full-scale and small-scale testing bench were used. For the full-scale test, the LNT operating temperature will be denoted as '450 ºC'. In order to reduce the testing errors and ensure the reliability of collected data, data recorded in the first and last cycle are removed. For each testing point, the data within a constant observation window (9 cycles: 540 s) were analysed and presented unless otherwise stated. It should be mentioned that constant amount of hydrogen was continually injected to the TWC-out exhaust stream during the whole test. Corresponding results will be discussed in section 6.3.1.

Table 6-1- Details of constant H_2 injection cases study under engine lean/rich cycle operation (50s at λ = 1.15 and 10s at λ = 0.9; H_2 is injected during the whole test)

Case	LNT operating temperature (°C)	H_2 injection amount (ppm)
1	150	10,000
2	200	5000
3	200	10,000
4	250	5000
5	250	10,000
6	450 (Full-scale)	1500
7	450 (Full-scale)	10,000

(2) Cyclic H_2 injection test

Hydrogen injection is used to regenerate the LNT catalyst instead of the periodical engine rich operation. The use of hydrogen to regenerate the LNT was performed under engine constant lean operation (λ = 1.15) via the small-scale testing bench. The operating temperature of LNT was chosen at 150, 200, and 250 °C respectively by the furnace under constant GHSV of 25,000 h^{-1}. During the tests, H_2 was injected to TWC-out exhaust gas in a cycling manner. An example of hydrogen cyclic injection profile is illustrated in Figure 6-1. It can be seen that each cycle consists of 10s of constant hydrogen injection (1%), followed by a pause of 50 s. The total duration of each cycle is 60 s, and the cycle will be repeated for five times. In the present study, different amounts of hydrogen injection were examined at fixed operating temperatures. Details of the hydrogen cyclic injection cases are summarized in Table 6-2.

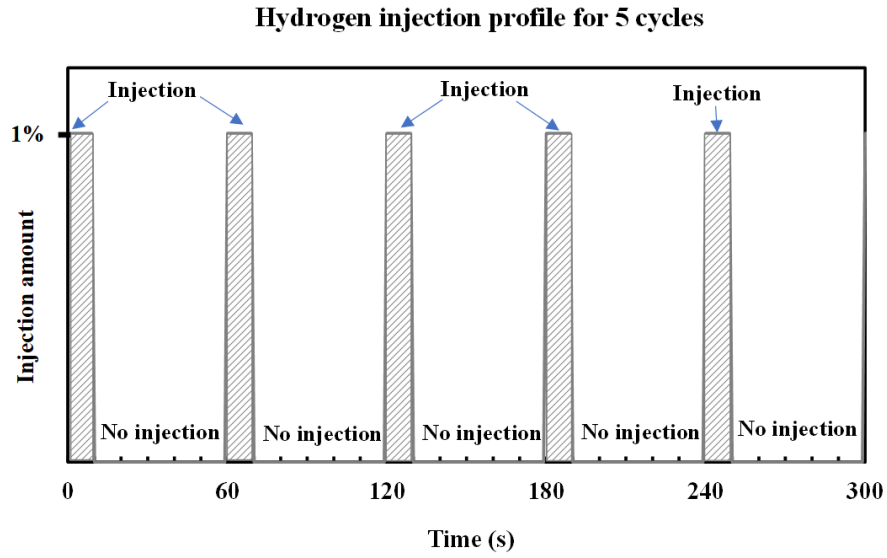

Figure 6-1. Example of periodical hydrogen injection profile for 5 cycles

Table 6-2- Details of cyclic H_2 injection cases study under engine constant lean operation (λ = 1.15; each injection cycle = 10 s of injection and 50 s of pause; 5 cycles in total)

Case	LNT operating temperature (°C)	H_2 injection amount
1	200	1%
2	200	2%
3	150	3.4%
4	250	3.4%

6.3 Results and discussion

6.3.1 Investigation on constant hydrogen injection on LNT performance

(1) Hydrogen effect at 150 °C (1% of H_2 addition)

At 150 °C, 1% of hydrogen was continually injected upstream the LNT under the engine lean/rich cycle operation of 50 s at λ = 1.15 and 10 s at λ = 0.9. Figure 6-2 compares the

species level (NO_x, and THC) measured at LNT-out for the case with 1% of hydrogen addition to the baseline case (no hydrogen addition). During the tests, it was observed that nearly all the CO were removed over the LNT catalyst for both conditions and the CO concentrations at LNT-out are very low (below 5 ppm). Thereby, the temporal profiles of CO concentrations are not presented here. As shown in Figure 6-2 (a), the average engine lambda value recorded by ATI is provided as reference to indicate the lean and rich phase. For the baseline condition, the majority of NO_x is stored on the LNT storage site during the lean phase; while engine switches to rich operation, the stored NO_x is released and subsequently reduced by reducing agents (like H_2, CO, THC, NH_3). However, NO_x spikes can be still observed at LNT out in the rich phase. When adding 1% of hydrogen to the exhaust feed to LNT, the NO_x slips are completely removed, yielding approximate 100% of NO_x conversion over the LNT. As for the THC levels at LNT out, similar spikes are observed for both conditions during rich phase. It is caused by the reason that the upstream TWC's conversion efficiency for THC and CO under rich condition are not as effective as that for lean condition. Also, it was previously reported that H_2 exhibits better reducing activity than CO and C_3H_6 in NO_x removal [102]. With 1% of hydrogen addition, the beneficial effect is also observed for THC conversion, with the THC peak values being slightly reduced.

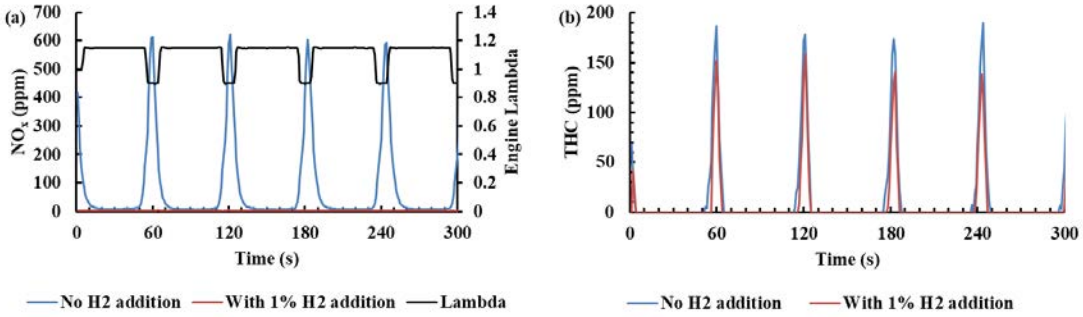

Figure 6-2. Comparison of (a) NO_x, (b) THC concentrations measured at LNT-out between the baseline condition (no H_2 addition) and the 1% H_2 addition condition at 150 ◦C under engine lean/rich cycle (50 s at λ = 1.15 and 10 s at λ = 0.9)

To better evaluate the hydrogen addition effect, the cycle-average conversion efficiencies of CO, THC, and NO_x are calculated for both conditions. Figure 6-3 presents the comparision. For both conditions, the average conversion efficicency of CO reaches around 100%. When the LNT is operating at low temperature (150 °C), there is nearly no THC conversion taking place over it. While around 20% of THC conversion is reached with 1% hydrogen addition. Regarding the NO_x reduction efficiency, it is increased from previous 84.70% to nearly 100% conversion with the extra 1% of hydrogen.

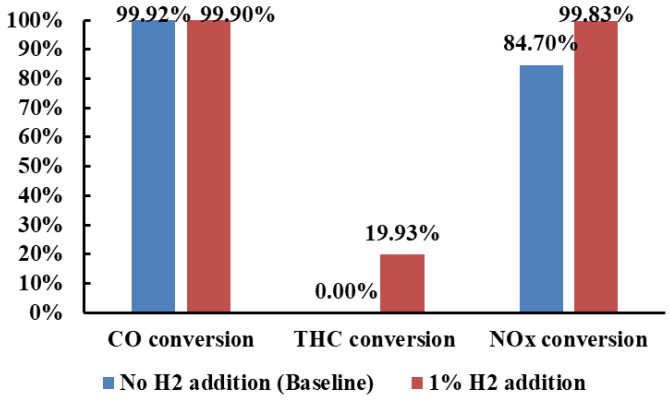

Figure 6-3. Hydrogen addition effect on the LNT catalyst performance at 150 °C under the engine lean/rich cycle (50 s at λ = 1.15 and 10 s at λ = 0.9)

Figure 6-4 shows the effect of 1% hydrogen addition on (a) the N_2O slips over the LNT

and (b) the average NO_x reduction selectivity to N_2O, NH_3 and N_2. It can be seen that the NO_x reduction selectivity to NH_3 is very low (below 2%) for both conditions at 150 ^oC. Thereby, the NH_3 concentrations at LNT-outlet are very low and the concentration profiles will not be presented here. As previously stated in Chapter 4 that hydrogen injection upstream a TWC is found to be beneficial in enhancing the NO_x light-off, but the enhancement effect is observed to be associated with certain amount of NH_3 and N_2O production. However, this issue is not captured here based on Figure 6-4. For the baseline condition (no H_2 addition), certain amount of N_2O is formed as by-product via NO_x reduction during the rich phase with the peak values reaching around 700 ppm at low temperature (150 ^oC). When adding 1% of hydrogen upstream the LNT, the peak values are significantly decreased to below 200 ppm. Based on the calculation of N_2O selectivity, it can be seen that with 1% of hydrogen addition, less fraction of NO_x (24.36%) is reduced to N_2O compared to the baseline condition (64.10%). DiGiulio et al. studied the NO_x reduction selectivity over a commercial LNT (Pt-Pd-Rh/Ba/CeO_2) catalyst under different operating conditions via laboratory bench flow reactor tests. They suggested that the N_2O selectivity is primarily dependent on the temperature with higher selectivity being observed at lower temperature [80]. Therefore, it is believed that the H_2 beneficial effect in moderating the N_2O generation is associated to the heat release of hydrogen oxidation. The hydrogen exothermic effect is indicated by Figure 6-5 which compares the exhaust gas temperature at LNT-outlet obtained for the case with 1% hydrogen addition to the baseline case. It should be mentioned that the LNT-inlet gas temperature for both

conditions is controlled by the furnace at 150 ± 5 ◦C (see the black line). Within the observation window, the exhaust gas temperature is slightly increased by 17 °C over the LNT for the baseline condition; While for the condition with 1% of hydrogen addition, larger temperature increment (73 °C) is perceived due to the exothermic effect of hydrogen addition.

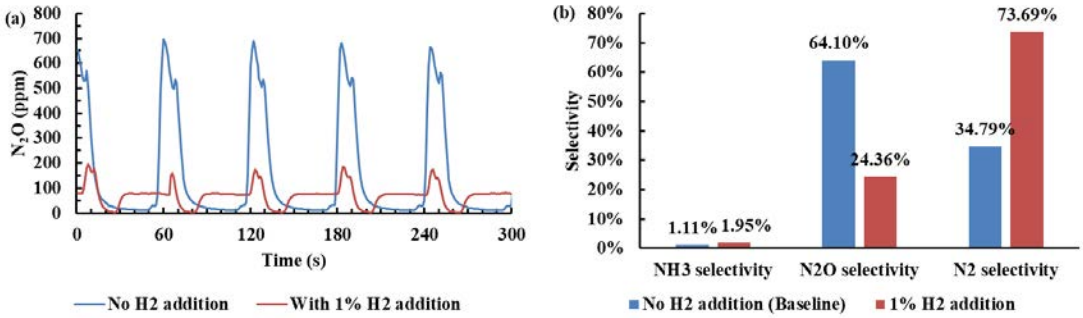

Figure 6-4. Hydrogen addition effect on (a) N_2O levels at LNT-out, (b) NO_x reduction selectivity over LNT at 150 °C under engine lean/rich cycle (50 s at λ = 1.15 and 10 s at λ = 0.9)

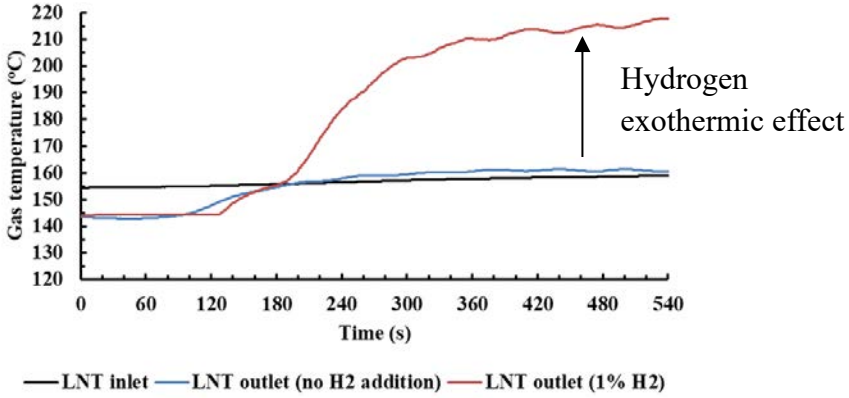

Figure 6-5. Exhaust gas temperature measured at the inlet and outlet of LNT with 1% H_2 addition under engine lean/rich cycle (Temperature obtained for the baseline condition is provided as reference)

(2) Hydrogen effect at different temperatures

For the 1% of hydrogen addition tests conducted at 200, 250, and 450 °C (Full-scale), similar hydrogen beneficial effect was observed. With 1% of hydrogen addition, the

cycle-averaged conversion efficiency of THC and NO_x was calculated for different temperature cases and compared to their corresponding baseline conditions. The comparison is given by Figure 6-6. Similar to what was previously discussed for 150 ºC condition, the CO and NH_3 concentrations measured at LNT-outlet for both with and without hydrogen addition are very low. Therefore, the discussion is focused on the conversion of THC and NO_x, and the selectivity to N_2O and N_2. With 1% of hydrogen addition, the THC conversion is improved to different degrees at all examined temperatures. Generally, the observed improvement is more effective at higher temperature with the largest improvement being obtained at the highest temperature (450 ºC). After injecting 1% of hydrogen, the average THC conversion is largely increased by 33% from previous 49% (baseline condition) to over 80% at 450 ºC. Similar to the THC conversion, the hydrogen improvement effect was also observed for NO_x conversion over the wide range of temperature. But the NO_x conversion curve as a function of temperature exhibits different trend. Larger improvement was observed at lower temperature, with the largest improvement (15.14%) being achieved for the 150 ºC case. While for the 450 ºC cases, with the same amount of hydrogen addition, the NO_x conversion was only improved by 9.90%.

Figure 6-7 presents the hydrogen effect on NO_x reduction selectivity observed at different temperatures. With 1% of hydrogen addition, the NO_x reduction selectivity to N_2O was reduced to different levels as a function of temperature. Larger reduction effect in N_2O selectivity was observed at lower temperature. It was previously discussed that the N_2 is

the dominated product of NO_x reduction with only a small fraction of NO_x being reduced to N_2O at higher temperature (see section 5.3.2). Therefore, at higher temperature, the hydrogen beneficial effect on moderating N_2O production is not that significant as that for the lower temperature cases. Generally speaking, adding 1% of hydrogen upstream the LNT is beneficial for promoting the LNT performance in terms of improving the THC and NO_x conversion, and reducing the N_2O generation, and the beneficial effect is observed to be temperature dependent.

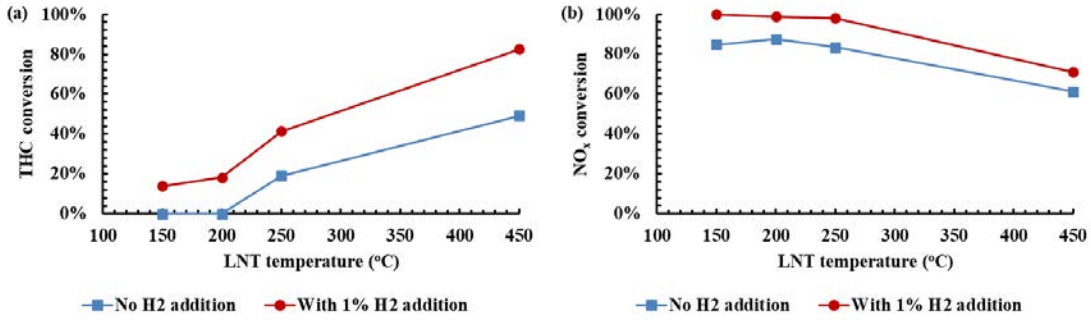

Figure 6-6. Hydrogen addition effect on LNT's (a) THC conversion, (b) NO_x conversion as a function of temperature under engine lean/rich cycle (50s at λ = 1.15 and 10s at λ = 0.9)

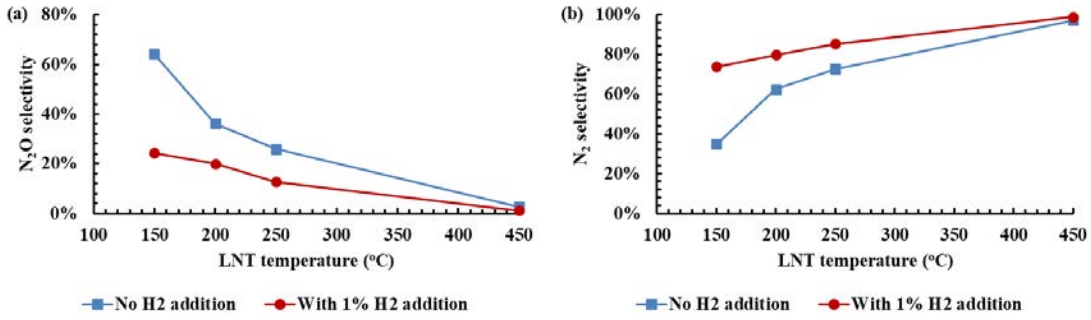

Figure 6-7. Hydrogen addition effect on LNT's NO_x reduction selectivity to (a) N_2O, (b) N_2 as a function of temperature under engine lean/rich cycle (50s at λ = 1.15 and 10s at λ = 0.9)

(3) Effect of hydrogen level

At 200 and 250 °C, hydrogen addition effect of lower amount (5000 ppm) was also

examined. The LNT performance versus the hydrogen addition amount at 200 °C is shown in Figure 6-8. For x-axis, 0, 5000, and 10000 represents the hydrogen addition amount (unit: ppm) to the exhaust feed into the LNT catalyst. 0 ppm means the baseline condition without extra hydrogen addition which is provided for reference. Around 100% of CO conversion was achieved for each case, therefore it is not discussed here. Regarding the NH_3 selectivity, it is very low for each case so only N_2O and N_2 selectivity will be focused. As for the influence on NO_x conversion, it can be seen that the beneficial effect is not proportional to the amount of hydrogen added. With 5000 ppm of hydrogen addition, the NO_x conversion is enhanced from the baseline level of 87.46% to 99.81%. Similar findings were reported by Salomons based on the experimental study on a commercial DOC [96]. Regarding the hydrogen beneficial effect in decreasing the N_2O selectivity, it can be seen that with more hydrogen addition, the N_2O is less favourably to be formed. Consequently, with larger amount of hydrogen addition, larger fraction of NO_x is converted to the harmless product N_2. This is because larger amount of hydrogen addition leads to more heat release and larger temperature increment over the LNT catalyst. Similar phenomenon can be found in Figure 6-9 for the cases study performed at 250 °C.

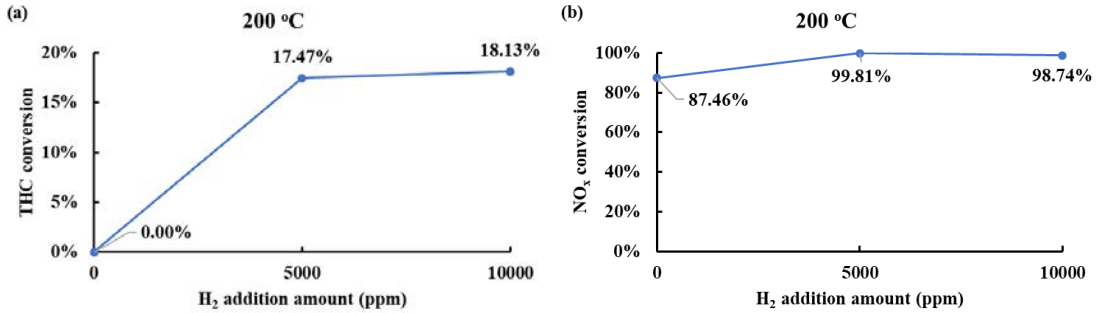

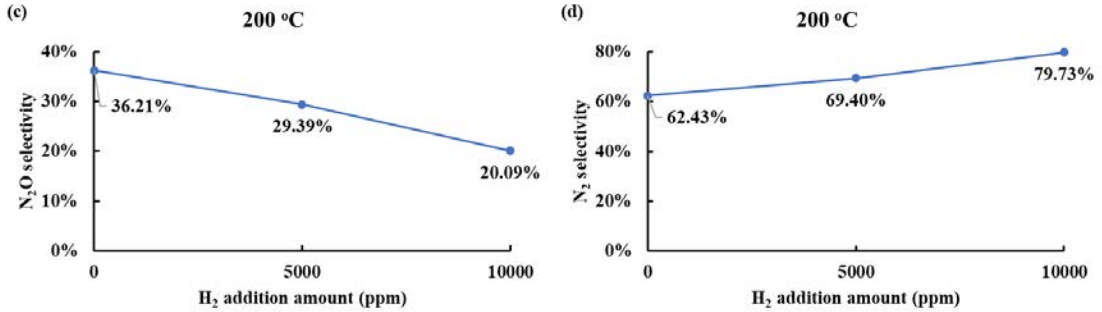

Figure 6-8. Hydrogen addition effect on (a) THC conversion, (b) NO_x conversion, (c) N_2O selectivity, and (d) N_2 selectivity as a function of H_2 addition amount at 200 °C under engine lean/rich cycle (50 s at λ = 1.15 and 10 s at λ = 0.9)

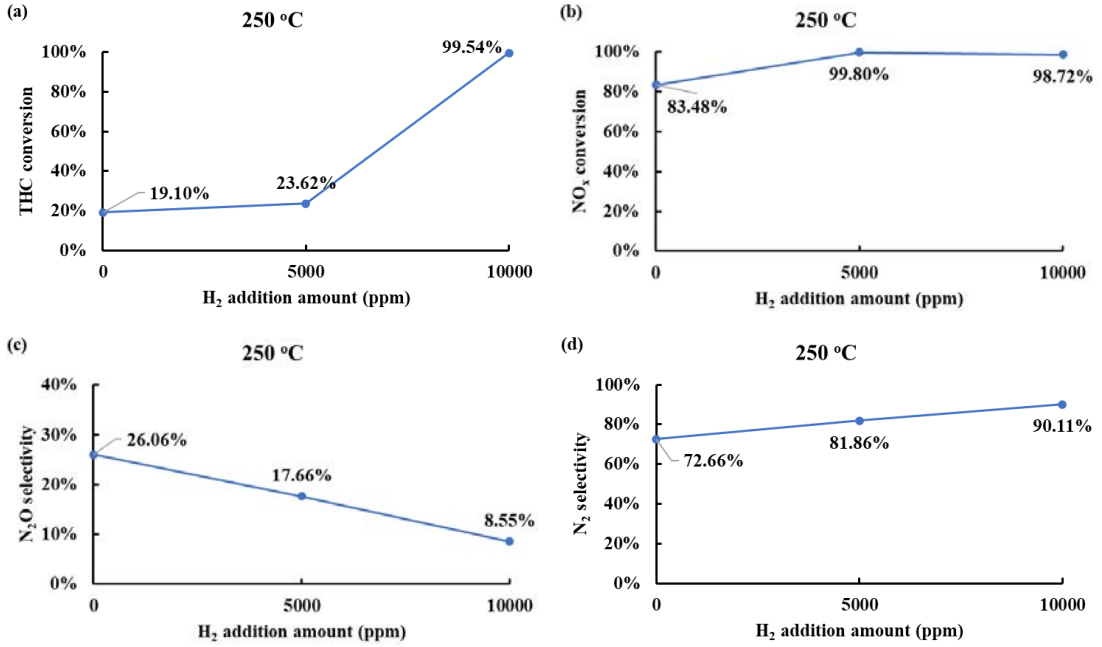

Figure 6-9. Hydrogen addition effect on (a) THC conversion, (b) NO_x conversion, (c) N_2O selectivity, and (d) N_2 selectivity as a function of H_2 addition amount at 250 °C under engine lean/rich cycle (50 s at λ = 1.15 and 10 s at λ = 0.9)

6.3.2 Assessing the feasibility of using cyclic hydrogen injection to regenerate the LNT catalyst

As aforementioned that rich phase (extra fuel) is required periodically to regenerate the LNT, which results in fuel penalty. The BSFC for engine constant lean operation (λ =1.15) and the engine lean/rich cycle operation (50 s at λ = 1.15 and 10 s at λ = 0.9) are

calculated. Compared to engine constant lean operation, it is found that an increment of 3.51% in fuel consumption is caused by the periodical rich operation. A reducing environment, where the excess oxygen must be consumed by H_2 and CO oxidation over the catalyst, is required for the LNT regeneration event. Therefore, relevant tests were performed to investigate the feasibility of regenerating the LNT through cyclic hydrogen injection under engine constant lean operation. Several testing scenarios were designed and examined. Details can be found in Table 6-2. As it was previously illustrated that hydrogen was injected into the exhaust feed to LNT inlet in a cycling manner during the tests. Take 1% of hydrogen cycling injection for instance, the hydrogen level measured at LNT inlet after hydrogen injection is shown in Figure 6-10. The baseline curve in red, which represents the LNT-inlet H_2 level under engine lean operation (λ = 1.15), is provided for reference. As we can see, with periodic H_2 injection, the hydrogen concentration measured at LNT-inlet under engine constant lean operation (λ = 1.15) shows similar trend as the H_2 profile observed under actual engine lean/rich cycle (see Figure 5-15 (a)).

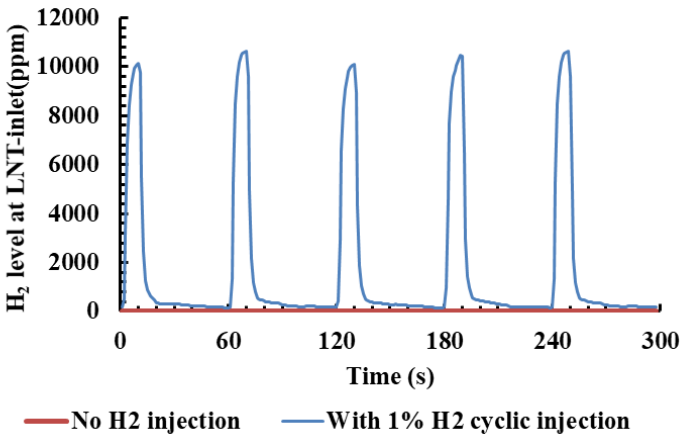

Figure 6-10. Temporal profile of H_2 concentration measured at LNT-inlet under engine

lean operation with H_2 cyclic injection at 1%

At 200 ºC, 1% and 2% of cyclic hydrogen injection were studied. For those two conditions, the LNT out CO, THC and NH_3 levels are low. Hence, only the NO_x and N_2O concentrations at LNT-out are presented in Figure 6-11. The grey shaded columns marked on the plot represent the hydrogen injection phase. For clear visualization, the hydrogen injection phases will not be marked for the N_2O profile. For both 1% and 2% of hydrogen addition cases, the NO_x concentration is gradually increasing as time elapses. This is because of the gradual NO_x storage on the LNT surface site. During the experiments, all the cases were performed after constant period of stoichiometric operation. Thereby the NO_x curves show an upward trend since the free storage sites are gradually occupied by the adsorbed NO_x. The occurrence of NO_x spikes is observed with the hydrogen injection pulse during the ON phase. This is similar to the observation for actual engine lean/rich cycle that the NO_x peaks are captured in the rich period (see Figure 6-2 (a)). Differently, for each hydrogen injection cycle (60 s), large amount of unreduced NO_x was emitted during the 50 s phase when there is no hydrogen injection. Although the results shown in Figure 6-2 and Figure 6-4 were obtained for the 150 ºC cases, similar curves were observed for other temperature conditions (200, 250, and 450 ºC) according to our experimental measurements. Therefore, those two figures can be used for comparison to analyse the general trend. As for N_2O, the concentration curve exhibits similar trend as Figure 6-4 (a) (blue line), but the peak values are lower than the baseline case which is measured to be around 700 ppm at 200 ºC. Since the majority of NO_x are unreduced,

thereby less N_2O will be produced.

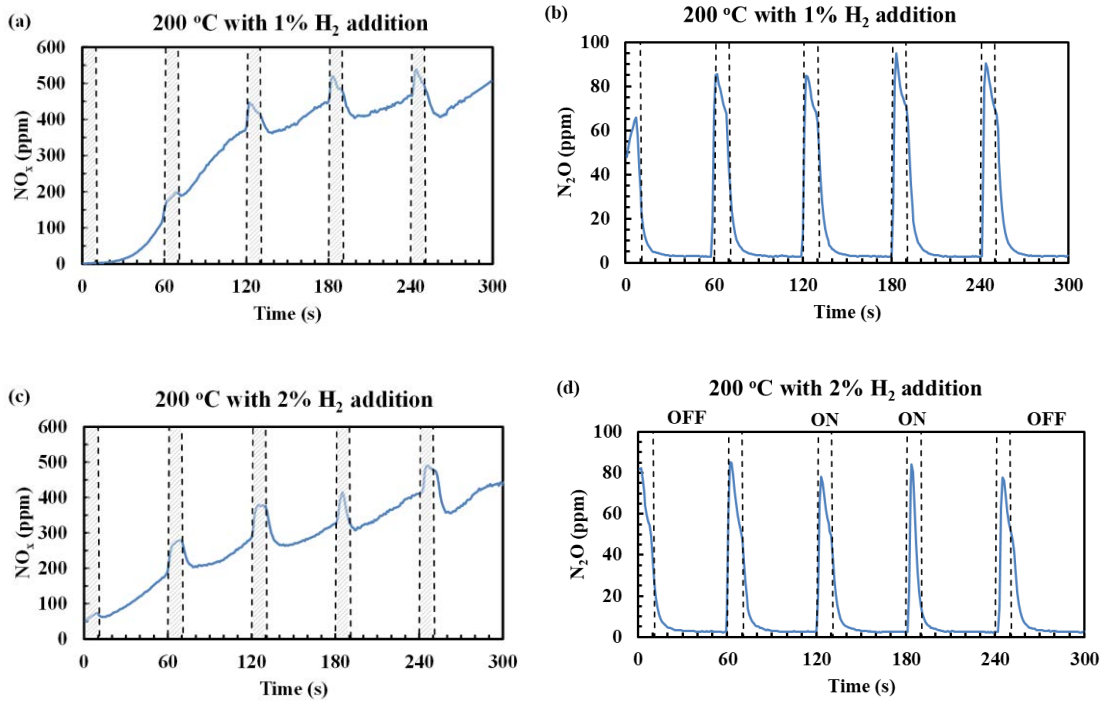

Figure 6-11. Temporal profile of NO_x and N_2O concentrations at LNT-out at 200 °C with (a-b) 1% and (c-d) 2% of hydrogen addition (H_2 injection phase is marked in grey shade as reference)

When engine is running with lean/rich cycle operation (50 s of λ = 1.15 and 10 s of λ = 0.9), H_2 level at LNT inlet during rich phase can reach approximate 3.4% according to the experimental measurement. Thereby, under engine constant lean operation (λ = 1.15), 3.4% of cyclic hydrogen addition was examined to simulate exhaust feed to LNT catalyst for the practical engine lean/rich cycle. This specific operation will be denoted as 'simulated engine lean/ 'rich' cycle. For those conditions, the NO_x and N_2O concentrations at LNT-out as a function of time are given by Figure 6-12. Similar trends are captured as previously discussed for the 200 °C cases. Large amount of unreduced NO_x was emitted during the 'no hydrogen injection phase' (50 s). It is assumed that the

extra hydrogen pulse of 1%, 2% and even 3.4% is not able to successfully create a rich atmosphere for the LNT regeneration. Therefore, the LNT catalyst is keeping adsorbing NO_x till its saturation, and the regeneration mode is not successfully initiated so further NO_x reduction reaction is not taking place. Accordingly, large amount of NO_x slips was observed.

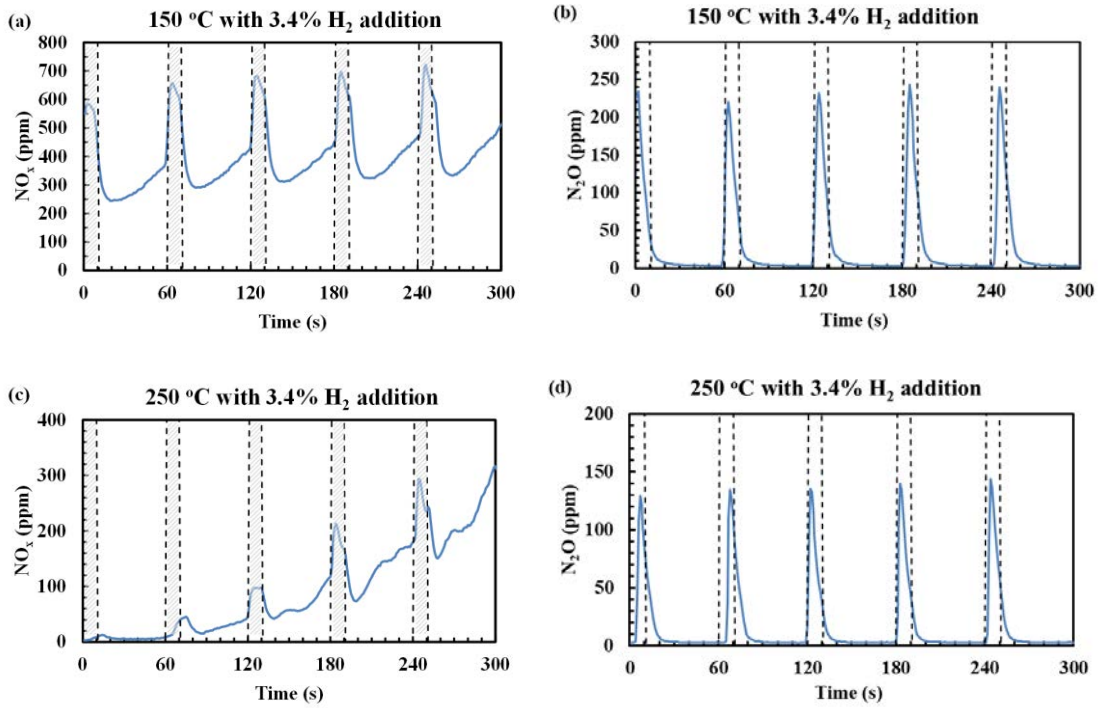

Figure 6-12. Temporal profile of NO_x and N_2O concentrations at LNT-out with 3.4% of hydrogen addition examined at (a-b) 150, and (c-d) 250 °C (H_2 injection phase is marked in grey shade as reference)

To better evaluate the exhaust gas stoichiometry, the lambda value of the exhaust stream at LNT inlet is calculated for the actual engine lean/rich cycle condition (50 s of λ = 1.15 and 10 s of λ = 0.9) and the simulated lean/ 'rich' cycle conditions (λ = 1.15 with 10s hydrogen addition at 1%, 2%, 3.4% occurring every 50 s) using Equation 3-29. The calculated lambda values are summarized in Table 6-3. It should be mentioned that for

the simulated cycle with hydrogen addition cases, 'rich' is corresponding to the phase with hydrogen addition and lean is equivalent to the remaining one. The lambda value is calculated at LNT-inlet (after TWC), thereby the lambda value is calculated to be around 1.16 which is slightly different from engine input lambda under lean operation (λ = 1.15). For the simulated cycle cases, during the lean period, the lambda value of exhaust gas at LNT inlet is the same for all cases at around 1.16, because there is no extra hydrogen addition. While during the rich period, different lambda values are obtained with different amount of hydrogen addition. Overall speaking, the upstream hydrogen addition shifts the lambda value towards a less lean region.

Table 6-3- Calculated lambda of exhaust gas at LNT inlet for different conditions

	Lean	'Rich' (with H_2 addition)
Actual engine lean/rich cycle	1.1634	0.8902
Simulated cycle (1% H_2 addition)	1.1634	1.1301
Simulated cycle (2% H_2 addition)	1.1634	1.0987
Simulated cycle (3.4% H_2 addition)	1.1634	1.0575

More detailed illustration is given by Figure 6-13, which compares the exhaust gas lambda profile calculated for the simulated cycle (3.4% H_2 addition) to the actual engine lean/rich cycle. For the red line which represents the simulated engine lean/ 'rich' cycle, during the hydrogen injection phase (10 s), the lambda value is reduced towards a level at around 1.06 due to hydrogen addition. Although the lambda value can be shifted towards rich region by hydrogen addition, it can be noticed that even with 3.4% of hydrogen addition the lambda value remains in the lean region. When engine is operating

with actual engine lean/rich cycle, the oxygen was completely consumed over the upstream TWC during the rich phase. As for engine constant lean operating conditions, there are certain amount of O_2 contained (2.73%) in the exhaust feed to LNT. Even with 3.4% of hydrogen addition, the required reducing environment is not successfully created for LNT regeneration. It is suggested that the extra added hydrogen is reacting with oxygen rather than functioning as a reducing agent, leading to large amount of NO_x slips over the LNT. Therefore, it is concluded that periodically injecting H_2 upstream is not able to regenerate the LNT catalyst under steady engine lean operation due to the surplus oxygen contained in the exhaust.

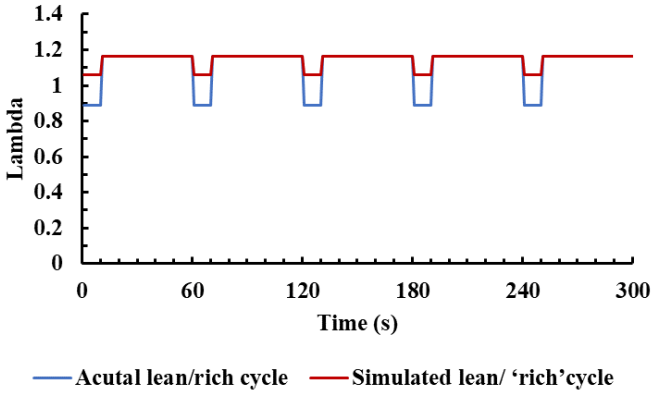

Figure 6-13. Comparison of the calculated lambda of exhaust gas at LNT-inlet between different conditions (Blue: actual engine lean/rich cycle, no H_2 addition; Red: simulated engine lean/ 'rich' cycle with periodical H_2 addition at 3.4%)

Apart from the aforementioned engine constant lean with cyclic hydrogen addition experiments, the effect of periodical hydrogen addition on LNT performance under engine lean/stoichiometric cycle operation was studied. During the test, the engine is operating under cycling operation of 50 s of lean (λ =1.15) plus 10 s of stoichiometric (λ =1), and specific amount of hydrogen is added into the LNT feed gas during the

stoichiometric period to simulate a rich exhaust environment. It is calculated that 3.4% of hydrogen addition to the exhaust feed shifts the lambda from previous 1 to rich at around 0.9. Thereby, for the following study, 3.4% of hydrogen was injected into the TWC-out exhaust stream during the stoichiometric period of engine operation. Relevant tests were performed via the small-scale LNT set-up at 150 and 250 °C, respectively.

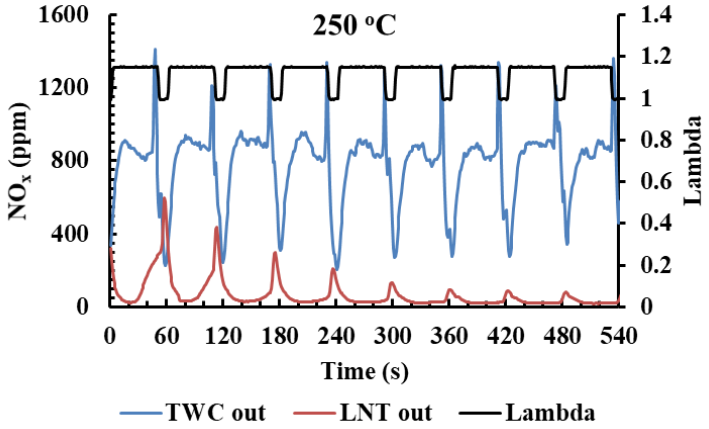

Figure 6-14. Temporal profile of NO_x concentrations measured at TWC out and LNT out under engine lean/ (stoichiometric with H_2 addition) cycle operation at 250 °C (Lambda profile is provided as reference)

Under engine lean/stoichiometric cycling operation, CO concentrations at both TWC-out and LNT-out are very low (below 5 ppm), so the CO concentrations is not presented here. The THC concentration at TWC out varies between the lean and stoichiometric condition. Overall, it is below 40 ppm, and it can be completely converted over the LNT catalyst. Therefore, only the NO_x profile will be our major interest. Figure 6-14 compares the NO_x levels measured at TWC-out and LNT-out under engine lean/stoichiometric operation with periodical hydrogen addition during the stoichiometric phase at 250 °C. The lambda profile recorded by ATI is given as reference to indicate the alternation of lean and

stoichiometric phase. It can be noticed that large amount of NO_x was escaped over the upstream TWC without being converted. During lean phase, these escaped NO_x emissions were effectively stored on the downstream LNT catalyst; while engine switching to stoichiometric operation with hydrogen addition to the LNT inlet exhaust feed, the regeneration and reduction process was initiated. Thereby, it is suggested that periodically injecting 3.4% of hydrogen into the exhaust feed to LNT is able to regenerate the LNT catalyst under engine lean/stoichiometric cycling operation. As previously discussed in Chapter 5, the stored NO_x could not be completely removed during the regeneration period when using gasoline (periodical rich operation) for LNT purging. However, it is noticed that the NO_x slips during the regeneration period significantly decrease towards a very low level (around 50 ppm) when using hydrogen for LNT purging.

Based on corresponding FTIR measurements, the average conversion efficiency of CO, THC and NO_x, as well as the NO_x reduction selectivity over the LNT catalyst are calculated for this case. Figure 6-15 compare the LNT performance for this case to the actual engine cycle case (50 s at λ = 1.15 and 10 s at λ = 0.9) at 250 ºC. For the engine lean/ (stoichiometric with H_2 addition) cycle case, the cycle-averaged conversion efficiency of CO, THC, NO_x for the LNT catalyst is 55.80%, 100%, and 93.09% respectively. Although the CO conversion only reaches 55.80%, it is noticed that the CO slips over LNT are very low. Therefore, this deficiency can be neglected. According to the comparison, it can be seen that the NO_x removal efficiency for this case (93.09%) is even higher than the actual engine lean/rich cycle case (83.48%). Regarding the NO_x

reduction selectivity, 83.09% of NO_x was converted to N_2 with 16.79% being reduced to N_2O under the engine lean/ (stoichiometric with H_2 addition) cycle at 250 °C. It is suggested that N_2O is more favourably to be formed under actual engine lean/rich cycle compared to the engine lean/ (stoichiometric with H_2 addition) cycle at the examined temperature.

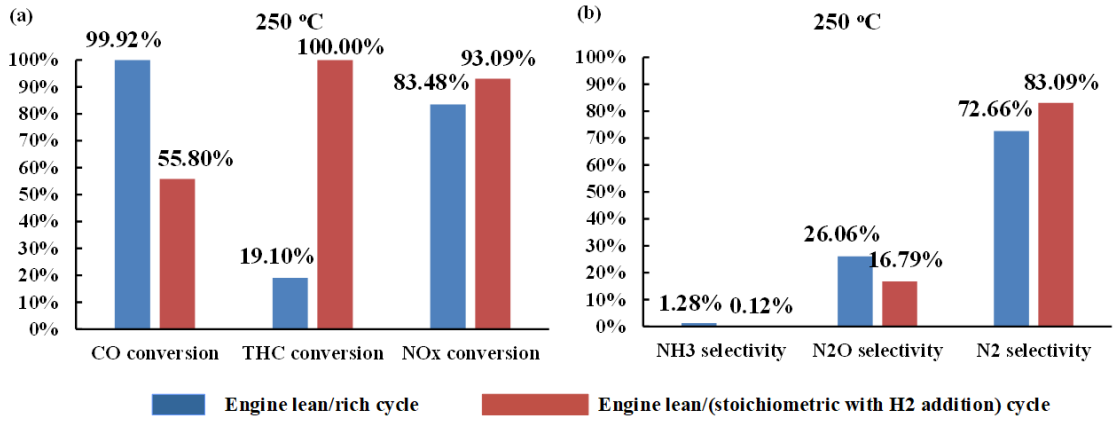

Figure 6-15. Comparison of LNT performance between the engine lean/rich cycle case and the engine lean/ (stoichiometric with H_2 addition) cycle case at 250 °C

Regarding the case examined at 150 °C, corresponding experimental results were given by Figure 6-16 and Figure 6-17. Similar to the 250 °C case, only minor amount of NO_x slips was observed over LNT under the engine lean/ (stoichiometric with H_2 addition) cycle. As time elapses, the NO_x peaks value at LNT out gradually decreases towards zero level. The cycle-averaged NO_x conversion efficiency for LNT is calculated to be 98.70%. As previously discussed in Chapter 5, the selectivity to NH_3 and N_2O is primarily dependent on temperature, and N_2O is preferred to be formed at lower temperature. Under engine lean/ (stoichiometric with H_2 addition) cycle operation at relative lower operating temperature (150 °C), certain amount of NH_3 (14.49%) was formed over the LNT catalyst

compared to the case examined under actual engine lean/rich cycle (1.11%). But less fraction of NO_x was reduced to N_2O. Overall speaking, under the engine lean/ (stoichiometric with H_2 addition) cycle, larger percentage of NO_x was converted into the harmless N_2 and fewer undesirable by-products were produced. During the test, the fuel consumption is also monitored for both conditions. It is observed that the BSFC of engine is reduced by 2.45% when engine is running at lean/stochiometric (50 s at λ = 1.15, 10 s at λ = 1) compared to the lean/rich cycle (50 s at λ = 1.15, 10 s at λ = 0.9). Although it is calculated that the fuel economy for engine only was improved when running engine at lean/stoichiometric with simultaneous hydrogen addition, it should be mentioned that the actual fuel economy of the whole system (engine plus hydrogen supply system) will also be affected by the hydrogen generation technology. Therefore, it is suggested that better LNT performance and fuel economy (engine only) is achieved when running engine at lean/stoichiometric with 3.4% of hydrogen addition during the stoichiometric period.

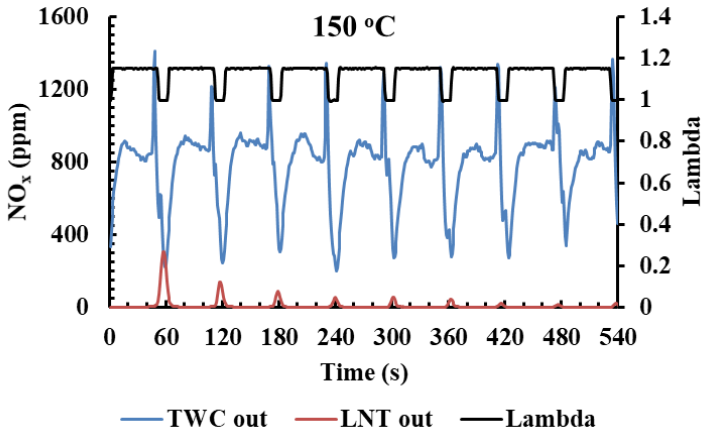

Figure 6-16. Temporal profile of NO_x concentrations measured at TWC out and LNT out under engine lean/ (stoichiometric with H_2 addition) cycle operation at 150 °C (Lambda profile is provided as reference)

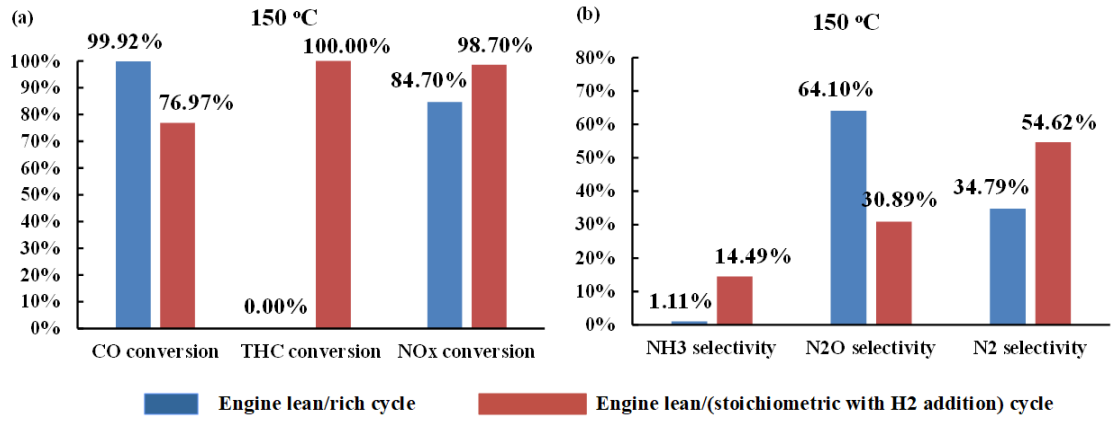

Figure 6-17. Comparison of LNT performance between the engine lean/rich cycle case and the engine lean/ (stoichiometric with H_2 addition) cycle case at 150 °C

6.4 Summary

In present chapter, the effect of hydrogen addition upstream the LNT catalyst on its performance was experimentally studied for a lean-burn gasoline engine.

Firstly, the engine was running at transient lean/rich cycle (50 s of λ = 1.15 and 10 s of λ = 0.9) with different amount of hydrogen being continually added to the exhaust feed to LNT inlet during the whole test at various temperatures (150, 200, 250, and 450 °C). The hydrogen addition was observed to be beneficial for LNT performance at all examined temperatures, including promoting the THC and NO_x conversion, reducing the NO_x reduction selectivity to N_2O. With the same amount of hydrogen addition (1%), it was found that the hydrogen promotion effect on THC conversion is more effective at higher temperature. While opposite trend was perceived for the promotional effect on NO_x conversion, with the greatest promotion being obtained at the lowest temperature

(150 °C). Similar phenomenon can be found for the selectivity to N_2O, larger reduction effect was observed at lower temperature. Comparing the results obtained with different amount of hydrogen addition, it is found that more effective impact is achieved with higher amount of hydrogen addition for improving the THC conversion and moderating the N_2O generation. As for NO_x conversion, significant improvement was achieved with 5000 ppm hydrogen addition, and no further improvements can be observed when increasing the hydrogen addition amount to 1%.

Besides that, the feasibility of injecting hydrogen to regenerate the LNT under engine lean operation was examined. The cycling injection strategy, where constant amount of hydrogen was injected into the exhaust feed to the LNT for 10 s and the injection event occurs every 50 s, was employed. Initially, engine was operating at constant lean condition (λ = 1.15) with different amount of hydrogen (1%, 2%, and 3.4%) being periodically injected upstream the LNT to artificially simulate the lean/ 'rich' exhaust environment. However, significant unreduced NO_x emissions are found after the LNT during the 'rich' phase. Experimental results show that the lambda of exhaust gas at LNT-inlet is shifted towards a lower level (less lean) by hydrogen addition, but the lambda (around 1.06) still remains in lean region even with 3.4% of hydrogen injection. It is suggested that injecting H_2 to the exhaust feed is not successful to regenerate the LNT catalyst under engine constant lean operation due to the surplus oxygen contained in the exhaust. Subsequently, the concept was examined with engine lean/stoichiometric cycling operation (50 s of λ = 1.15 and 10 s of λ =1) where 3.4% of hydrogen was injected

upstream LNT during the stoichiometric period. Compared to the engine lean/rich cycle operation, it is found that 2.45% of fuel consumption reduction is achieved for the engine. Experimental results implied that the NO_x regeneration and reduction process was successfully initiated, with over 93% of NO_x conversion being achieved for the LNT. Additionally, it was noticed that N_2O is less favourably to be formed over the LNT catalyst under certain simulated cycle compared to that for the actual engine lean/rich cycle. In general, running engine at lean/stoichiometric (with hydrogen adding to the exhaust feed) is able to purge the LNT catalyst with better LNT performance and fuel economy being attained simultaneously. Results and analysis from present work highlight the potential of using hydrogen as promoters to expand the optimum operating window of LNT to a larger variety of temperatures. Additionally, the potential of using hydrogen addition instead of periodical engine rich operation to regenerate the LNT for better fuel economy was highlighted.

CHAPTER 7 CONCLUSIONS AND FUTURE WORK

This thesis presents the investigation of potential hydrogen effect on the aftertreatment system of a lean-burn GDI engine, including a commercial TWC and LNT catalyst. Major conclusions obtained from the present research are summarized in this chapter. Subsequently, recommendations regarding potential future works on this research topic will be briefly discussed.

7.1 Concluding remarks

Overall, the experimental studies presented in this thesis show that hydrogen addition to the exhaust stream is beneficial for lean-burn gasoline engine aftertreatment performance, in terms of reducing the low temperature CO and THC slips over the catalysts and improving the lean-NO_x removal performance. Accordingly, it is suggested that hydrogen could be potentially used as promoters for catalyst to achieve fast light-off and control the lean-NOx emissions. This hydrogen promotional effect highlights the potential of extending the optimum operating window of the catalysts system to a larger variety of temperature (i.e., low temperature 150 ^{o}C) and exhaust stoichiometry (i.e., periodical rich engine operation is not required). Key findings obtained in the present study are

summarized below in the sequence of each research chapter.

Chapter 4 Effect of hydrogen addition on the light-off performance of TWCs

- As an overall trend, the addition of hydrogen (5000 ppm) to GDI engine-out exhaust stream was shown to be beneficial of decreasing the TWC light-off temperatures of regulated species CO, THC, and NO_x under both stoichiometric and lean conditions, especially lean conditions.
- The amount of hydrogen addition to lean exhaust environment of the GDI engine was observed to be critical in advancing or retarding the CO and HC light-off. It was found that insufficient amount of hydrogen addition (i.e., 1000 ppm) has detrimental effect on CO and HC conversion. Finding out the threshold and optimal value of hydrogen addition amount will be necessary.
- The hydrogen effect on promoting TWC low temperature and lean-NO_x performance can be attributed to multiple factors, including the rapid temperature increment caused by hydrogen oxidation, and the strong CO inhibition feature moderated by hydrogen.
- Certain amount of NH_3 and N_2O formation was observed to be accompanied with the hydrogen addition. The NH_3 slips could aid with NO_x reduction over the downstream LNT which has been discussed in Chapter 5. The N_2O slips could be utilized for *in situ* soot oxidation by designing a hybrid zoned TWC which can effectively reduce the gaseous and particulate emissions from a fuel-efficient lean-burn GDI engine.

Chapter 5 Study of a TWC-LNT system performance on a gasoline engine

- Implementing a downstream LNT to the gasoline engine aftertreatment system was shown to be advantageous in improving the overall conversion of engine-out legislated pollutants, such as lean NO_x abatement was achieved via effective NO_x storage, regeneration, and reduction, the unreduced CO and THC emissions from TWC-out were removed by the LNT.
- Under engine periodical lean/rich operation, the majority of NO_x was stored on the surface sites during lean phase, and effective regeneration and reduction process was triggered by the rich exhaust environment, yielding an overall NO_x reduction efficiency of above 70% at all examined temperatures (150 to 450 ºC). However, certain amount of NO_x slips over the LNT can be still observed during the rich phase, which can be explained by the reason that NO_x emissions are over the LNT storage capacity.
- The LNT activity was primarily controlled by the operating temperature. The NO_x conversion efficiency exhibited 'bell curve' feature, yielding relatively lower conversion at low (150 ºC) and high operating temperatures (450 ºC). It was also observed that N_2O is favourably to be formed as by-products at low temperatures.
- The LNT performance was also dependent on the reductant concentrations. Regarding the reductant concentrations (CO, H_2, HC, NH_3), they were greatly affected by the upstream TWC. CO and HCs were consumed over the TWC to form H_2 and NH_3 through WGS and SR reactions.

Chapter 6 Effect of hydrogen addition on the performance of a LNT catalyst

- As an overall trend, hydrogen addition to the exhaust feed to LNT was observed to be advantageous for improving the LNT performance, in terms of enhancing the THC and NO_x conversion and moderating the N_2O formation.
- The extent of the observed hydrogen beneficial effect was temperature dependent. Larger improvement in THC conversion is achieved at higher temperature, while opposite trend was observed for the effect of promoting NO_x conversion and inhibiting N_2O selectivity.
- When engine was operating with lean/stochiometric cycle, adding hydrogen to the stoichiometric exhaust environment upstream the LNT was shown to be able to regenerate the LNT. Better LNT performance and reduced engine fuel consumption was achieved compared to the standard lean/rich condition. Therefore, it is suggested that the periodical rich operation required for LNT regeneration could be replaced by hydrogen addition which can improve LNT performance and engine fuel economy simultaneously.

7.2 Future work suggestion

Present work explored the potential effect of hydrogen addition to improve the low temperature and lean-NO_x removal performance of a GDI engine aftertreatment catalysts system, including a commercial TWC and a LNT catalyst. There are still works required

to be done in this research topic to further expand the understanding of hydrogen beneficial effect on the exhaust system of lean-burn GDI engine and help the design of advanced aftertreatment system to utilize the 'hydrogen effect'. Suggestions on future works regarding this research topic are introduced as follow.

Hydrogen effect under various engine operations

In Chapter 4, the beneficial effect of different amount of hydrogen addition was examined at engine speed of 2100 rpm and load of 2.2 bar BMEP. Therefore, further experimental works could be conducted to expand the investigation to a larger variety of engine operating conditions such as at lower load and speed (0.63 BMEP and 1000 rpm), and higher condition (3.77 bar BMEP and 2100 rpm). This can help to identify the optimal amount of hydrogen addition for different engine operating conditions. Additionally, as it was previously discussed the amount of hydrogen addition is critical for whether advancing or retarding the CO and HC light-off under lean conditions. Further tests are required to include the hydrogen effect study on the amount of 1000 to 5000 ppm to identify the threshold of hydrogen addition amount. For example, the hydrogen addition of 1500, 2000, and 2500 ppm etc. could be studied. Consequently, various combinations of those parameters (speed, load, and hydrogen addition amount) could be designed and further tested. Regarding the hydrogen effect on LNT catalyst, it is also necessary to explore the ideal amount of hydrogen addition. Corresponding results could be used to help developing the catalysts converters which can effectively utilize the 'hydrogen promotional impact'.

Expand the TWC model to include detailed kinetics mechanism

In the simulation of TWC light-off, global reaction mechanisms were employed to simplify the calculation. Although the hydrogen enhancement effect on CO light-off could be correctly explained by weakening the CO self-inhibition term, this could also be further complemented by incorporating detailed kinetics mechanism with specific washcoat fractions information to deliver better understanding on how hydrogen affects the oxidation and reduction reactions on catalyst surface sites (like Pt-, Pd-, and Rh-based sites). Also, combined with relevant experimental data, the developed model and reaction terms can be expanded to include more operating points (different engine operations & different amounts of hydrogen addition), and possibly to quantify the hydrogen effect on catalytical oxidation and reduction activity as a function of different conditions.

Use on-board generated H_2-rich reforming gas to improve the catalyst performance

For practical applications, the hydrogen added upstream of the catalysts can be generated by the on-board exhaust gas fuel reforming instead of being stored in a storage tank. Therefore, a mini exhaust gas fuel reformer can be possibly integrated with the catalyst system to supply hydrogen for enhancing the catalysts low temperature activity. Subsequently, the influence of adding hydrogen-enriched reforming gas on catalysts activity needs to be assessed. Apart from hydrogen, it should be mentioned that the reforming gas also contains CO, steam, CH_4, and various other HCs. Therefore, the investigation of the effect of those fuel reforming product compositions on the catalyst performance is of great necessity. Also, it should be mentioned that adding reforming gas

into the engine exhaust is a possible approach for LNT regeneration rather than periodical engine intake throttling. Therefore, relevant study on on-board exhaust gas fuel reforming to supply right amount of reductants (H_2, and CO) to the LNT catalyst needs to be carried out. For example, examining the optimal oxygen to fuel ratio (to the reformer) for achieving maximum NO_x removal efficiency and minimum fuel penalty. As it was stated that the hydrogen beneficial effect on improving catalysts low temperature activity could be utilized for reducing the cold start emissions. Therefore, it is necessary to study the whole process of hydrogen production, and addition to the exhaust while engine is starting up to help design advanced control and operation strategy for minimizing the time required to generate sufficient amount of hydrogen-enriched reforming gas.

LIST OF REFERENCES

1. Smith, M.N. *World Economic Forum - The number of cars worldwide is set to double by 2040.* 2016 [cited 2021 June 01]; Available from: https://www.weforum.org/agenda/2016/04/the-number-of-cars-worldwide-isset-to-double-by-2040.
2. EuropeanUnion, *Regulation (EC) No 715/2007 of the European Parliament and of the Council of 20 June 2007 on type approval of motor vehicles with respect to emissions from light passenger and commercial vehicles (Euro 5 and Euro 6)*. 2007.
3. Chen, B.H.-Y. and H.-L. Chang, *Development of Low Temperature Three-Way Catalysts for Future Fuel Efficient Vehicles.* Johnson Matthey Technology Review, 2015. **59**(1): p. 64-67.
4. Dabill, D.W., et al., *The oxidation of hydrogen and carbon monoxide mixtures over platinum.* Journal of Catalysis, 1978. **53**(1): p. 164-167.
5. Sun, M., et al., *Steady-state multiplicity and superadiabatic extinction waves in the oxidation of CO/H2 mixtures over a Pt/Al2O3-coated monolith.* Industrial & engineering chemistry research, 2003. **42**(1): p. 37-45.
6. Katare, S.R. and P.M. Laing, *Hydrogen in diesel exhaust: effect on diesel oxidation catalyst flow reactor experiments and model predictions.* SAE International Journal of Fuels and Lubricants, 2009. **2**(1): p. 605-611.
7. Salomons, S., et al., *CO and H2 oxidation on a platinum monolith diesel oxidation catalyst.* Catalysis Today, 2006. **117**(4): p. 491-497.
8. Satokawa, S., et al., *Promotion effect of H2 on the low temperature activity of the selective reduction of NO by light hydrocarbons over Ag/Al2O3.* Applied Catalysis B: Environmental, 2003. **42**(2): p. 179-186.
9. Burch, R., et al., *Exceptional activity for NO x reduction at low temperatures using combinations of hydrogen and higher hydrocarbons on Ag/Al 2 O 3 catalysts.* Topics in Catalysis, 2004. **30**(1-4): p. 19-25.
10. Herreros, J.M., et al., *Enhancing the low temperature oxidation performance over a Pt and a Pt–Pd diesel oxidation catalyst.* Applied Catalysis B: Environmental, 2014. **147**: p. 835-841.
11. Zhao, H., *Overview of gasoline direct injection engines*, in *Advanced Direct Injection Combustion Engine Technologies and Development*. 2010. p. 1-19.
12. Harada, J., et al., *Development of direct injection gasoline engine*. 1997, SAE Technical Paper.
13. Mock, P., *European vehicle market statistics.* Pocketbook, Lugano, Switzerland, 2014.
14. Zhao, H., *Advanced direct injection combustion engine technologies and development: diesel engines*. Vol. 2. 2009: Elsevier.

15. Takagi, Y., *The role of mixture formation in improving fuel economy and reducing emissions of automotive SI engines.* FISITA Technical Paper, 1996(P0109).
16. Zhao, F., M.-C. Lai, and D.L. Harrington, *Automotive spark-ignited direct-injection gasoline engines.* Progress in energy and combustion science, 1999. **25**(5): p. 437-562.
17. Andersson, J., et al., *Particle and sulphur species as key issues in gasoline direct injection exhaust.* Nippon Kikai Gakkai, 1999. **15**: p. 449-452.
18. Mathis, U., M. Mohr, and A.-M. Forss, *Comprehensive particle characterization of modern gasoline and diesel passenger cars at low ambient temperatures.* Atmospheric Environment, 2005. **39**(1): p. 107-117.
19. Henkel, S., et al., *Injector fouling and its impact on engine emissions and spray characteristics in gasoline direct injection engines.* SAE International Journal of Fuels and Lubricants, 2017. **10**(2): p. 287-295.
20. Arters, D.C. and M.J. Macduff, *The effect on vehicle performance of injector deposits in a direct injection gasoline engine.* SAE transactions, 2000: p. 2044-2052.
21. Spicher, U. and T. Heidenreich, *Stratified-charge combustion in direct injection gasoline engines*, in *Advanced Direct Injection Combustion Engine Technologies and Development*. 2010. p. 20-44.
22. Brunekreef, B. and S.T. Holgate, *Air pollution and health.* The lancet, 2002. **360**(9341): p. 1233-1242.
23. Vautard, R., P. Yiou, and G.J. Van Oldenborgh, *Decline of fog, mist and haze in Europe over the past 30 years.* Nature Geoscience, 2009. **2**(2): p. 115.
24. Fowler, D., et al., *Atmospheric composition change: ecosystems–atmosphere interactions.* Atmospheric Environment, 2009. **43**(33): p. 5193-5267.
25. Van Vorst, W.D., *Impact of the California clean air act.* International journal of hydrogen energy, 1997. **22**(1): p. 31-38.
26. Agency, E.E. *CO2 performance of new passenger cars in Europe*. [cited 2021 05/05]; Available from: https://www.eea.europa.eu/data-and-maps/indicators/average-co2-emissions-from-motor-vehicles-1/assessment.
27. AECC. *LEGISLATION FOR SUSTAINABLE MOBILITY - AECC - Euro7 and Euro VII*.
28. Myers, P., O. Uyehara, and H. Newhall, *Engine exhaust emissions*, in *Engine Emissions*. 1973, Springer. p. 1-31.
29. Stone, R., *Introduction to internal combustion engines*. Vol. 3. 1999: Springer.
30. Heywood, J.B., *Internal combustion engine fundamentals.* 1988.
31. Shimotani, K., et al., *Characteristics of gasoline in-cylinder direct injection engine.* JSAE review, 1996. **17**(3): p. 267-272.
32. Anderson, R., et al., *Understanding the thermodynamics of direct injection spark ignition (DISI) combustion systems: an analytical and experimental investigation.* SAE transactions, 1996: p. 2195-2204.
33. Kittelson, D.B., *Engines and nanoparticles: a review.* Journal of aerosol science, 1998. **29**(5-6): p. 575-588.
34. Tree, D.R. and K.I. Svensson, *Soot processes in compression ignition engines.* Progress in Energy and Combustion Science, 2007. **33**(3): p. 272-309.

35. EPA, D., *Integrated science assessment for particulate matter.* US Environmental Protection Agency Washington, DC, 2009.
36. Mansurov, Z., *Soot formation in combustion processes.* Combustion, Explosion and Shock Waves, 2005. **41**(6): p. 727-744.
37. Ramanathan, V. and G. Carmichael, *Global and regional climate changes due to black carbon.* Nature geoscience, 2008. **1**(4): p. 221-227.
38. Richter, J.M., et al., *Application of catalyzed gasoline particulate filters to GDI vehicles.* SAE International Journal of Engines, 2012. **5**(3): p. 1361-1370.
39. Chan, T.W., et al., *Evaluation of a gasoline particulate filter to reduce particle emissions from a gasoline direct injection vehicle.* SAE International Journal of Fuels and Lubricants, 2012. **5**(3): p. 1277-1290.
40. Ito, Y., et al., *Advanced ceramic wall flow filter for reduction of particulate number emission of direct injection gasoline engines*. 2013, SAE Technical Paper.
41. Fennell, D., et al., *GDI Engine Performance and Emissions with Reformed Exhaust Gas Recirculation (REGR)*, in *SAE Technical Paper Series*. 2013.
42. Bogarra, M., et al., *Study of particulate matter and gaseous emissions in gasoline direct injection engine using on-board exhaust gas fuel reforming.* Applied Energy, 2016. **180**: p. 245-255.
43. Bowman, C.T., *Kinetics of pollutant formation and destruction in combustion.* Progress in energy and combustion science, 1975. **1**(1): p. 33-45.
44. Alger, T., T. Chauvet, and Z. Dimitrova, *Synergies between high EGR operation and GDI systems.* SAE International Journal of Engines, 2009. **1**(1): p. 101-114.
45. Summers, J.C. and L.L. Hegedus, *Effects of platinum and palladium impregnation on the performance and durability of automobile exhaust oxidizing catalysts.* Journal of Catalysis, 1978. **51**(2): p. 185-192.
46. Agency, E.E. *Fleet composition*. Available from: https://www.eea.europa.eu/publications/ENVISSUENo12/page032.html.
47. Kašpar, J., P. Fornasiero, and N. Hickey, *Automotive catalytic converters: current status and some perspectives.* Catalysis Today, 2003. **77**(4): p. 419-449.
48. Degobert, P., *Automobiles and Pollution, Society of Automotive Engineers.* Inc., Warrendale, PA, 1995. **146**.
49. Zheng, Q., et al., *Part I: a comparative thermal aging study on the regenerability of Rh/Al2O3 and Rh/CexOy-ZrO2 as model catalysts for automotive three way catalysts.* Catalysts, 2015. **5**(4): p. 1770-1796.
50. Fornasiero, P., et al., *Metal-loaded CeO2-ZrO2 solid solutions as innovative catalysts for automotive catalytic converters.* Catalysis today, 1996. **29**(1-4): p. 47-52.
51. Hu, Z., et al., *Performance and structure of Pt–Rh three-way catalysts: mechanism for Pt/Rh synergism.* Journal of Catalysis, 1998. **174**(1): p. 13-21.
52. Heck, R.M. and R.J. Farrauto, *Automobile exhaust catalysts.* Applied Catalysis A: General, 2001. **221**(1-2): p. 443-457.

53. Turkcan, A., et al., *Numerical and experimental investigations of the effects of the second injection timing and alcohol-gasoline fuel blends on combustion and emissions of an HCCI-DI engine.* Fuel, 2018. **219**: p. 50-61.
54. Wei, H., et al., *Gasoline engine exhaust gas recirculation–a review.* Applied energy, 2012. **99**: p. 534-544.
55. Fennell, D., J. Herreros, and A. Tsolakis, *Improving gasoline direct injection (GDI) engine efficiency and emissions with hydrogen from exhaust gas fuel reforming.* International Journal of Hydrogen Energy, 2014. **39**(10): p. 5153-5162.
56. Ball, D.J., *Distribution of warm-up and underfloor catalyst volumes*. 1992, SAE Technical Paper.
57. Nunan, J., et al., *HC Traps for Gasoline and Ethanol Applications.* SAE International Journal of Fuels and Lubricants, 2013. **6**(2): p. 430-449.
58. Ning, J. and F. Yan, *Temperature control of electrically heated catalyst for cold-start emission improvement.* IFAC-PapersOnLine, 2016. **49**(11): p. 14-19.
59. Li, W., et al., *Passive ammonia SCR system for lean-burn SIDI engines.* SAE International Journal of Fuels and Lubricants, 2010. **3**(1): p. 99-106.
60. Prikhodko, V.Y., et al., *Ammonia Generation and Utilization in a Passive SCR (TWC+SCR) System on Lean Gasoline Engine.* SAE International Journal of Engines, 2016. **9**(2): p. 1289-1295.
61. Mejia-Centeno, I. and G.A. Fuentes, *Nitrous oxide formation during light-off over a commercial pd-containing three-way catalytic converter: The effect of low-sulfur gasoline.* Chemical Engineering Communications, 2009. **196**(10): p. 1140-1151.
62. Pihl, J.A., et al., *Product selectivity during regeneration of lean NOx trap catalysts*. 2006, SAE Technical Paper.
63. Davies, C., et al., *Simultaneous removal of NOx and soot particulate from diesel exhaust by in-situ catalytic generation and utilisation of N2O.* Applied Catalysis B: Environmental, 2018. **239**: p. 10-15.
64. Roy, S. and A. Baiker, *NO x storage− reduction catalysis: from mechanism and materials properties to storage− reduction performance.* Chemical Reviews, 2009. **109**(9): p. 4054-4091.
65. Iwamoto, S.K., S.; Yoshida, S.; Inui, T. , In Progress in Zeolite and Microporous Materials, 1997. **105**.
66. Olympiou, G.G. and A.M. Efstathiou, *Industrial NOx control via H2-SCR on a novel supported-Pt nanocatalyst.* Chemical engineering journal, 2011. **170**(2-3): p. 424-432.
67. Theis, J.R., J. Kim, and G. Cavataio, *Passive TWC+ SCR systems for satisfying tier 2, bin 2 emission standards on lean-burn gasoline engines.* SAE International Journal of Fuels and Lubricants, 2015. **8**(2): p. 460-473.
68. Burch, R., J. Breen, and F. Meunier, *A review of the selective reduction of NOx with hydrocarbons under lean-burn conditions with non-zeolitic oxide and platinum group metal catalysts.* Applied Catalysis B: Environmental, 2002. **39**(4): p. 283-303.

69. Lindfors, L.-E., et al., *Silver/alumina catalyst for selective catalytic reduction of NO x to N 2 by hydrocarbons in diesel powered vehicles.* Topics in Catalysis, 2004. **28**(1): p. 185-189.
70. Burch, R. and M. Coleman, *An investigation of the NO/H2/O2 reaction on noble-metal catalysts at low temperatures under lean-burn conditions.* Applied Catalysis B: Environmental, 1999. **23**(2-3): p. 115-121.
71. Nanba, T., et al., *Improvements in the N2 selectivity of Pt catalysts in the NO–H2–O2 reaction at low temperatures.* Applied Catalysis B: Environmental, 2003. **46**(2): p. 353-364.
72. Costa, C.N. and A.M. Efstathiou, *Transient Isotopic Kinetic Study of the NO/H2/O2 (Lean de-NO x) Reaction on Pt/SiO2 and Pt/La− Ce− Mn− O Catalysts.* The Journal of Physical Chemistry B, 2004. **108**(8): p. 2620-2630.
73. Kobylinski, T.P. and B.W. Taylor, *The catalytic chemistry of nitric oxide: II. Reduction of nitric oxide over noble metal catalysts.* Journal of Catalysis, 1974. **33**(3): p. 376-384.
74. Costa, C.N., et al., *An investigation of the NO/H2/O2 (lean de-NOx) reaction on a highly active and selective Pt/La0. 7Sr0. 2Ce0. 1FeO3 catalyst at low temperatures.* Journal of Catalysis, 2002. **209**(2): p. 456-471.
75. Shibata, J., et al., *Factors controlling activity and selectivity for SCR of NO by hydrogen over supported platinum catalysts.* The Journal of Physical Chemistry B, 2004. **108**(47): p. 18327-18335.
76. Machida, M., *NO x-Sorbing Metal Oxides, MnO x–CeO 2. Oxidative NO Adsorption and NO x–H 2 Reaction.* Catalysis surveys from Japan, 2002. **5**(2): p. 91-102.
77. Rohr, F., et al., *On the mechanism of sulphur poisoning and regeneration of a commercial gasoline NOx-storage catalyst.* Applied Catalysis B: Environmental, 2005. **56**(3): p. 201-212.
78. Forzatti, P., et al., *Reaction pathway of the reduction by CO under dry conditions of NOx species stored onto PtBa/Al2O3 Lean NOx Trap catalysts.* Journal of Catalysis, 2010. **274**(2): p. 163-175.
79. Liu, L., et al., *Effect of exhaust gases of Exhaust Gas Recirculation (EGR) coupling lean-burn gasoline engine on NOx purification of Lean NOx trap (LNT).* Mechanical Systems and Signal Processing, 2017. **87**: p. 195-213.
80. DiGiulio, C.D., et al., *NH3 formation over a lean NOX trap (LNT) system: Effects of lean/rich cycle timing and temperature.* Applied Catalysis B: Environmental, 2014. **147**: p. 698-710.
81. Abdulhamid, H., E. Fridell, and M. Skoglundh, *Influence of the type of reducing agent (H 2, CO, C 3 H 6 and C 3 H 8) on the reduction of stored NO x in a Pt/BaO/Al 2 O 3 model catalyst.* Topics in catalysis, 2004. **30**(1-4): p. 161-168.
82. Parks, J.E., et al., *Lean gasoline engine reductant chemistry during lean NOx trap regeneration.* SAE International Journal of Fuels and Lubricants, 2010. **3**(2): p. 956-962.
83. Ito, Y., et al., *Next generation of ceramic wall flow gasoline particulate filter with integrated three way catalyst*. 2015, SAE Technical Paper.

84. Myung, C.-L., et al., *Nanoparticle filtration characteristics of advanced metal foam media for a spark ignition direct injection engine in steady engine operating conditions and vehicle test modes.* Energies, 2015. **8**(3): p. 1865-1881.
85. Guan, B., et al., *Review of the state-of-the-art of exhaust particulate filter technology in internal combustion engines.* Journal of environmental management, 2015. **154**: p. 225-258.
86. Saito, C., et al., *New particulate filter concept to reduce particle number emissions*. 2011, SAE Technical Paper.
87. Xia, W., et al., *Catalyzed gasoline particulate filter (GPF) performance: effect of driving cycle, fuel, catalyst coating*. 2017, SAE Technical Paper.
88. Heimrich, M.J. and C.C. Andrews, *On-board hydrogen generation for rapid catalyst light-off.* SAE transactions, 2000: p. 1117-1124.
89. Muraki, H., et al., *The effect of steam and hydrogen in promoting the oxidation of carbon monoxide over a platinum on alumina catalyst.* Journal of Chemical Technology & Biotechnology, 1991. **52**(3): p. 415-424.
90. Kärcher, V., P. Hellier, and N. Ladommatos, *Effects of Exhaust Gas Hydrogen Addition and Oxygenated Fuel Blends on the Light-Off Performance of a Three-Way Catalyst*. 2019, SAE Technical Paper.
91. Sitshebo, S., A. Tsolakis, and K. Theinnoi, *Promoting hydrocarbon-SCR of NOx in diesel engine exhaust by hydrogen and fuel reforming.* International Journal of Hydrogen Energy, 2009. **34**(18): p. 7842-7850.
92. Nova, I., et al., *Experimental investigation of the reduction of NOx species by CO and H2 over Pt–Ba/Al2O3 lean NOx trap systems.* Catalysis Today, 2010. **151**(3-4): p. 330-337.
93. Botas, J.A., et al., *Kinetic considerations of three-way catalysis in automobile exhaust converters.* Applied Catalysis B: Environmental, 2001. **32**(4): p. 243-256.
94. Hepburn, J.S., et al., *The pulse flame combustor revisited.* SAE Transactions, 1996: p. 2296-2331.
95. Bhatia, D., M.P. Harold, and V. Balakotaiah, *Kinetic and bifurcation analysis of the cooxidation of CO and H2 in catalytic monolith reactors.* Chemical Engineering Science, 2009. **64**(7): p. 1544-1558.
96. Salomons, S., R.E. Hayes, and M. Votsmeier, *The promotion of carbon monoxide oxidation by hydrogen on supported platinum catalyst.* Applied Catalysis A: General, 2009. **352**(1-2): p. 27-34.
97. Hauptmann, W., et al., *Modeling the simultaneous oxidation of CO and H2 on Pt – Promoting effect of H2 on the CO-light-off.* Applied Catalysis A: General, 2011. **397**(1-2): p. 174-182.
98. Rankovic, N., et al., *Kinetic Modeling Study of the Oxidation of Carbon Monoxide–Hydrogen Mixtures over Pt/Al2O3 and Rh/Al2O3 Catalysts.* The Journal of Physical Chemistry C, 2011. **115**(41): p. 20225-20236.
99. Hoyle, N., et al., *Catalysis of H2, CO and alkane oxidation–combustion over Pt/Silica catalysts: evidence of coupling and promotion.* Catalysis today, 1999. **47**(1-4): p. 45-49.

100. Oh, S.H. and J.C. Cavendish, *Transients of monolithic catalytic converters. Response to step changes in feedstream temperature as related to controlling automobile emissions.* Industrial & Engineering Chemistry Product Research and Development, 1982. **21**(1): p. 29-37.
101. Stewart, C., et al., *Unraveling the H2 Promotional Effect on Palladium-Catalyzed CO Oxidation Using a Combination of Temporally and Spatially Resolved Investigations.* ACS Catal, 2018. **8**(9): p. 8255-8262.
102. J. Theis, H.J., R. Mccabe, M. Sharma, V. Balakotaiah, M.P. Harold, Society of Automotive Engineers (SAE). **01**(1067).
103. Gu, H., K.M. Chun, and S. Song, *The effects of hydrogen on the efficiency of NO x reduction via hydrocarbon-selective catalytic reduction (HC-SCR) at low temperature using various reductants.* International Journal of Hydrogen Energy, 2015. **40**(30): p. 9602-9610.
104. Kong, Y., et al., *NOx trap regeneration with an on-board hydrogen generation device.* SAE transactions, 2004: p. 316-322.
105. Park, C., et al., *The influence of hydrogen-enriched gas on the performance of lean NOx trap catalyst for a light-duty diesel engine.* International journal of hydrogen energy, 2010. **35**(4): p. 1789-1796.
106. Ngan, E., et al., *Final Tier 4 Emission Solution Using An Aftertreatment System With A Fuel Reformer, LNT, DPF And Optional SCR*, in *SAE Technical Paper Series*. 2011.
107. Ivancic, T.M., et al., *Discovery of a new Al species in hydrogen reactions of NaAlH4.* The Journal of Physical Chemistry Letters, 2010. **1**(15): p. 2412-2416.
108. Andújar, J.M. and F. Segura, *Fuel cells: History and updating. A walk along two centuries.* Renewable and sustainable energy reviews, 2009. **13**(9): p. 2309-2322.
109. Manoharan, Y., et al., *Hydrogen fuel cell vehicles; current status and future prospect.* Applied Sciences, 2019. **9**(11): p. 2296.
110. Ahmed, S. and M. Krumpelt, *Hydrogen from hydrocarbon fuels for fuel cells.* International journal of hydrogen energy, 2001. **26**(4): p. 291-301.
111. Al-Baghdadi, M.A.-R.S. and H.A.-K.S. Al-Janabi, *Improvement of performance and reduction of pollutant emission of a four stroke spark ignition engine fueled with hydrogen–gasoline fuel mixture.* Energy conversion and management, 2000. **41**(1): p. 77-91.
112. Ji, C., et al., *Effect of hydrogen addition on combustion and emissions performance of a gasoline rotary engine at part load and stoichiometric conditions.* Energy Conversion and Management, 2016. **121**: p. 272-280.
113. Suzuki, T. and Y. Sakurai, *Effect of hydrogen rich gas and gasoline mixed combustion on spark ignition engine*. 2006, SAE Technical Paper.
114. Stone, R., H. Zhao, and L. Zhou, *Analysis of combustion and particulate emissions when hydrogen is aspirated into a gasoline direct injection engine*. 2010, SAE Technical Paper.
115. Abdalla, A.M., et al., *Hydrogen production, storage, transportation and key challenges with applications: A review.* Energy conversion and management, 2018. **165**: p. 602-627.

116. Ahluwalia, R.K., T.Q. Hua, and J.K. Peng, *On-board and Off-board performance of hydrogen storage options for light-duty vehicles.* International Journal of Hydrogen Energy, 2012. **37**(3): p. 2891-2910.
117. Zeng, K. and D. Zhang, *Recent progress in alkaline water electrolysis for hydrogen production and applications.* Progress in energy and combustion science, 2010. **36**(3): p. 307-326.
118. Ursua, A., L.M. Gandia, and P. Sanchis, *Hydrogen production from water electrolysis: current status and future trends.* Proceedings of the IEEE, 2011. **100**(2): p. 410-426.
119. Jamal, Y. and M. Wyszynski, *On-board generation of hydrogen-rich gaseous fuels—a review.* International journal of hydrogen energy, 1994. **19**(7): p. 557-572.
120. Lorenzut, B., et al., *Hydrogen production through alcohol steam reforming on Cu/ZnO-based catalysts.* Applied Catalysis B: Environmental, 2011. **101**(3-4): p. 397-408.
121. Fennell, D., et al., *Thermochemical recovery technology for improved modern engine fuel economy – part 1: analysis of a prototype exhaust gas fuel reformer.* RSC Advances, 2015. **5**(44): p. 35252-35261.
122. Jamal, Y., T. Wagner, and M. Wyszynski, *Exhaust gas reforming of gasoline at moderate temperatures.* International Journal of Hydrogen Energy, 1996. **21**(6): p. 507-519.
123. Ashur, M., et al., *On board exhaust gas reforming of gasoline using integrated reformer & TWC*. 2007, SAE Technical Paper.
124. Tsolakis, A., A. Megaritis, and M. Wyszynski, *Application of exhaust gas fuel reforming in compression ignition engines fueled by diesel and biodiesel fuel mixtures.* Energy & fuels, 2003. **17**(6): p. 1464-1473.
125. Tsolakis, A., et al., *Low-load dual-fuel compression ignition (CI) engine operation with an on-board reformer and a diesel oxidation catalyst: effects on engine performance and emissions.* Energy & Fuels, 2010. **24**(1): p. 302-308.
126. Tsolakis, A. and A. Megaritis, *Partially premixed charge compression ignition engine with on-board H2 production by exhaust gas fuel reforming of diesel and biodiesel.* International Journal of Hydrogen Energy, 2005. **30**(7): p. 731-745.
127. Braun, J., et al., *Three-dimensional simulation of the transient behavior of a three-way catalytic converter*. 2002, SAE Technical Paper.
128. Mukadi, L. and R. Hayes, *Modelling the three-way catalytic converter with mechanistic kinetics using the Newton–Krylov method on a parallel computer.* Computers & chemical engineering, 2002. **26**(3): p. 439-455.
129. Zygourakis, K., *Transient operation of monolith catalytic converters: a two-dimensional reactor model and the effects of radially nonuniform flow distributions.* Chemical Engineering Science, 1989. **44**(9): p. 2075-2086.
130. Jeong, S.-J. and W.-S. Kim, *A numerical approach to investigate transient thermal and conversion characteristics of automotive catalytic converter*. 1998, SAE Technical Paper.
131. Jeong, S.-J. and W.-S. Kim, *Three-dimensional numerical study on the use of warm-up catalyst to improve light-off performance*. 2000, SAE Technical Paper.

132. Guojiang, W. and T. Song, *CFD simulation of the effect of upstream flow distribution on the light-off performance of a catalytic converter.* Energy Conversion and Management, 2005. **46**(13-14): p. 2010-2031.
133. Hayes, R.E., et al., *CFD modelling of the automotive catalytic converter.* Catalysis Today, 2012. **188**(1): p. 94-105.
134. Somorjai, G. and Y. Li, *Introduction to surface chemistry and catalysis Wiley.* New York, 1994.
135. Voltz, S.E., et al., *Kinetic study of carbon monoxide and propylene oxidation on platinum catalysts.* Industrial & Engineering Chemistry Product Research and Development, 1973. **12**(4): p. 294-301.
136. Misono, M., *Basis of heterogeneous catalysis*, in *Studies in surface science and catalysis*. 2013, Elsevier. p. 1-23.
137. Kuipers, E., et al., *Surface-molecule proton transfer: A demonstration of the Eley-Rideal mechanism.* Physical review letters, 1991. **66**(1): p. 116.
138. Rettner, C., *Dynamics of the direct reaction of hydrogen atoms adsorbed on Cu (111) with hydrogen atoms incident from the gas phase.* Physical review letters, 1992. **69**(2): p. 383.
139. Stampfl, C. and M. Scheffler, *Anomalous Behavior of Ru for Catalytic Oxidation: A Theoretical Study of the Catalytic Reaction CO+ 1 2 O 2→ CO 2.* Physical review letters, 1997. **78**(8): p. 1500.
140. Baxter, R. and P. Hu, *Insight into why the Langmuir–Hinshelwood mechanism is generally preferred.* The Journal of chemical physics, 2002. **116**(11): p. 4379-4381.
141. Kim, Y.-D. and W.-S. Kim, *Re-evaluation and modeling of a commercial diesel oxidation catalyst.* Industrial & Engineering Chemistry Research, 2009. **48**(14): p. 6579-6590.
142. Koltsakis, G., P. Konstantinidis, and A. Stamatelos, *Development and application range of mathematical models for 3-way catalytic converters.* Applied Catalysis B: Environmental, 1997. **12**(2-3): p. 161-191.
143. Siemund, S., et al., *Three-way monolithic converter: simulations versus experiments.* Chemical Engineering Science, 1996. **51**(15): p. 3709-3720.
144. Shamim, T., et al., *A comprehensive model to predict three-way catalytic converter performance.* Journal of engineering for gas turbines and power, 2002. **124**(2): p. 421-428.
145. Ceviz, M.A., et al., *Determination of cycle number for real in-cylinder pressure cycle analysis in internal combustion engines.* Energy, 2011. **36**(5): p. 2465-2472.
146. Gopujkar, S.B., J. Worm, and D. Robinette, *Methods of pegging cylinder pressure to maximize data quality*. 2019, SAE Technical Paper.
147. GmbH, A.L., *BOOST Users Guide*. 2018.
148. Peters, B.J., et al., *Integrated 1D to 3D simulation workflow of exhaust aftertreatment devices*. 2004, SAE Technical Paper.
149. Ramanathan, K., D.H. West, and V. Balakotaiah, *Optimal design of catalytic converters for minimizing cold-start emissions.* Catalysis today, 2004. **98**(3): p. 357-373.

150. Kaviany, M., *Principles of heat transfer in porous media*. 2012: Springer Science & Business Media.
151. VDI-Wärmeatlas, V., *Berechnungsblätter für den Wärmeübergang.* Siebte, erweiterte Auflage. VDI-Verlag, 1994.
152. Hawthorn, R. *Afterburner catalysts-effects of heat and mass transfer between gas and catalyst surface*. in *AIChE Symp. Ser*. 1974.
153. Ullah, U., et al., *Monolithic reactors: mass transfer measurements under reacting conditions.* Chemical Engineering Science, 1992. **47**(9-11): p. 2413-2418.
154. Votruba, J., et al., *Heat and mass transfer in honeycomb catalysts—II.* Chemical Engineering Science, 1975. **30**(2): p. 201-206.
155. Perry, R.H., D.W. Green, and J.O. Maloney, *Perry's chemical engineers' handbook*. 1997, McGraw-Hill, New York.
156. Subramaniam, B. and A. Varma, *Reaction kinetics on a commercial three-way catalyst: the carbon monoxide-nitrogen monoxide-oxygen-water system.* Industrial & engineering chemistry product research and development, 1985. **24**(4): p. 512-516.
157. Brinkmeier, C., *Automotive three way exhaust aftertreatment under transient conditions: measurements, modeling and simulation*. 2006, University of Stuttgart.
158. Germann, H., S. Taglaiferri, and H.P. Geering, *Differences in pre-and post-converter lambda sensor characteristics*. 1996, SAE Technical Paper.
159. Silvis, W.M., *An algorithm for calculating the air/fuel ratio from exhaust emissions*. 1997, SAE Technical Paper.
160. Mejía-Centeno, I., S. Castillo, and G.A. Fuentes, *Enhanced emissions of NH3, N2O and H2 from a Pd-only TWC and supported Pd model catalysts: Light-off and sulfur level studies.* Applied Catalysis B: Environmental, 2012. **119-120**: p. 234-240.
161. Mannila, P., et al., *Stationary kinetics of essential reactions on automobile exhaust PtRh/Al2O3 catalyst.* Applied Catalysis B: Environmental, 1996. **7**(3-4): p. 179-198.
162. Pihl, J.A., et al., *Lean NOx trap chemistry under lean-gasoline exhaust conditions: impact of high NOx concentrations and high Temperature.* Topics in Catalysis, 2013. **56**(1-8): p. 89-93.
163. Sharma, M., M.P. Harold, and V. Balakotaiah, *Analysis of Storage and Reaction Phases of LNT for Diesel Engine Exhaust Treatment*. 2005, SAE Technical Paper.
164. West, B., et al., *Assessing reductant chemistry during in-cylinder regeneration of diesel lean NOx traps.* SAE transactions, 2004: p. 1975-1985.
165. Maurer, M., et al., *Investigations of Lean NOx Trap (LNT) Regeneration Strategies for Diesel Engines*. 2017, SAE Technical Paper.
166. Ren, Y. and M.P. Harold, *NO x Storage and Reduction with H2 on Pt/Rh/BaO/CeO2: Effects of Rh and CeO2 in the Absence and Presence of CO2 and H2O.* Acs Catalysis, 2011. **1**(8): p. 969-988.
167. Theis, J.R., et al., *NO x release characteristics of lean NO x traps during rich purges.* SAE transactions, 2003: p. 758-775.

APPENDIX

A. Screening tests for LNT activity study

(1) LNT storage memory effect study

During the tests, the LNT catalyst is found to have a 'NO_x storage memory'. Namely, the NO_x level measured at post-LNT will be different even the measurement is carried out under same operating condition. Therefore, repeated FTIR measurements were performed under engine lean/rich cycle (50 s lean at λ =1.15, 10 s rich at λ =0.9) at 150 and 250 ^{o}C respectively. For both two temperature cases, the 1st measurement was conducted after LNT being exposed to a long period of stoichiometric engine exhaust, while the 2nd measurement was conducted after lean operation. Both two measurements were performed under the same condition and follow same testing procedure.

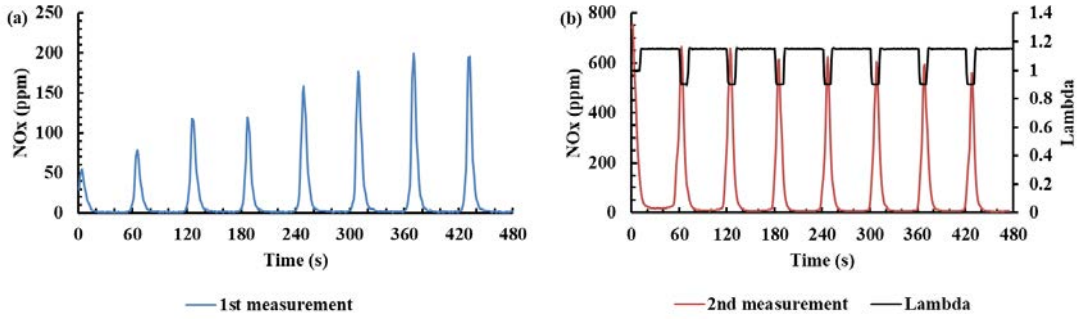

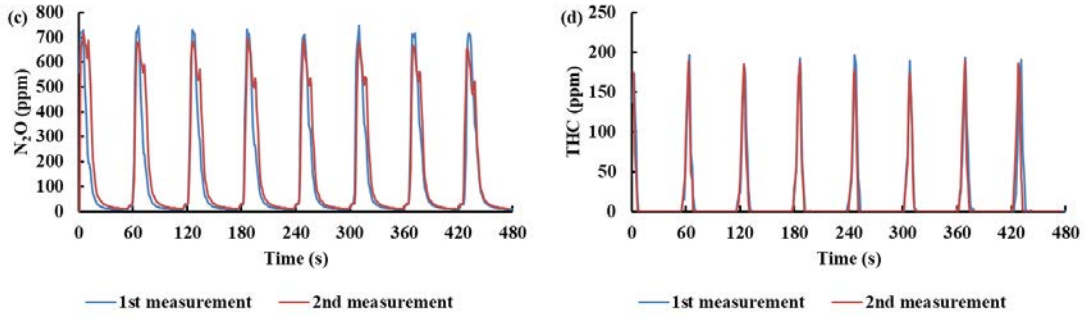

Figure A-1. Temporal profile of (a)-NO_x, (b)-N_2O, and (c)-THC concentrations at LNT out obtained from repeated measurements under engine cycle operation at 150 ºC (lambda value provided as reference)

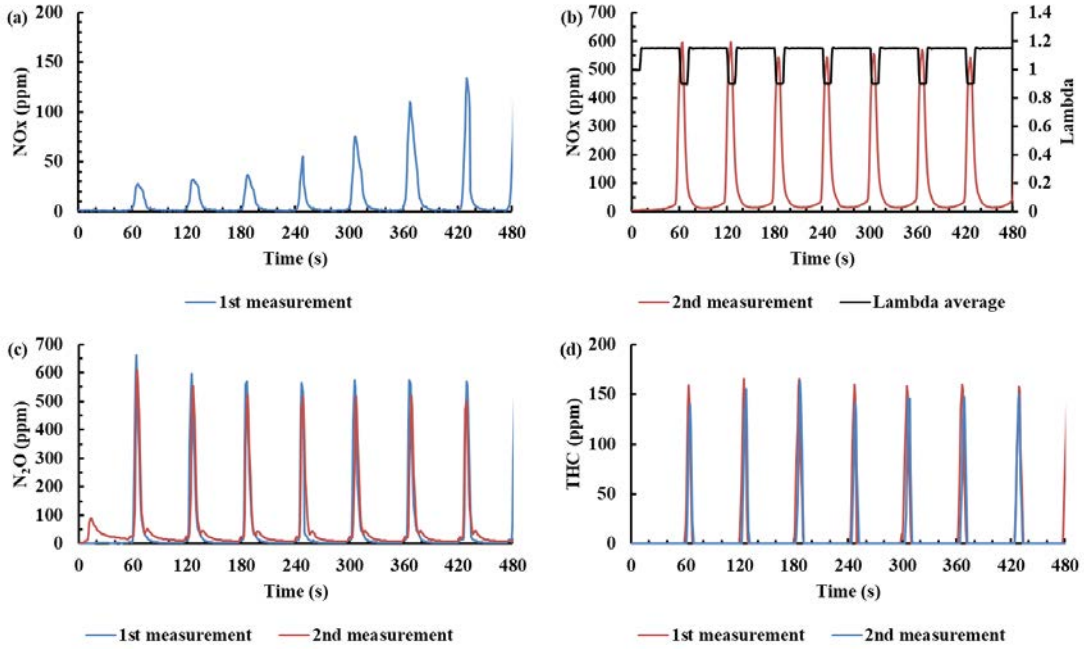

Figure A-2. Temporal profile of (a-b)-NO_x, (c)-N_2O, and (d)-THC concentrations at LNT out obtained from repeated measurements under engine cycle operation at 250 ºC (lambda value provided as reference)

Figure A-1 compares the NO_x, N_2O and THC profiles at LNT out from two separate measurements at 150 ºC. The performed lambda cycle keeps the same for these two measurements and is shown in Figure A-1 (b). It can be seen that the NO_x level varies for the 1st and 2nd measurement, while the N_2O and THC concentrations are quite similar. This is believed to be resulted from the LNT storage memory effect on NO_x. For the 1st

measurement, the NO_x slips over LNT are getting up as time increases. It is assumed that most of the NO_x storage sites are free when the LNT is exposing to stochiometric condition for a long period. Thereby, when we measured just after that, the NO_x slips over LNT will be very low at the beginning and show an increasing trend as the storage sites are gradually occupied. After a point, the NO_x levels will be stable. As for the 2nd measurement, NO_x level stabilizes at around 650 ppm, which is believed to be related to the fact that the LNT is saturated so that the NO_x slips will not change as a function of time.

Figure A-2 presents the repeated measurement study but for 250 ºC. Similarly, an upward trend was perceived for the NO_x which was measured after LNT experiencing long period of stoichiometric exhaust, and another NO_x was recorded to be stable. As for the THC and N_2O profiles obtained from these two measurements, the variance can be neglected. Therefore, for the following experimental study of different scenarios, not only the operating parameters but also the beforehand engine operation should keep the same to minimize the experimental errors and ensure the reliability and comparability of recorded data under various conditions.

Additionally, the change in species concentrations in response to corresponding engine transition from both stoichiometric to lean and the reverse operation were recorded by FTIR and HSense at LNT outlet. The temporal profiles of NO_x, H_2 and CO levels are presented in Figure A-3. Under the transient engine operation from stoichiometric to lean, the THC and N_2O levels are very low, so they are not presented here. In the previous study

of our research group, the time delay from changing engine operating parameters to observing any change in the instrument reading (FTIR and HSense) was investigated through relevant tests. Thereby, the averaged time delay of 5s will be considered in present study to well illustrate how the NO_x level responses to engine transient operation. The average engine out species concentration measured under steady lean (λ =1.15) and stoichiometric (λ =1) conditions are summarized in Table A-1 for reference.

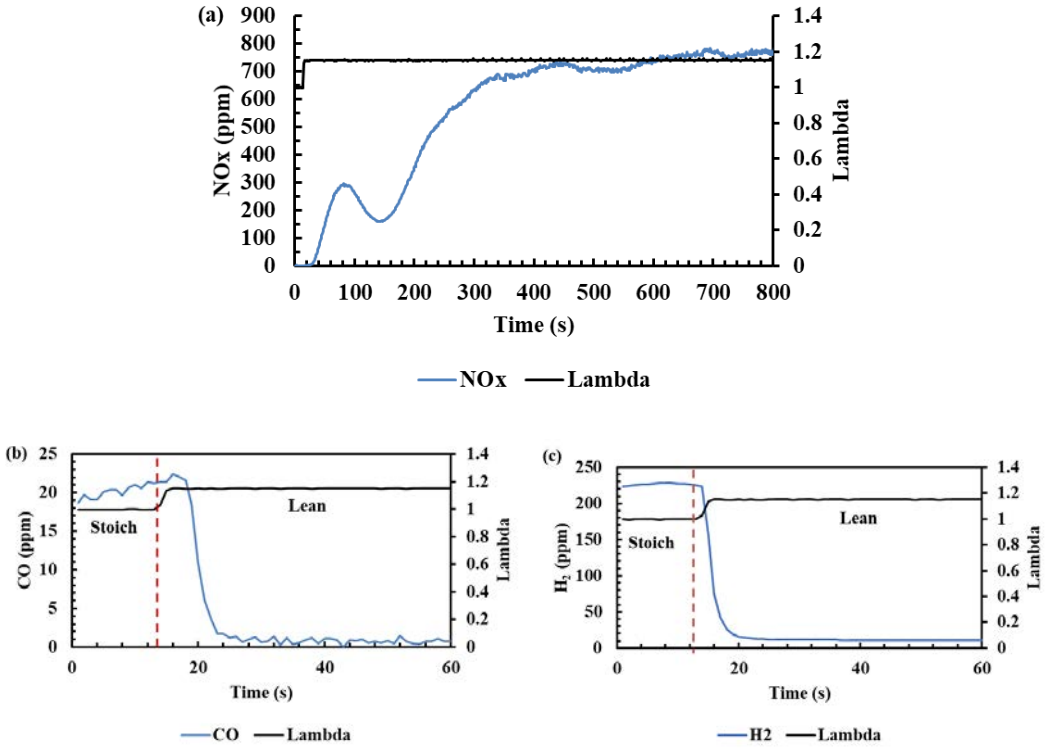

Figure A-3. Species concentration after LNT with engine transient operation from stoichiometric to lean (lambda value provided as reference)

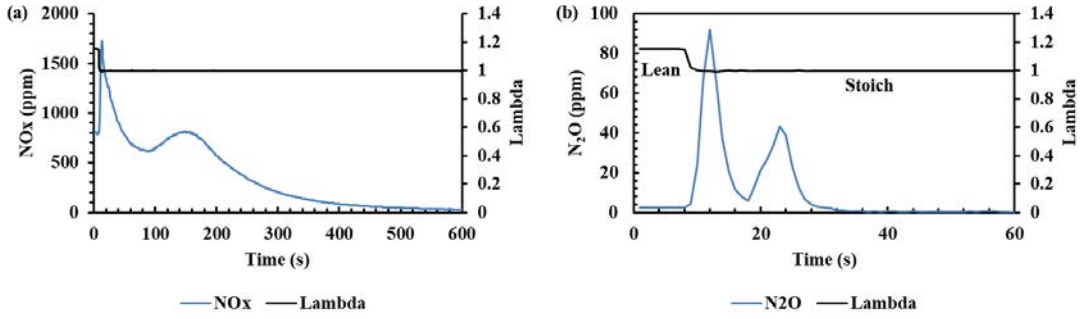

Figure A-4. Species concentration after LNT with engine transient operation from lean to stoichiometric (lambda value provided as reference)

According to Figure A-3 (b-c), as engine operation switches from stoichiometric (stated as 'stoich' in the plot) to lean, the measured CO and H_2 concentrations quickly drop to zero level. As for NO_x, it was observed that the LNT took around 450 s to saturated and NO_x slips reach an equilibrium. It should be noted that the duration of LNT to be saturated greatly depends on the operating temperature, which explains the slow growing trend of NO_x at low temperature in Figure A-1 (a) and Figure A-2 (a). Figure A-4 captures transient species concentration change at post-LNT with switching engine from lean to stoichiometric. Other species levels are very low under this operation, thereby only the NO_x and N_2O concentration profiles are presented here. A peak in NO_x curve can be observed with the transient change in exhaust stoichiometry, which is assumed to be resulted from following reasons: 1) As engine switches to stoichiometric operation, more NO_x is generated from in-cylinder combustion (see Table A-1) and certain amount of NO_x were escaped from TWC unreduced at the instant; 2) The adsorbed NO_x is suddenly released from the LNT storage site due to the instantaneous change in exhaust stoichiometry. Corresponding N_2O curve reveals similar story. Consequently, in the following study, it is critical to keep the consistency of beforehand exhaust condition when performing different testing scenarios.

Table A-1. Average engine out species concentrations under steady engine operation

	Lean λ =1.15	Rich λ =0.9	Stoichiometric λ =1
H_2 (ppm)	155.77	11950.33	2735.65
CO (ppm)	988.67	24284.47	6863.04

CO_2 (%)	11.24	9.92	11.47
H_2O (%)	11.19	12.73	12.49
O_2 (%)	3.03	0.30	0.80
N_2O (ppm)	0.84	0	2.37
NH_3 (ppm)	0.14	4.17	12.50
THC (ppm)	1488.58	2138.31	1520.70
NO_x (ppm)	811.97	889.55	1316.70

(2) Examine the LNT performance under various engine cycles

Prior to the tests, the LNT performance under various engine lean/rich cycles were studied at constant operating temperatures 150, 200, and 250 ºC respectively using the small-scale set up. The details of examined cycles are shown in Table A-2.

Table A-2. Details of different engine lean/rich cycles at 150 ºC

Examined engine cycles	Lean/rich phase duration (s)	Lean/rich phase λ
50/10 s cycle	50&10	1.15&0.9
50/10 s (rich at 0.925) cycle	50&10	1.15&0.925
55/5 s cycle	55&5	1.15&0.9

The temporal profiles of NO_x levels at LNT out under different cycles are shown in Figure A-5. The calculated cycle-based average conversion efficiency of CO, THC and NO_x under the examined cycles are presented in Figure A-6. As indicated by Figure A-5, the NO_x levels measured during lean phase are very low (around zero) for the 50&10 s case,

suggesting that the majority of NO_x was adsorbed on the LNT; While for the 55&5 s case, large amount of NO_x escape from LNT unadsorbed during lean period, thereby resulting in relative higher NO_x peaks. Similarly, for the 50&10 s (rich at 0.925) case, certain amount of NO_x was slipped over the LNT comparing to the 50&10 s case. Since the majority of NO_x was emitted unconverted over the LNT for those two cases, the corresponding NO_x removal efficiency will be lower than the 50&10 s case, which is in accordance with the observation in Figure A-6 that an average NO_x conversion efficiency at around 90% was achieved by the 50&10 s engine cycle. As for the 55&5 s and 50&10 s (rich at 0.925) cases, approximate 60% and 15% of NO_x conversion were observed. It is suggested that among the tested engine cycles, the optimum NO_x removal performance over LNT was perceived for the 50&10 s case. As for CO, nearly 100% of conversion is reached for all three cases, while THC exhibits different features. For the 50&10 s case, extremely low THC conversion was captured. As switching to the other two cases, the average THC conversion was greatly improved.

Although N_2 is the primary product of NO_x reduction over the catalyst, N_2O and NH_3 is also generally formed as by-products under certain conditions. The selectivity and yields of NH_3 and N_2O calculated over the LNT catalyst under different engine cycles are shown in Figure A-7 and Figure A-8. The selectivity to N_2 for these three cases was calculated based on the NH_3 and N_2O selectivity and are shown in Figure A-9. It was reported that the NH_3 and N_2O selectively primarily depends on the temperature and the duration of lean/rich cycle was of secondary importance on the selectivity [80]. The temperature

dependence of NO_x reduction selectivity was discussed previously in Chapter 5.3.3. The selectivity to N_2 is fairly lower for the 50&10 s lean/rich duration comparing to the 55&5 s. At 150 °C, only a small fraction of stored NO_x (below 5%) was converted to NH_3 for all examined cycles; While as for N_2O, the selectivity is relatively higher (around 50% for the 50&10 s cases, and 12% for the 55&5 s case).

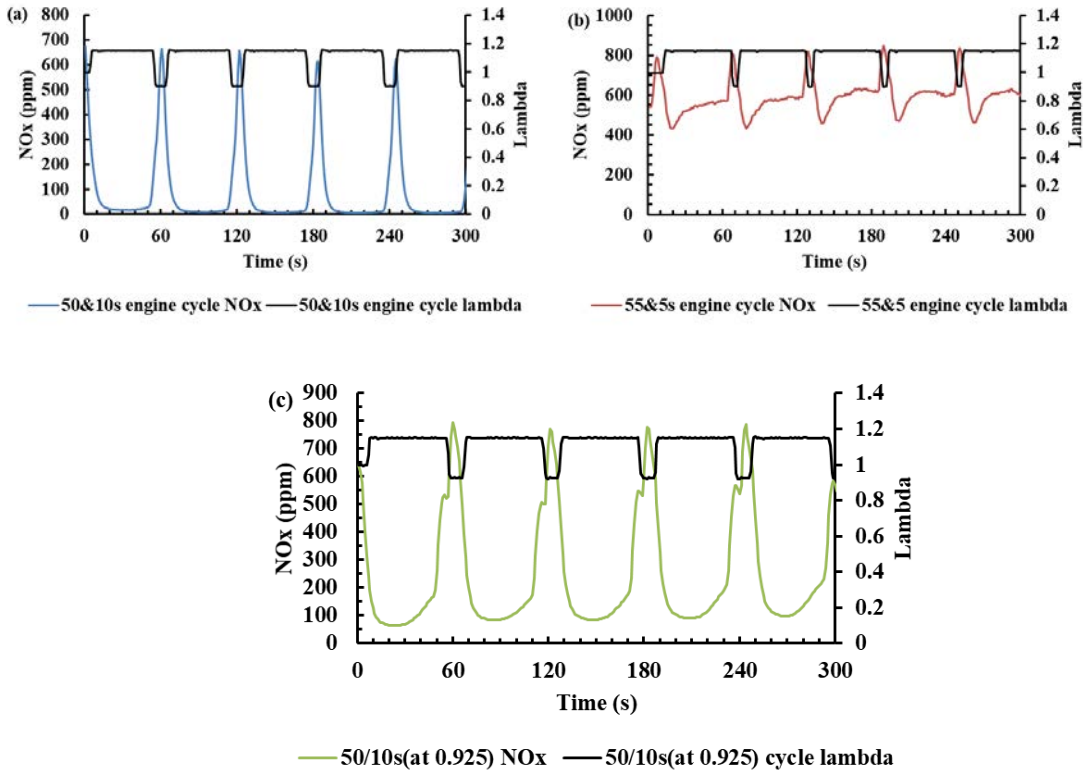

Figure A-5. Measured NO_x concentrations at LNT outlet different engine cycles at 150 °C (lambda value are provided as reference)

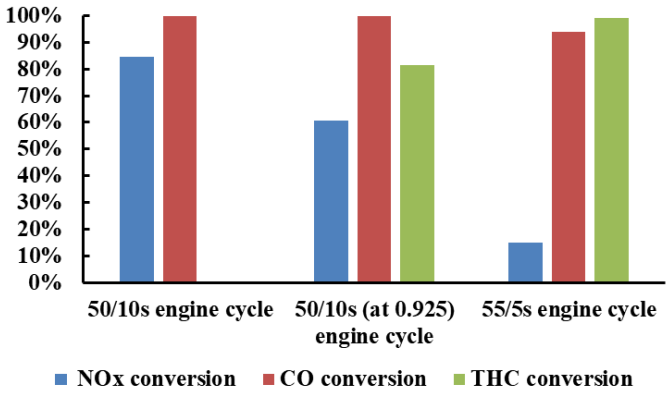

Figure A-6. Cycle averaged conversion efficiency of NO_x, CO, and THC for the LNT under different engine cycles at 150 ºC (THC conversion for 50/10 s engine cycle is near zero)

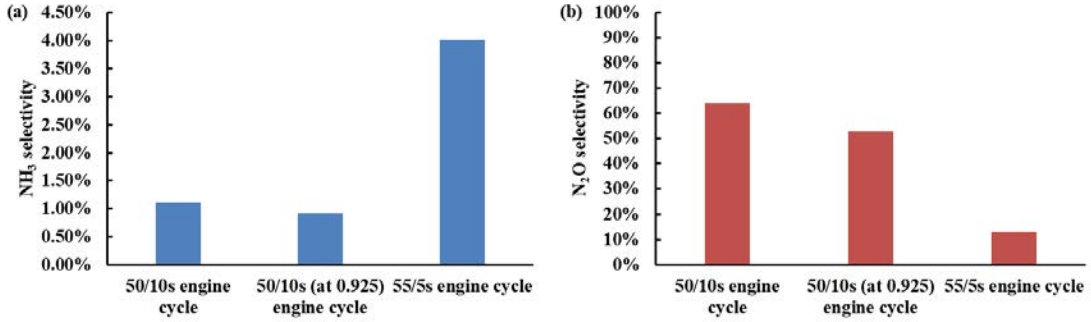

Figure A-7. Cycle averaged selectivity of (a) NH_3 and (b) N_2O for the LNT under different engine cycles at 150 ºC

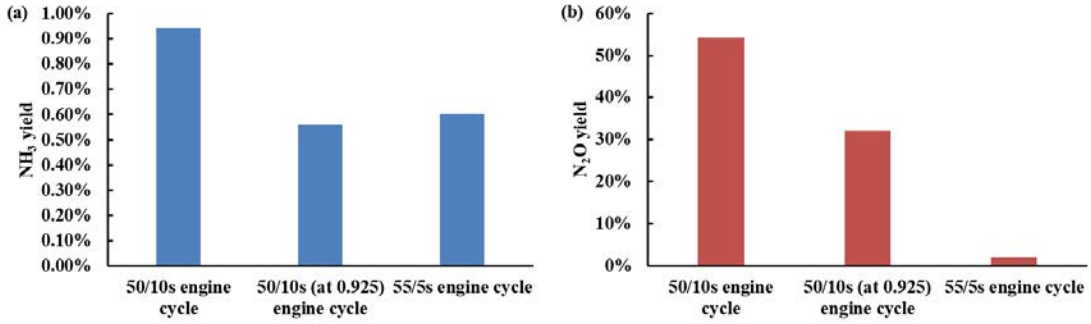

Figure A-8. Cycle averaged yield of (a) NH_3 and (b) N_2O for the LNT under different engine cycles at 150 ºC

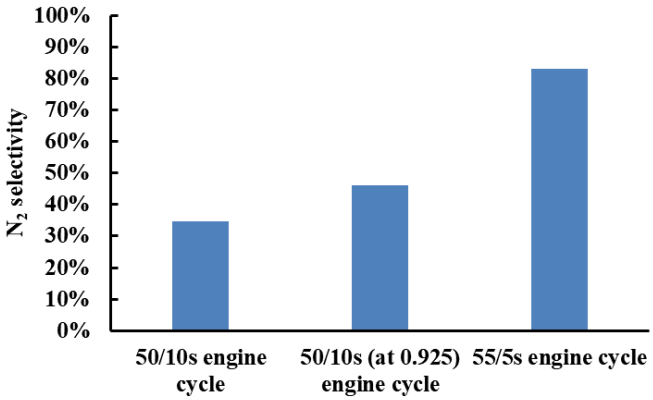

Figure A-9. Cycle averaged selectivity to N_2 for the LNT under different engine cycles at 150 ^oC

As it was observed, better NO_x removal efficiency was achieved for the 50&10s engine cycle operation. Although the selectivity to N_2O for this case is relatively high (58.15%), it should be mentioned that the NOx reduction selectivity to N_2O and NH_3 is strongly dependent on operating temperature. This observed higher selectivity to N_2O is considered to be resulted from the examined temperature (150 ^oC). The selectivity at different temperature will be discussed in next section. Therefore, the lean/rich cycle of 50s/10s duration at lambda value of 1.15/0.9 is selected as the representative and baseline cycle for the following LNT study. And this cycle will be denoted as 'the baseline engine lean/rich cycle' unless otherwise mentioned.

Similar to the 150 ^oC case, temporal profiles of NO_x concentration measured at LNT outlet, and the lambda value recorded by ATI were plotted for each case at 200 and 250 ^oC. The cycle-based average conversion of CO, THC, and NO_x were calculated and plotted to compare the LNT performance for 50&10 s case and 55&5 s case. Additionally, for NOx reduction, the selectivity and yields of NH_3 and N_2O were also obtained and

presented. The N_2 selectivity was also provided based on the nitrogen-containing species mass balance theory. At both 200 and 250 °C , similarly, better NO_x removal performance was observed for 50&10s case than 55&5 s case. Similar results were obtained for NH_3 and N_2O selectivity. The NH_3 selectivity is low for all cases at both 200 and 250 °C; While the N_2O selectivity is significantly higher for 50/10 s case than 55/5 s case, but it is decreased as temperature rises. Therefore, the lean/rich cycle of 50 s/10 s duration at lambda value of 1.15/0.9 is selected as the representative and baseline cycle for the following LNT study.

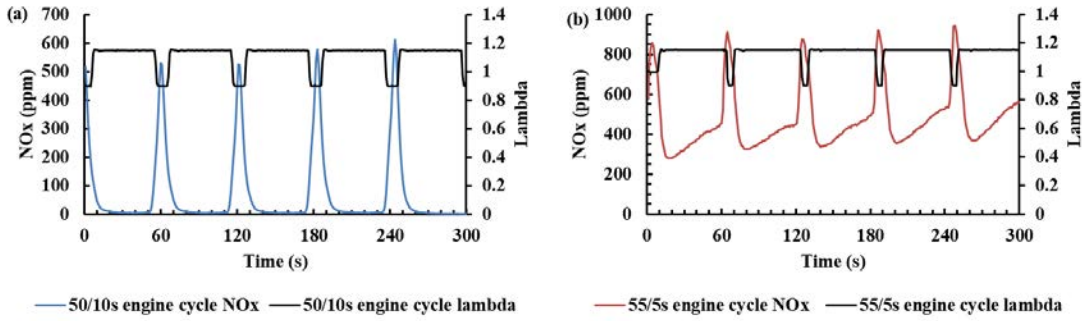

Figure A-10. Measured NO_x concentrations at post-LNT under different engine cycles at 200 °C (lambda value are provided as reference)

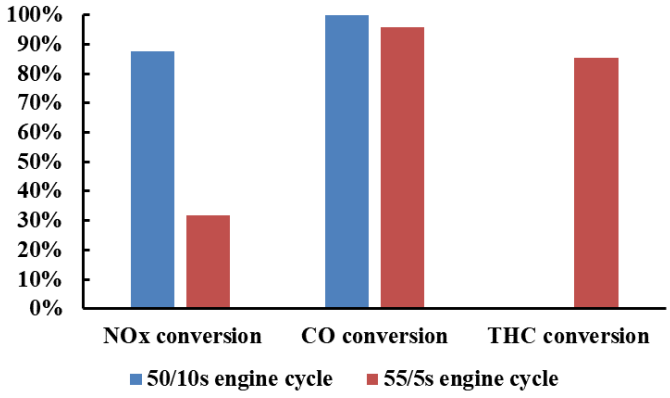

Figure A-11. Cycle averaged conversion efficiency of NO_x, CO, and THC for the LNT under different engine cycles at 200 °C

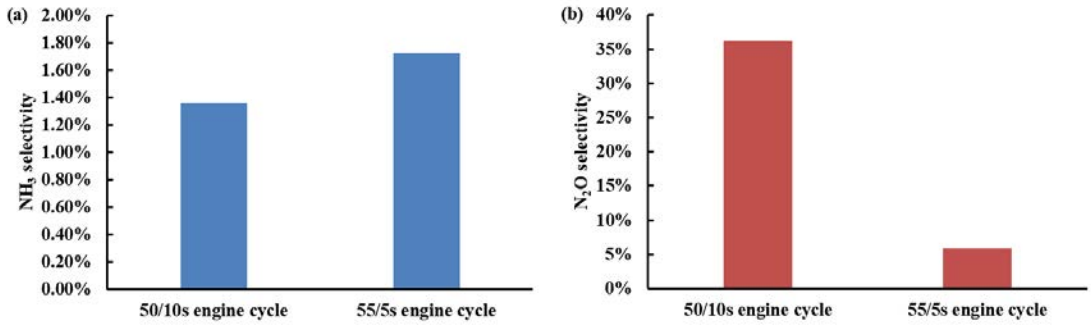

Figure A-12. Cycle averaged selectivity of (a) NH_3 and (b) N_2O for the LNT under different engine cycles at 200 °C

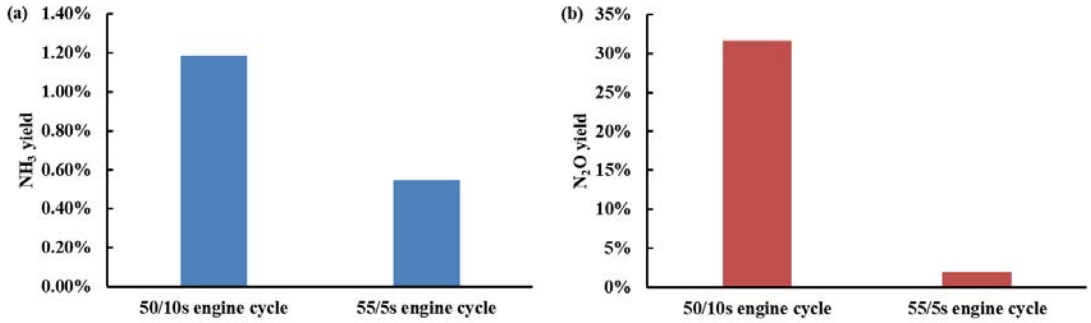

Figure A-13. Cycle averaged yields of (a) NH_3 and (b) N_2O for the LNT under different engine cycles at 200 °C

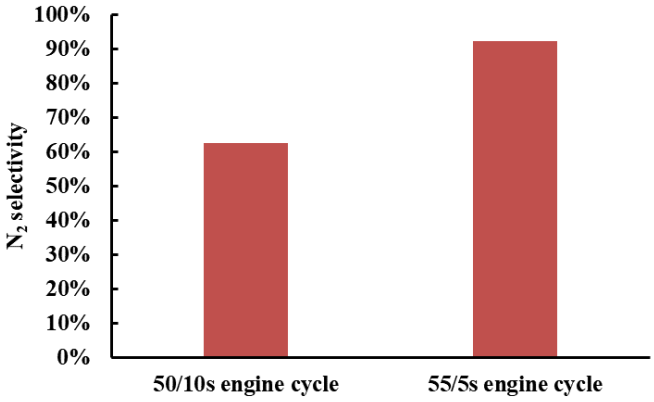

Figure A-14. Cycle averaged selectivity to N_2 for the LNT under different engine cycles at 200 °C

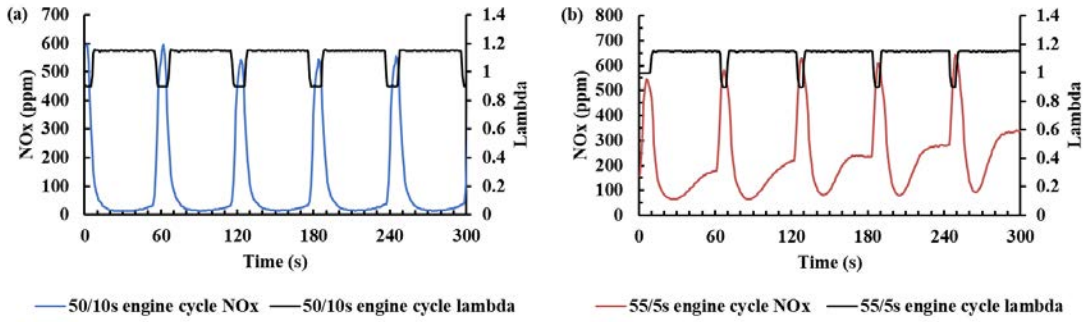

Figure A-15. Measured NO_x concentrations at LNT outlet different engine cycles at 250 °C (lambda value are provided as reference)

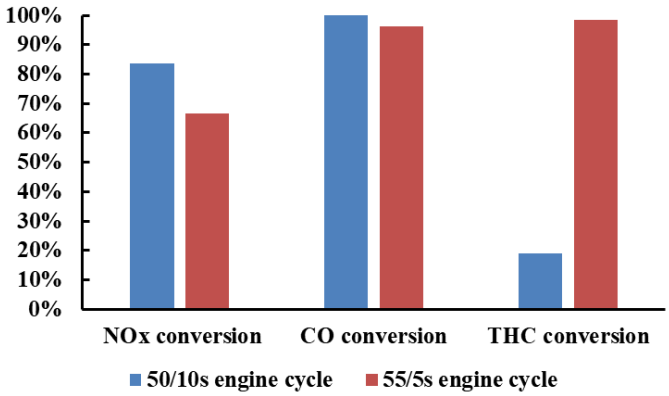

Figure A-16. Cycle averaged conversion efficiency of NO_x, CO, and THC for the LNT under different engine cycles at 250 °C

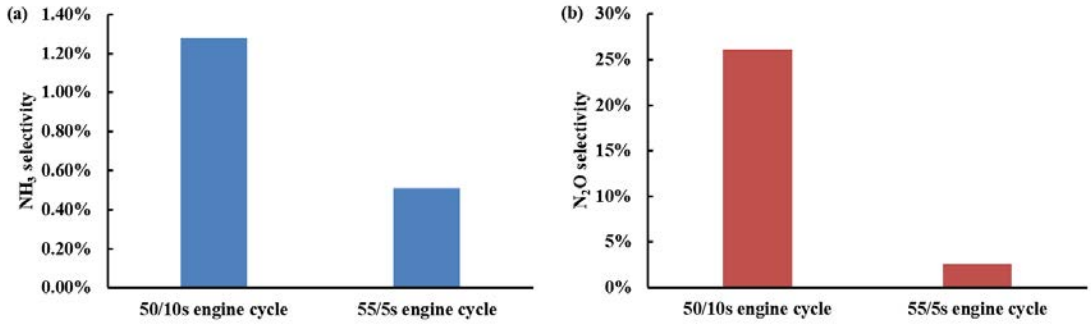

Figure A-17. Cycle averaged selectivity of (a) NH_3 and (b) N_2O for the LNT under different engine cycles at 250 °C

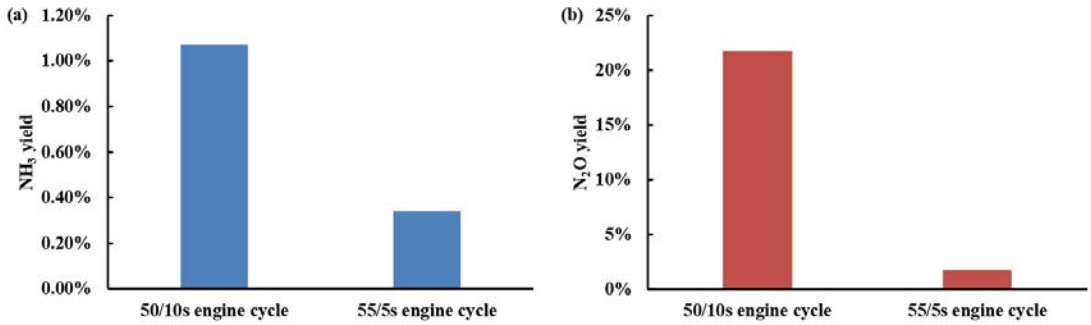

Figure A-18. Cycle averaged yields of (a) NH_3 and (b) N_2O for the LNT under different engine cycles at 250 °C

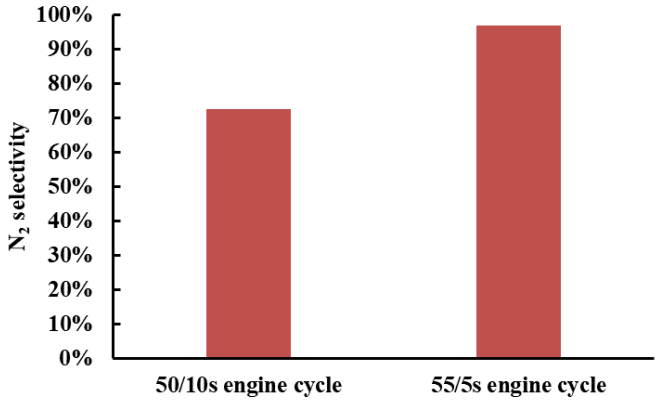

Figure A-19. Cycle averaged selectivity to N_2 for the LNT under different engine cycles at 250 °C

B. Measuring instruments specifications

Table B-1.Technical specifications for the MKS MultiGas^{TM} 2030 FTIR analyser

Measurement/control system specifications	
Measurement Technique	FTIR Spectrometry
Gases and Vapours Measurable	Most molecules except for N_2, H_2, and O_2
Ranges	Concentration between 10ppb and 100% full scale
FTIR	2102 Process FTIR
Spectral Resolution	0.5 – 16cm^{-1}
Scan Speed	1 scan/sec @ 0.5cm^{-1}
Scan Time	1-300 sec
Infrared Source	Silicon Carbide
Reference Laser	Helium Neon (15798.2cm^{-1})
Detector	LN_2 –cooled MCT; TE–cooled MCT
Purge Pressure	20 psig (1.5 bar) max
Pressure Transducer	MKS Baratron® capacitance manometer

Table B-2.Measuement accuracy of the MKS MultiGas^{TM} 2030 FTIR analyser

Measurement accuracy for various gaseous compositions (%)									
CO	CO_2	NO	NO_2	N_2O	NH_3	H_2O	CH_4	C_2H_2	THC
±3	±2	±3	±3	±3	±3	±5	±5	±5	±5

Table B-3.Technical specifications for the Bronkhorst digital mass flow controller (model EL-FLOW *Select* F-201AV)

Measurement/control system specifications	
Flow range	min. 0,4…20 l_n/min
	max. 2…100 l_n/min (based on N_2)
Accuracy	± 0,5 % RD plus ±0,1% FS
Settling time (in control, typical)	standard: 1…2 seconds
Control stability	< ± 0,1 % FS
Operating temperature	-10 … +70 °C
Temperature sensitivity	zero: < 0,05% FS/°C; span: < 0,05% Rd/°C
Warm-up time	30 min. for optimum accuracy

Table B-4. Technical specifications for the V&F hydrogen& helium mass spectrometer (HSense)

Measurement/control system specifications	
Mass range	2 - 4 amu (atomic mass unit)
Dissolution	<1 amu
Measuring range *	0- 50,000 ppm, 0- 100% by volume
reproducibility	$< \pm$ 3%
accuracy	$< \pm$ 2%
Analysis time	$\geq$ 20 mesc/amu
Response time *	T90 < 1 sec
Detection limit *	<1 ppm for H_2, <20 ppb for He

Table B-5. Technical specifications for the Testo 340 Flue Gas Analyzer

Measurement/control system specifications	
Measuring range	0 to 25 Vol.%
Accuracy	± 0.2 Vol.%
Resolution	0.01 Vol.%
Reaction time t_{90}	< 20 s
Operating temperature	-5 to +50 °C

Table B-6. Technical specifications for the Rheonik Coriolis fuel flow meter (RHM015)

Measurement/control system specifications	
Measuring range	0.004 to 0.6 kg/min
Accuracy	± 0.1% of rate
Operating temperature	-50 to +210 °C
Maximum pressure	1379 bar
Materials	SS 316, Alloy C22, SuperDuplex